SYNTHESIS AND FUNCTIONALIZATION OF POLY-L-LYSINE-GRAFTED-POLYETHYLENE GLYCOL COPOLYMER NANOPARTICLE COMPLEXES FOR PROTEIN DELIVERY

By

NICHOLAS FLYNN

Bachelor of Science in Chemical Engineering
The University of Oklahoma
Norman, OK
2011

Master of Science in Chemical Engineering
Oklahoma State University
Stillwater, OK
2014

Submitted to the Faculty of the
Graduate College of the
Oklahoma State University
in partial fulfillment of
the requirements for
the Degree of
DOCTOR OF PHILOSOPHY
July, 2018

SYNTHESIS AND FUNCTIONALIZATION OF POLY-L-LYSINE-GRAFTED-POLYETHYLENE GLYCOL COPOLYMER NANOPARTICLE COMPLEXES FOR PROTEIN DELIVERY

Dissertation Approved:

Dr. Joshua D. Ramsey

Dissertation Adviser

Dr. Heather Gappa-Fahlenkamp

Dr. Ashlee N. Ford Versypt

Dr. Steve Hartson

ACKNOWLEDGEMENTS

I would like to thank everyone who helped me and gave me the opportunity to do the work described here. First, I would like to thank Dr. Pope, Dr. Hartson, Dr. Ford Versypt, and Dr. Fahlenkamp for serving on my committee. I would also like to thank Dr. Pope, Dr. Hartson, Dr. Jing Pope, and Dr. Ranjan for giving me the chance to work with and learn from them as part of my research experience here. Finally, I would like to thank my advisor, Dr. Josh Ramsey, for all of his guidance and support ever since the beginning of my time here. I am really very grateful for all that I have learned from the faculty here at OSU.

Next, I would like to thank my friends and family who have always been supportive and helped me along the way. I am especially thankful to my parents for their encouragement and all that they have done to help me.

Finally, I would like to thank the School of Chemical Engineering at Oklahoma State University for all of the great opportunities provided to me.

Name: NICHOLAS FLYNN

Date of Degree: JULY, 2018

Title of Study: SYNTHESIS AND FUNCTIONALIZATION OF POLY-L-LYSINE-GRAFTED-POLYETHYLENE GLYCOL COPOLYMER NANOPARTICLE COMPLEXES FOR PROTEIN DELIVERY

Major Field: CHEMICAL ENGINEERING

Abstract: Proteins are a large group of biomolecules that are capable of a broad range of biochemical functions. Utilizing the biochemical capabilities of proteins is of significant interest toward improving human health. For proteins to be useful, they must be appropriately delivered to perform the task for which they are needed. This work investigates how the cationic copolymer, poly-l-lysine-grafted-polyethylene glycol (PLL-g-PEG), may be used to modify proteins in order to improve aspects of their delivery. PLL-g-PEG was found to associate with a model protein, BSA, to form nanoparticle complexes through electrostatic interaction between the protein and copolymer. Molecular characteristics of the copolymer, such as PLL molecular weight and PEG grafting were found to impact both the ability of the copolymer to associate with the protein and also the stability of the resulting complexes. The nanoparticle complexes were functionalized with cell-penetrating peptides (CPPs) to impart the ability to enter into a broad range of cell types. The impact CPP functionalized nanoparticle complexes had on albumin in the physiological environment was investigated. CPPs were found to induce conformational changes in albumin, with the extent of albumin denaturation correlating with CPP charge and arginine content. The denaturation of albumin played a role in uptake of the nanoparticle complexes by macrophages. Cell specific delivery of PLL-g-PEG nanoparticle complexes was demonstrated by functionalizing PLL-g-PEG with an anti-PSMA monoclonal antibody. The anti-PSMA-PLL-g-PEG nanoparticle complexes were able to deliver a cytotoxic protein, glucose oxidase, to prostate specific membrane antigen (PSMA)-expressing LNCaP cells, while inducing negligible cytotoxicity in PC-3 cells, which lack PSMA. Together, these studies demonstrate the wide utility of PLL-g-PEG to provide a base for altering the characteristics of proteins which may be used to improve their delivery.

TABLE OF CONTENTS

Chapter Page

Chapter Page

LIST OF TABLES

Table Page

LIST OF FIGURES

Figure Page

Figure Page

CHAPTER I

INTRODUCTION

1.1 Proteins as Therapeutics and Challenges to Delivery

Proteins are relatively large biomolecules that, due to their vast variety of potential structures, carry out a wide number of biochemical tasks that are needed for the normal function of cells, tissues, and organs within an organism. When a protein is not present in quantities needed or is not sufficiently active, cells are unable to function normally, resulting in poor health and disease. Many health conditions are a result of a loss of appropriate protein function. For this reason, the ability to replace proteins that have lost function or to utilize proteins that can be used to accomplish biochemical tasks is of significant interest to improve human well-being.

Although some proteins, such as insulin, albumin, and antibodies, have already been successfully applied toward the improvement of human health, other proteins still face challenges to their use [1]. There may be several reasons that a protein is not able to be utilized therapeutically, but two common reason are poor delivery to specific sites within the body and rapid removal from circulation due to immunogenicity [1, 2]. A

protein may also not be adequately delivered if it needs to be delivered into the cell interior, as the cell membrane is effective at prohibiting large hydrophilic biomolecules like proteins from crossing into the cell interior [1, 3]. The development of novel approaches to either modify proteins or to encapsulate them into drug delivery vehicles has, therefore, become of substantial interest to attempt to overcome challenges to poor protein delivery.

1.2 Cationic Copolymers and Nanoparticles for Protein and Drug Delivery

Nanomaterials have become a popular approach to deliver therapeutics, ranging from small molecule anti-cancer drugs to macromolecules such as peptides, proteins, and nucleic acids [4, 5]. Nanomaterials can include a wide variety of structures, including nanoparticles (NPs), nanorods, nanosheets, and nanotubes, but NPs are one of the most common nanomaterials for drug delivery. The advantage of NP-based systems is that, through the manipulation of the material used to construct the NP, the delivery and release of therapeutic cargos can potentially be better controlled than that of the non-encapsulated molecules [6]. Additionally, the nano-scale is conducive for the passage and interaction of therapeutics with both the extracellular environment as well as components of the cell interior [6, 7]. NPs can be tailored with functionalities to protect their cargos during extracellular transport, as well as with mechanisms to allow for cell binding and internalization during delivery [8-10]. Despite all of these advantages, there remains significant room for improvement in production and efficiency of many NP-based drug delivery systems [11].

One of the most important aspects of NP delivery systems is the material used to synthesize the NP. Although several biomaterials have been developed that have characteristics conducive to drug delivery, our group has particular interest in the cationic

grafted copolymer, poly-l-lysine-grafted-polyethylene glycol (PLL-g-PEG, Figure 1.1). One part of the PLL-g-PEG copolymer, polyethylene glycol (PEG), is a hydrophilic polymer that has been widely used to reduce clearance and improve the biocompatibility of biomaterials, NPs, and pharmaceutics [12]. PEG coating or PEGylation prevents liver and kidney clearance of molecules, and is already being used commercially to improve the circulation characteristics of several proteins such as asparaginase (Oncaspar®) and interferon (Pegasys®) [13-15].

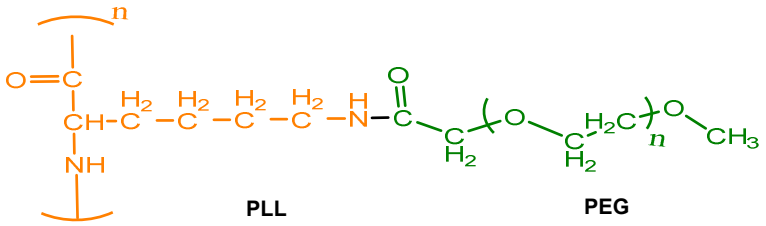

Figure 1.1. Chemical Structure of PLL-grafted-PEG.

One of the reasons PEG is able to impart these beneficial properties is through the reduction of serum protein adsorption onto NP surfaces. PEG has been used to prevent protein adsorption onto NPs and to reduce NP uptake by cells to about 10% of comparable bare NPs [16]. Others have established that PEG molecular properties, such as molecular weight and extent of copolymer grafting, also impact serum protein adsorption onto NPs. Rausch et al. found that 10-20% PEGylation of PLL was sufficient to prevent large aggregates from forming between the polymer and other serum proteins [17]. Additionally, Gref et al. found 5kDa PEG best prevented plasma proteins from being adsorbed on the surface of polylactic acid (PLA) NPs [18]. The work of these studies provided guidelines toward the grafting of PEG onto PLL as part of the synthesis of PLL-g-PEG NPs, which will be discussed in greater detail in subsequent sections.

The ϵ- amino groups of PLL-g-PEG are cationic at physiological conditions (pI 9.5), allowing the polymer to electrostatically self-assemble with negatively charged molecules to form into a type of NP, often called a polyion complex [19-23]. Synthetic gene delivery applications have utilized PLL and other cationic polymers to self- assemble with nucleic acids and utilize specialized functionalities to enhance their delivery efficiency [24-26]. In addition to nucleic acids, charged polymers and copolymers have also been used to deliver proteins, such as lysozyme, IgG, butyrylcholinesterase (BChE), superoxide dismutase (SOD1), and catalase [27-32]. These studies suggested the significant potential of PLL-g-PEG copolymers to self-assemble with a wide variety of proteins to form NP complexes and alter the delivery of proteins. However, the characteristics of cationic copolymers, such as PLL-g-PEG, best suited for protein delivery have not been well described. This prompted us to investigate what copolymer structural characteristics significantly impact protein association with the PLL-g-PEG during NP synthesis and what characteristics this imparts on the resulting NP complexes.

1.3 Identifying PLL-g-PEG Characteristics Beneficial to Protein Delivery

The first section describing experimental work, Chapter 3, focused on identifying PLL-g-PEG cationic copolymer characteristics that are likely to be favorable for the delivery of proteins [9]. A library of PLL-g-PEG copolymers with varying structural characteristics, such as PLL molecular weight and PEG grafting ratio, were synthesized to better understand what aspects of cationic copolymers significantly impact protein delivery. In this section of the work, Chapter 3 (Figure 1.2.), our group encapsulated a model protein, bovine serum albumin (BSA), to better understand how properties of the copolymer materials impact delivery characteristics of the encapsulated protein. A broad range of PLL molecular weights

were grafted with 2 and 5 kDa PEG at different ratios to both encapsulate the protein into nanoscale complexes and to also enable the future planned multi-functionalization of the NP complexes with targeting and cell internalization ligands. Ligand functionalization and cell delivery will be discussed further in later sections of the *Introduction* and in subsequent chapters. BSA was used as a model protein for these studies, due to its availability and high degree of similarity in isoelectric point and molecular weight to recombinant BChE (BSA: pI; 4.7, MW; 66.5 kDA; BChE: pI; 5.0, $MW_{monomer}$; 85 kDa), a protein of much more significant interest in improving its delivery [30, 33-35]. Our group found that minor alterations in PLL-g-PEG material properties, such as polymer molecular weight, could impart unique characteristics to the PLL-g-PEG/BSA NP complex, such as variation in protein-copolymer association and resistance to NP complex instability. Additionally, while BSA could not be released from the NP complex, the protein retained activity toward a small molecule substrate.

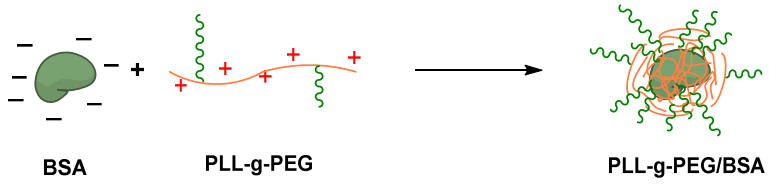

Figure 1.2. Chapter 3: Effect of cationic grafted copolymer structure on the encapsulation of bovine serum albumin.

Forming NP complexes with BSA and cationic copolymers aimed to serve as a guide for forming similar complexes with BChE. BChE is an enzyme of great interest in defense and anti-terrorism applications, due to its ability to bind and scavenge organophosphate type toxicants that compose several types of chemical weapons [33]. Recombinant BChE has the potential to be economically produced compared to native forms of the enzyme, but is

cleared from blood circulation too quickly to provide protection against organophosphate poisoning for prolonged periods of time [33]. We were part of a collaborative team that found BChE formed NP complexes with PLL-g-PEG, which also retained significant enzyme activity, organophosphate binding, and resistance to proteolysis [36, 37]. With the ability to form PLL-g-PEG/BChE NP complexes encapsulating functional enzyme, our groups proceeded to functionalize BSA and BChE NP complexes with CPPs and targeting ligands to attempt to impart the ability bind and enter red blood cells.

1.4 Ligand Functionalization and Cell Penetrating Peptides

One approach that has been shown to improve cellular binding of polyion NPs is the use of targeting ligands to bind to cell-specific molecular features on the cell surface [38]. Our group took a similar approach to functionalize our NPs, using two ligands to aid NP binding and internalization. The first ligand was a 2 kDa, peptide called ERY1, which was developed by Kontos et al. [39]. ERY1 binds to Glycophorin A, an abundant protein on red blood cells (RBCs) [39]. Using RBCs or RBC-like materials as carriers can potentially improve the circulation characteristics of proteins or NPs, which naturally circulate for long periods of time [40]. ERY1 has been used to transport proteins and nanoparticles to RBCs, while having minimal impact on RBC function [41, 42]. Our group developed NPs that have been functionalized with ERY1 that were able to bind to RBCs *in vitro* and in a model system of simulating RBCs under flowing conditions [43, 44]. The second ligand that was used to functionalize NP complexes is another 2 kDa peptide called low molecular weight protamine (LMWP). LMWP is a highly cationic cell-penetrating peptide (CPP) that was developed by Park et al. for transporting siRNA and protein cargos into several cell types, including RBCs [45-48]. CPPs, as their name suggests, are peptides with the ability to

traverse the cell membrane. Our group aimed to similarly use the LMWP CPP to deliver NPs into RBCs. Due to our group's interest in utilizing CPPs and the wide applicability of these peptides to deliver therapeutic cargos, we briefly reviewed CPPs from their discovery to their recent applications, which is found in Chapter 2 of this work [49]. Although CPPs are not the primary focus of this work, our group's efforts to apply them toward improving the NPs our group produced made a review on the subject beneficial. While reviewing CPPs, it was found that most work investigating CPPs focused on their transport through cells or their application, but the interactions of CPP-functionalized NPs with proteins in the biological environment in their route to delivery have received considerably less attention. As little exploration on the interactions that serum proteins with CPP-functionalized NPs had been done, another portion of this work aimed to combine aspects of what is known about the protein corona of NPs in order to learn more about utilizing CPPs for NP delivery.

1.5 Nanoparticles and the Protein Corona

Recently, Cedervall et al. discovered that NPs placed in a biological medium become surrounded by a halo of proteins, also known as a "protein corona" [50, 51]. The protein corona is akin to the Vroman effect, in which surfaces that come into contact with plasma become coated with proteins [52, 53]. This protein corona is highly important as the corona confers a new biological identity to NPs, altering how NPs interact with cells and other components of the biological environment [54-56]. For example, NP clearance by macrophages and half-life in circulation have been correlated to individual corona proteins of polystyrene NPs [57]. Tenzer et al. also found that factors, such as thrombocyte activation, hemolysis, and endothelial cell death can all be induced by protein corona formation on polystyrene and silica NPs [58]. These studies, along with several others, demonstrate that

the protein corona confers a new biological surface to NPs that may significantly impact how the NPs interact with cells [59-61]. Therefore, in order to design novel biomaterials and nanodevices intended for therapeutic delivery, characterizing the protein corona is an important factor for using materials that will ultimately perform best *in vivo* [58, 62].

1.6 Proteins of the Nanoparticle Protein Corona

Characterizing what types of individual and groups of proteins bind to NPs is one key part to understanding the corona composition and predict biological outcomes from protein binding. There are over 3,700 proteins in the plasma, each of which could compose part of a NP protein corona [63]. Some of the most common proteins observed on almost all studied NPs are also some of the most abundant proteins in plasma, such as albumin, IgG, and fibrinogen [64]. These and other groups of proteins that bind and coat the NP can each influence how NPs interact with cells [53]. For example, NPs that primarily bind groups of proteins called dysopsonins, proteins inhibitory to cellular uptake, could often be expected to aid the NPs persistence in circulation [64]. Some commonly observed typical dysopsonins found to bind to NPs include albumin and apolipoproteins [64]. Others have observed opsonins, such as complement proteins C3, C4, C5, and IgG, in the NP protein corona, which increases cellular uptake [65, 66]. Due to the large number of effects that different proteins may have on NP delivery, characterizing which proteins bind to different types of NPs is an important part to more accurately predicting how successful NPs will be at delivery.

1.7 Nanoparticle Binding and Uptake with the Protein Corona

The protein corona has been found to be critically important in NP-cellular interactions, such as cell binding and uptake. For example, it has been found that the protein

corona adversely affects NPs that have been functionalized with targeting ligands, reducing the ability of ligands to target NPs to specific cell types [67, 68]. The protein corona also affects the cellular uptake of NPs. Caracciolo et al. found that adsorption of the protein corona around DC-DOPE-cholesterol liposomes, encapsulating DNA, strongly influenced the liposome cellular uptake mechanism, altering uptake from clatherin- to caveolae-mediated endocytosis, thereby improving transfection efficiency in the presence of serum [69]. Additionally, Ritz et al. formed protein coronas with individual proteins found as part of the protein corona of NPs and discovered that ApoA4 and ApoC3 proteins decreased cellular uptake, while ApoH increased cellular uptake [70]. These studies indicate that individual proteins within the protein corona, in addition to NP surface properties, can potentially play an important role in the cellular uptake of NPs.

The protein corona significantly impacts macrophage binding and uptake of NPs. Macrophages, particularly in the liver and spleen, are often responsible for most of the removal of nanomaterials administered *in vivo* [71]. The enrichment of certain proteins on the NP surface have been found to be closely tied with either preventing or promoting macrophage NP uptake [72]. For example, the association of the protein clusterin with PEG was found to be correlated with significantly reduced macrophage uptake [73]. Conversely, NP surface properties, such as hydrophobicity, have been found to promote corona formation which favor greater macrophage uptake [72]. In each of these cases, the type of NP surface played an important role in what type of protein corona was formed and what effect it had on macrophage uptake.

1.8 Protein Structure Within the Nanoparticle Protein Corona

Individual proteins within the NP protein corona may also act to favor or inhibit NP uptake, depending on the structural state of the protein [74]. Albumin, one of the most abundant proteins in blood, was found by multiple groups to undergo denaturation that lead to NP uptake by macrophages and other cell types [57, 60]. These structural changes were observed to be induced by cationic NPs, however, other types of NPs have also been observed to cause protein denaturation [60, 74].

Although the protein corona has been characterized for several NP systems, including gold, silica, polystyrene, and liposomes, the corona for most NPs, particularly those of polymeric gene and protein vectors such as PLL-g-PEG or those that have been functionalized with ligands, have not been extensively studied [54, 62, 75, 76]. Because of our group's interest in delivering CPP functionalized PLL-g-PEG NP to RBCs *in vivo*, another major aim of this work was to determine how albumin binding to CPP-functionalized NP complexes impacted albumin structure and if this structural change could lead to uptake of the complexes by macrophage cells, which is described in Chapter 4 (Figure 1.3).

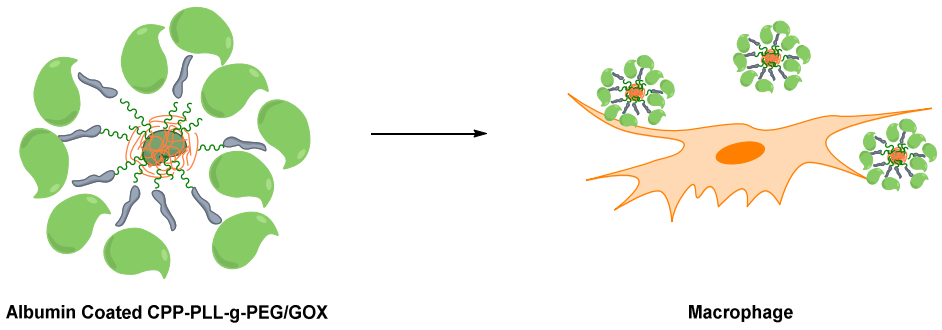

Figure 1.3. Chapter 4: Albumin Denaturation Impacts Macrophage Uptake of CPP Functionalized PLL-g-PEG/GOX Complexes.

Because most CPPs are highly charged, CPP functionalized PLL-g-PEG complexes were also expected to cause similar denaturation of albumin as that observed in the studies described earlier [57, 60]. Determining what CPP characteristics induce lower extents of albumin denaturation and therefore potentially less macrophage uptake could potentially serve to guide in the design of CPP-functionalized NP protein delivery systems.

1.9 Targeted Nanoparticle Delivery

CPPs are effective at delivering cargos into a wide variety of cells. However, this property also results in poor cell specificity. Because PLL-g-PEG NP binding to targeted cell types was also an important component to our group's efforts to deliver proteins, a ligand with greater cell specificity was needed to be able to better control the delivery of PLL-g-PEG NP complexes. Chapter 5 (Figure 1.4) describes another part of our group's efforts to demonstrate that delivery of PLL-g-PEG NP complexes can be preferentially delivered to specific cells. While much of our work has focused on attempting to improve the binding and internalization of PLL-g-PEG NP complexes to red blood cells, we also aimed to explore other applications for which these NP complexes could be used. In this section, targeted delivery of a cytotoxic protein, glucose oxidase (GOX), was delivered to cancer cells expressing prostate membrane specific antigen (PSMA). GOX catalyzes the oxidation of glucose into gluconic acid and hydrogen peroxide [77]. Hydrogen peroxide is cytotoxic due to the oxidative damage it causes to lipids, proteins, and nucleic acids within cells [78]. GOX has long been of interest as an anti-cancer agent, but localized delivery of the protein to tumors is necessary for the enzyme to be cytotoxic to tumors and not the host [79-81]. By delivering a cytotoxic protein intracellularly to PSMA-expressing cells, we demonstrate that

PLL-g-PEG NPs, encapsulating GOX and other proteins, can be selectively delivered to cells of interest.

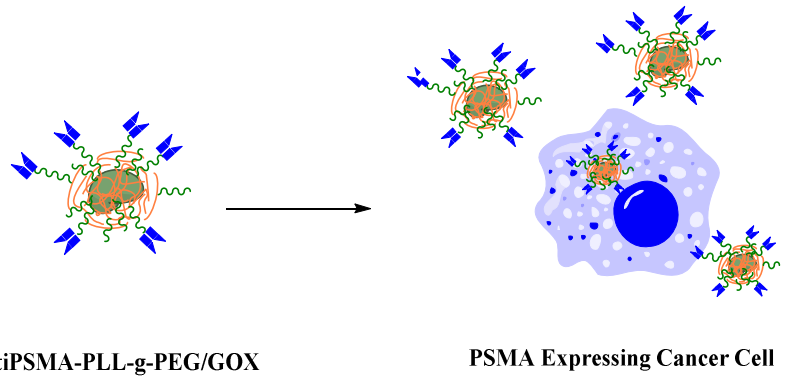

Figure 1.4. Chapter 5: Intracellular delivery of glucose oxidase for enhanced cytotoxicity to PSMA-expressing prostate cancer cells.

1.10 Summary

The overall aim of this work was to use the cationic polymers and other biomaterials to give proteins new properties that improve their delivery. We focused primarily on cationic copolymers of PLL-g-PEG, which we show are able to effectively associate with proteins and self-assemble into NP complexes. Chapter 3 of this work focuses on how structural characteristics of the copolymer impact both association of a model protein, BSA, into NPs and how this impacts several aspects of protein delivery. Upon demonstrating that proteins could be formed into NP complexes, our group proceeded to functionalize the NP complexes with CPPs to enable them to be more efficiently delivered intracellularly. Chapter 2 of this work reviews the origins and current applications of CPPs. Chapter 4 of this work investigates the role of serum albumin in the protein corona on the uptake of CPP functionalized NPs by macrophage cells. As one of the primary drawbacks of utilizing CPPs for the delivery of therapeutic cargos is poor cell specificity, Chapter 5 of this work focuses

on antibody functionalization of the NP complexes to demonstrate that specificity for particular cells can be imparted on these complexes. This work consisted of delivering the cytotoxic protein, GOX, as part of the PLL-g-PEG NP complex to PSMA-expressing prostate cancer cells. Collectively, these studies demonstrate that PLL-g-PEG NP complexes can be tuned to interact with the biological environment in many different ways and also show potential in a wide variety of protein delivery applications.

CHAPTER II

CELL-PENETRATING PEPTIDES TRANSPORT THERAPEUTICS INTO CELLS

2.1 Introduction

Cells are adept at preventing small molecules, proteins, genetic material, and larger protein complexes from entering in a nonspecific manner. The exterior of the cell is composed of a fluid phospholipid bilayer that is coated with proteoglycans. The lipid bilayer that makes up the cell membrane has a polar surface with a nonpolar interior. Together, the contrasting nature of the membrane lipid bilayer prevents most molecules from passively diffusing directly through the cell membrane. Instead, cells use a combination of ion channels and carrier proteins to transport important molecules such as ions, sugars, and amino acids across the lipid bilayer. Cells also may use endocytosis or exocytosis to transport material in bulk across the membrane.

While precise control of transport across the cell membrane is generally advantageous for the cell, many potential therapeutic drug targets are located within the interior of the cell and require entry of pharmaceutical molecules in order to be

effectively treated. This has long been a challenge in the field of gene therapy [82], where a therapeutic gene must not only be transported across the cell membrane, but must also be transported to the nucleus of the cell where it can be transcribed and translated into a therapeutic protein. Similarly, siRNA must also be transported across the cell membrane to the cell cytosol where it can act on the mRNA of the gene being silenced. Likewise, there are a growing number of intracellular targets for cancer therapy. In some cases, cancer treatment may benefit from the intracellular delivery of a particular protein, such as a cytotoxic protein or a tumor suppressor protein that is not natively expressed in an active state [83-86]. Cancer therapy may also benefit from delivery of peptides that act as inhibitors. Examples include peptides that act by preventing STAT3 from binding to DNA in tumor cells [87], peptides that inhibit angiogenesis by hindering β protein kinase C [88, 89], and peptides that induce apoptosis by disrupting the membrane of mitochondria [90, 91].

Large macromolecular drugs, such as genetic material or proteins, are often designed to be transported into target cells through either non-specific or receptor-mediated endocytosis. In contrast, many small molecule therapeutics are believed to undergo transport through some combination of passive diffusion and carrier-mediated transport. There is currently a very spirited debate on where this balance falls [92, 93]. Dobson and Kell have argued previously that carrier-mediate transport is the predominant mechanism for drug entry [94], while Sugano et al. made a case for a combination of both passive diffusion and carrier-mediate transport [95].

Regardless of how much each mechanism plays in the transport of the drug, cell entry remains a focus for those working in drug design and discovery. An exciting and

relatively new approach to transporting pharmaceutical agents into cells is making use of cell-penetrating peptides (CPPs) (recent reviews include: [96-99]). CPPs are relatively short peptides, typically less than 30 amino acids, that have been shown to be relatively nontoxic and capable of traversing the cell membrane. They are typically classified as either polycationic, amphipathic, or hydrophobic. Most importantly, they have been used to facilitate the transport of many different therapeutic agents into cells, including plasmid DNA, siRNA, therapeutic proteins, viruses, imaging agents, and other various nanoparticles.

2.2 Discovery of Cell-Penetrating Peptides

Some of the first studies that led directly to the discovery of CPPs were published in 1988. Up until that time, transport of proteins and peptides through the cell membrane was generally regarded as difficult given their large molecular weight and hydrophilicity [100]. Frankel and Pabo, however, discovered that purified *trans*-activator protein (TAT), from human immunodeficiency virus type 1 (HIV-1), was readily taken up from cell culture medium by HL3T1 cells [101]. They also showed that uptake of TAT was enhanced when chloroquine was added to the medium, suggesting that uptake was likely occurring through endocytosis. At the same time, Green and Loewenstein independently demonstrated that only a portion of the 86 amino acid TAT protein was necessary for both cellular uptake and enzymatic activity [102]. By investigating various N-terminal and C-terminal deletion mutants, Green and Loewenstein showed that TAT (37 – 57) entered cells and retained ~ 40 % of the activity of the full-length TAT protein.

Nearly 10 years after the initial discovery of the TAT peptide, even smaller TAT peptides were shown to translocate through the cell membrane. In one study, Vivès et al.

found that TAT (48 – 60) was able to enter cells and that cellular uptake of the peptide was not inhibited at 4 ºC [103], implying an alternative to the endocytic mechanism suggested earlier by the findings of Frankel and Pabo. Further, Vivès et al. were able to rule out potocytosis and caveolae-mediated endocytosis by using respective pathway inhibitors. At the same time, Vivès et al. published a second paper in which they showed that the C-terminal end of the TAT peptide could be further truncated to TAT (48 – 57) without significant loss of translocation ability [104]. Park et al. followed up this study showing that the peptide could be truncated even more to TAT (49 – 57) [105].

Around the same time as the discovery of TAT, the Prochiantz group identified a 60 amino acid region of the *Drosophila* antennapedia homeobox protein (pAntp) that was capable of penetrating differentiated neurons [106]. Joliot et al. were investigating the effects of injecting the DNA-binding peptide on nerve cell differentiation when they discovered that the peptide was able to penetrate differentiated nerve cells (i.e., without injection) and accumulate in the nucleus. While the entry mechanism was unclear, they were able to rule out internalization due to cell damage by comparing the uptake of the pAntp peptide with proteolytic fragments of fluorescent ovalbumin.

Prochiantz's group followed this initial report with a study investigating the uptake mechanism and also the minimal sequence required for cell entry [107]. Earlier studies had shown that the third α-helix of the pAntp peptide, which consists of three α-helices with a β-turn between the second and third helix, may be especially important in cell entry; there is a high degree of phylogenetic kinship in the third α-helix and studies showed that internalization of the peptide was especially sensitive to mutations in this region [108]. Derossi et al. went on to show that truncation of the third α-helix by

deletion of the C-terminal glutamate produced a 16 amino acid peptide capable of translocating through cell membranes [107]. Further, they were able to show that entry of the peptide was not limited to neuronal cells nor was it dependent on binding a specific transporter. Once again, the mode of cell entry was not clear, but this time Prochiantz's group demonstrated that internalization was energy-independent, occurring at 4 °C and avoiding the endolysosomal uptake pathway.

Hundreds of additional CPPs have been discovered in the two decades that have passed since the discovery of TAT and the pAntp peptide. Table 2.1 provides a short list of some of these peptides, their source, peptide sequence, and examples of the cargo they have been used to transport. CPPs are typically classified by either their physical-chemical properties or by their origin. The peptides listing in Table 2.1 have been grouped based on their physical-chemical properties: cationic, amphipathic, or hydrophobic.

Table 2.1. Examples of some common cell-penetrating peptides and their applications.

Name	Source	Sequence	Cargo	References
		Cationic Peptides		
TAT (48–60)	HIV TAT Protein	GRKKRRQRRRPPQ	Gene Vectors, Proteins, Peptides, Label	[109-111]
Penetratin	Antennapedia	RQIKIWFQNRRMKWKK	Gene Vectors, Proteins, Peptides, Label	[112-116]
Polyarginine	Synthetic	$RRRR_n$	Gene Vectors,	[117-120]

			Liposome, Label	
Oct4	Oct4 Protein	DVVRVWFCNRRQKGKR	Protein, Label	[121]
WT1-pTj	Wilms Tumor Protein 1	KDCERRFSRSDQLKRHQR RHTGVKPFQ	Label	[122]
DPV3	Heparin Binding Protein	RKKRRRESRKKRRRES	Proteins	[123]
Amphipathic Peptides				
Transportan	Galanin and Mastoparan	GWTLNSAGYLLGKINLKA LAALAKKIL	Gene Vector, Label	[124, 125]
MAP	Synthetic	KLALKLALKALKAALKLA	Label	[126]
VP22	Herpes Virus Structural Protein	DAATATRGRSAASRPTER PRAPARSASRPRRPVE	Proteins	[127-129]
Pep1	SV 40 NLS and a hydrophobic domain	KETWWETWWTEWSQPK KKRKV	Proteins, Gene Vectors	[114, 130, 131]
KW	Synthetic	KRKRWHW	Small Molecule	[132]
Hydrophobic Peptides				
KFGF	Kaposi Fibroblast Growth Factor	AAVLLPVLLAAP	Peptides, Antibodies	[133, 134]
FGF12	Fibroblast Growth Factor 12	PIEVCMYREP	Proteins	[135, 136]
Integrin β3 Peptide	Integrin β3	VTVLALGALAGVGVG	Used for Peptide Sequence Function	[137]

			Studies	
C105Y	α1-Antitrypsin	PFVYLI	Gene Vector, Peptide, Liposome	[138-140]
TP2	Synthetic	PLIYLRLLRGQF	Label	[141, 142]

Similar to TAT and the pAntp peptide, many of the CPPs were derived from natural proteins or peptides, including viral proteins, heparin-binding proteins, DNA/RNA-binding proteins, homeoproteins, signal peptides, and antimicrobial peptides. The VP22 peptide, for example, was derived from a herpes virus structural protein [127]. The origin of DPV3 was a heparin binding protein [123]. TAT, which comes from the HIV-1 virus, was derived from the RNA-binding, *trans*-activator protein. The origin of the pAntp peptide was a homeoprotein, which is a class of DNA-binding proteins. K-FGF was derived from the signal peptide in Kaposi's sarcoma fibroblast growth factor [133], and while none are included in Table 2.1, there are many known CPPs that were derived from antimicrobial peptides such as Bac7, buforin 2, tachyplesin and melittin [143-146].

Some CPPs are derived from a combination of natural proteins or peptides and are referred to as chimeric. Transportan and Pep1 are two peptides listed in Table 1 that are chimeric. Transportan was produced by combining the neuropeptide galanin and the wasp venom peptide mastoparan [124]. A common approach with chimeric CPPs has been to combine signal peptides with NLS peptides. Pep1 is a result of this approach, where a tryptophan-rich hydrophobic domain that associates with cell membranes has been fused to a SV40 NLS peptide [130]. MPG is another chimeric peptide produced

using this approach. MPG combines the SV40 NLS peptide with a signal peptide taken from HIV glycoprotein 41 [147].

Synthetic peptides are the final classification group based on the origin of the CPP. Model amphipathic peptide (MAP) and polyarginine are both listed in Table 2.1 and were two of the first synthetic peptides developed. These early synthetic peptides were designed to mimic CPPs based on natural proteins. For example, polyarginine was investigated for its cell-penetrating ability because of its similarity to TAT, which also has a large number of arginine residues [118, 120]. MAP was meant to be a model peptide that had amphipathic alpha helical secondary structure, which could be used to study if unique structural features were necessary for membrane passage, as was thought to be the case with the pAntp peptide [148]. Since the discovery of these two synthetic peptides, and many more like them, molecular cloning techniques and screening tools such as phage display have enabled high-throughput screening of large peptide libraries. These libraries have yielded additional synthetic CPPs that, unlike polyarginine and MAP, tend to be more hydrophobic and lack amphipathic structure [149].

Lastly, there has been recent interest in developing non-peptide mimics of CPPs. These mimics of CPPs are typically built upon polymer backbones. By modifying the polymer side chains an array of polymers have been synthesized that show robust transduction of cells. While these non-peptide mimics of CPPs are not the focus of this paper, the interested reader is referred to a recent review on the subject [150].

2.3 Mechanism of Cellular Entry

From the beginning there has been considerable interest in exactly how CPPs enter cells. The mechanisms are still not entirely understood, but what we are beginning to

recognize is that the mechanisms by which CPPs enter cells seems dependent on not only the type of CPP but also its concentration [151], the cargo that it transports, and the cell line on which it is being tested. Arriving at this understanding has not been easy, as early studies provided contradictory findings. As described above, Frankel and Pabo (1988) found that chloroquine enhanced the uptake of Tat peptide, implying that an endocytic mechanism was likely [109]. Vives, Brodin, and Lebleu (1997), however, showed that the uptake of TAT occurred at 4 °C, which implied that endocytosis was unlikely [103]. In addition, the Prochiantz group showed that pAntp was also able to enter cells at 4°C , thereby lending further evidence to an energy-independent, non-endosomal uptake mechanism for CPPs [107]. The concern with these studies, and many other early studies, was that they predominantly relied on fluorescence microscopy of fixed cells or flow cytometry to measure uptake of CPPs. In 2002, it was shown that fixation of cells could lead to artifactual redistribution of peptides that had otherwise simply been bound to the cell membrane [152, 153]. Both of these studies also showed that despite extensive washing, cationic CPPs remained bound to the cell membrane, which could erroneously lead one to conclude from flow cytometry that the CPPs had been internalized. Taking into account the issues with flow cytometry and cell fixation, Richard et al. (2003) were able to show that the uptake of the TAT peptide is indeed inhibited at 4 °C. Endosomal distribution and the kinetics of uptake also helped confirm that TAT, under the conditions described in the study, was internalized in an endocytic manner.

Figure 2.1 summarizes the different routes by which a CPP might enter a cell. While direct translocation across the cell membrane occurs in some cases, it is generally

accepted that most CPPs and CPP-cargo complexes enter cells through endocytosis, including macropinocytosis, clathrin-mediated endocytosis, and caveolae/lipid raft-mediated endocytosis. Some CPPs have been shown to use more than one of these internalization routes and to sometimes use different routes simultaneously. Investigations into the TAT peptide, for example, have shown that TAT is internalized through macropinocytosis [154], clathrin-mediated endocytosis [155], and caveolae-mediated endocytosis [156].

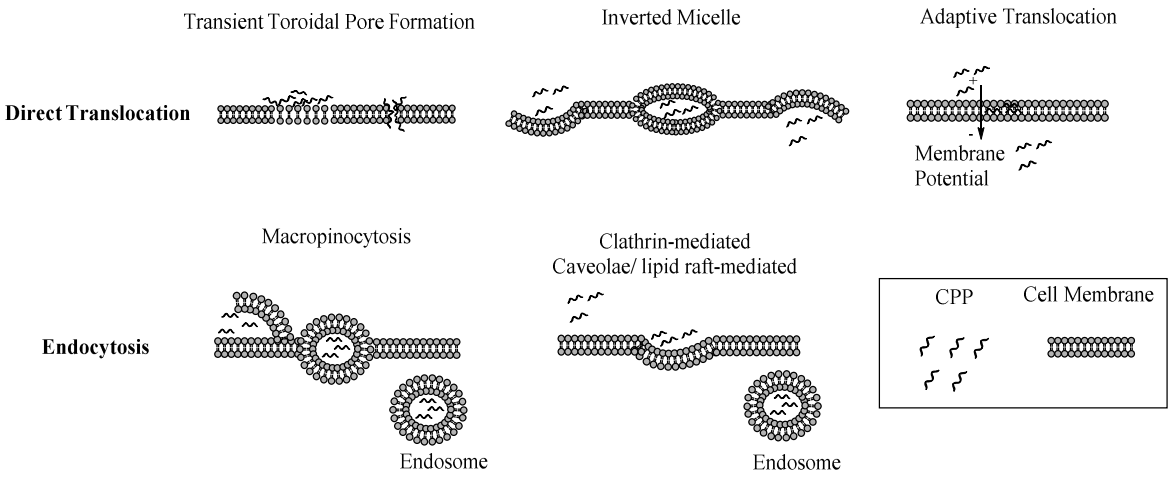

Figure 2.1. Proposed mechanisms for cellular entry of cell-penetrating peptides.

In spite of some of the early errors assessing cellular entry, CPPs have been shown to directly penetrate the cell membrane in a non-endocytic manner, especially at high concentrations of the peptide [157, 158]. Many different models have been proposed to explain this observation, a few of which include inverted micelles, transient toroidal pores, and adaptive translocation.

Derossi et al. were the first to suggest CPPs may be entering through an inverted micelle [159]. They hypothesized that the pAntp was entering cells through either an

inverted micelle or through fluid phase pinocytosis. The authors went on to provide ample justification for the inverted micelle model, including an explanation that substitution of the CPP tryptophan residues, which are known to induce formation of inverted micelles, abolished cell penetration.

The formation of transient toroidal pores, similar to the carpet model [160], has also been suggested as a possible mechanism for direct translocation. Molecular dynamics simulations of the TAT peptide interacting with a lipid bilayer showed that at high concentrations of the TAT peptide transient pores could form in the membrane [161]. The model showed that attraction of the TAT peptide with the phospholipid head groups on both the outer and inner lipid leaflets leads to a thinning of the lipid bilayer and ultimately penetration of the membrane. The lack of observable membrane leakage has led many to discount this mechanism. The transient nature of the pores, however, combined with the cellular membrane repair response may explain why no membrane leakage or cell damage is observed [162].

Another proposed mechanism for direct translocation of the cell membrane by cationic CPPs is adaptive translocation. The idea that a hydrophilic, charged peptide could directly migrate through the hydrophobic lipid bilayer initially seems improbable. Rothbard et al., however, proposed a mechanism by which they suggested cationic peptides form transient ion pair complexes with negatively charged membrane components; the reduced, yet still positive charge associated with the ion pair complex allows the peptide to adaptively diffuse through the cell membrane, where the driving force for diffusion is the membrane potential [163]. Rothbard et al. supported their proposed model by explaining that reduced membrane potential resulted in reduced

cellular uptake of the peptide without any noticeable effect on endocytosis. Further, they showed that increased membrane potential resulted in increased cellular uptake of CPPs.

In addition to the models described here, there may be a newly discovered model that is not entirely understood. A recent study by Hirose et al. found that arginine-rich CPPs conjugated to hydrophobic small molecules directly translocated the cell membrane at sites where the peptides formed unique "particle-like" structures composed of multiple vesicles on the plasma membrane [164]. Penetration into the cell occurred through both direct translocation and endocytosis. Further, direct translocation was found to be dependent on the presence of the hydrophobic fluorescent dye Alexa488 that was attached to the peptide.

The importance of the Alexa488 in the study performed by Hirose et al. brings us back to an issue raised earlier; the mechanism used by CPPs to enter cells depends not only on the peptide but also other factors such as the size and physicochemical nature of its cargo [165]. For example, when TAT was fused to a protein, cellular uptake of the complex occurred through caveolae-mediated endocytosis [166]. When the peptide was conjugated to a fluorophore, however, uptake occurred through clathrin-mediated endocytosis [155]. Further, internalization of TAT/fusion protein complexes was largely limited to endocytosis, but TAT/small peptide complexes were internalized through both endocytosis and rapid, direct membrane translocation [167].

Understanding cellular internalization means not only studying the CPP complex as a whole, but also considering the potential limitations of the different techniques used to study internalization. One concern with many of the methods that have been used to study endocytosis of CPPs is the use of chemical inhibitors. While chemical inhibitors

can be used to help understand the role of different endocytic uptake pathways in the internalization of CPPs, they also have a substantial impact on cell viability, thereby significantly affecting cells in ways that may make interpretation of the results difficult. Additionally, the performance of chemical inhibitors can be highly dependent on the cell line used. Holm, Andaloussi, and Langel recently wrote a book chapter describing several methods (including fluorescence microscopy, HPLC, flow cytometry, spectrofluorometry, electron microscopy, and mass spectroscopy) for studying the uptake of CPPs, which can avoid the use of chemical inhibitors [168]. The authors provide a list of the advantages and drawbacks associated with the different methods and advocate for the use of more than one approach in order to avoid the negative aspects of the different methods.

2.4 Applications using Cell-Penetrating Peptides

CPPs have been used in a wide number of applications, ranging from simple cell culture transfection to the systemic delivery of therapeutics. The focus here is to highlight a few of the many instances where CPPs have been used to deliver therapeutics, specifically nucleic acids, proteins, small molecules, and imaging agents. Many of the examples of *in vivo* delivery are limited to small animals, and application of CPPs to human therapeutics has yet to prove effective. CPPs enhance the general uptake of a therapeutic but in doing so reduce the specificity. This loss of specificity is not only likely to impact efficacy but also safety. Much of the recent work has focused on using CPPs along with targeting ligands to improve delivery of a therapeutic. As approaches to improve the targeted delivery of biomolecules are combined with CPPs, therapeutics may be delivered more efficiently, thereby greatly improving treatment outcomes.

Nucleic Acid Delivery

One of the first biomedical applications of CPPs was delivery of nucleic acids into cells. As previously mentioned, large hydrophilic molecules, such as nucleic acids, are generally inefficient at passing through the cell membrane. To improve the delivery of nucleic acids, plasmid DNA has been complexed with cationic polymers or liposomes, which condense DNA into particles capable of entering cells through endocytosis. Similar to these polymeric and liposomal materials, cationic CPPs have also been used to condense plasmid DNA into small particles. One of the first studies showing this was by Morris et al., who demonstrated that CPPs could be complexed with oligonucleotides through electrostatic attraction, which resulted in improved gene delivery [147]. Soon after, Transportan and pAntp were used to deliver peptide nucleic acid (PNA) by covalently linking the CPPs to the PNA [169]. These developments spurred additional investigations into using CPPs to deliver nucleic acids. Recently, van Asbeck et al. sought to better understand what physicochemical and molecular factors most influence the successful delivery of CPP/siRNA complexes [170]. The authors discovered that CPP/siRNA complexes with the most negative zeta-potentials in serum were the most resistant to siRNA release over a 20 hour incubation period compared to less negatively charged complexes. They also found that the zeta-potential of CPP/siRNA complexes in serum did not correlate with improved cellular association, which they explained could demonstrate the importance of serum proteins or CPP conformation on the ability of CPP/siRNA complexes to associate with the cell membrane.

CPPs have also been coupled recently to other molecules to improve gene delivery after entry into the cell. Favaro et al., for example, investigated combining TAT with a

fusion protein partially composed of the intracellular transport protein dynein light chain Rp3 for improving DNA delivery to the nucleus [171]. They found that using the CPP and the transport protein improved gene delivery by more than 7-fold compared to the transport protein alone. Similarly, Lindberg et al. functionalized CPPs to not only penetrate the cell membrane but to also facilitate better intracellular trafficking by disrupting endolysosomes [172]. They delivered anti-microRNA oligonucleotides into cells by combining the endosomolytic agent trifluoromethylquinoline to the PepFect14 CPP, producing a new CPP that the authors named PepFect15. Compared to the PepFect14 complexes, PepFect15 produced a one-fold improvement in anti-microRNA delivery at the optimum CPP:oligonucleotide molar ratio.

CPPs have been used also to enhance existing synthetic gene vectors *in vivo*. Hayashi et al. demonstrated that polyarginine functionalized lipoplexes efficiently silenced genes in a mouse liver [173]. An interesting and unexpected finding in subsequent work was that CPPs seemed to improve the long-term gene expression from vectors that normally only provide for very transient gene expression. One example of this was a TAT-PEI vector that extended the gene expression period from about 1 month to nearly 7 months compared to TAT or PEI alone [174]. Another demonstration of this effect by Yamano et al., showed that a TAT-modified liposome could be used to deliver a reporter gene with reasonable levels of expression for up to 7 months [175].

One of the main limitations of gene vectors utilizing CPPs is low cell specificity. A popular approach for improving synthetic gene vectors has been to incorporate targeting ligands with CPPs to better control cell-specific attachment. Interestingly, synergism between the CPP and the targeting ligand has often been observed. In a recent study,

Fang et al. found that the coupling of a vascular endothelial growth factor receptor-1 targeting peptide to TAT internalized siRNA into cancer cells more readily than the CPP alone [176]. Improved and/or more selective gene delivery has also been reported with targeting ligands, such as mannose, folate, and RGD [177-179]. The same approach has also been applied to the delivery of siRNA using folate and penetratin [180]. The authors suggested that the multiple ligand approach increased the avidity for their siRNA nanoparticles toward folate expressing cancer cells.

Interestingly, CPPs have also been demonstrated to transport nucleic acids to poorly accessible tissues such as the skin and brain. Recently, Chen et al. used the SPACE peptide to deliver siRNA encapsulated in liposomes topically to the skin [181]. Other hard to reach tissues, such as the brain, have also become more accessible to therapeutics because of CPPs. TAT-functionalized micelles were used to deliver a dual formulation of siRNA and camptothecin to a glioma through the nasal cavity in mice [182]. Similarly, a polyarginine CPP and a transferrin targeting ligand improved delivery of plasmid DNA encapsulated in a liposome to the brain [117].

In addition to synthetic vectors, CPPs have been used also to improve viral gene delivery vectors. Viral vectors are typically only efficient at gene delivery to cells that have the receptors that a virus needs for cell attachment and entry. CPPs have been combined with viral vectors, however, to widen the range of cell types that viral vectors are able to infect. By forming complexes through electrostatic attraction, several types of CPPs were found to improve the infectivity of an adenovirus gene vector, including cells poorly permissive to infection [114, 183]. Similarly, the ability of adeno-associated virus and baculovirus to deliver genes has also been improved using CPPs [184, 185].

Together, these studies demonstrate that viral vectors can be modified to deliver genes to a much wider range of targets, including various cancers and stem cells. In one study, TAT was shown to increase the infectivity of an oncolytic adenovirus, which led to improved survival of tumor bearing mice [186]. Park et al. recently investigated the effects of oligomeric CPPs on adenoviral gene delivery to transduce stem cells [187]. They found that tetramers of CPPs were better than CPP monomer at delivering adenovirus to mesenchymal stem cells.

Some CPPs have been proven also to be effective antimicrobials and capable of penetrating into other types of non-mammalian cells. With the prevalence of multidrug resistant bacteria, the development of peptides to either act as antimicrobials or to deliver antimicrobial agents is an area of growing interest. Bai et al. and Rajasekaran et al. delivered PNA into gram-negative bacteria, as well as intracellular bacteria strains using CPPs [188, 189]. Both CPP-PNA constructs inhibited microbial growth, demonstrating that gene silencing can be an effective approach to control bacteria. Although many antimicrobial CPPs have been discovered, the mechanism behind their broad penetration ability remains an area of active investigation. In one recent study, Rodriguez et al. found that the membrane potential is a key factor for cell entry of the model antimicrobial peptide Iztli-1 [190]. This provides a basis for further studies to understand why many CPPs can also act as antimicrobial peptides.

Peptides, Proteins, and Enzymes

As with gene delivery, proteins are typically unable to passively enter cells. Because many therapeutic targets are inside of cells, CPPs provide an ideal means for

intracellular delivery of the growing number of pharmaceutically relevant proteins [191]. Early studies on the *in vivo* behavior of CPP conjugates of β-galactosidase coupled to TAT demonstrated that CPPs can facilitate the delivery of proteins into most cell types [192]. These prior successes have been built upon recently with CPPs transporting proteins into cells for treating specific diseases. TAT has been used to deliver the herpes virus E2 protein to induce apoptosis in cervical cancer cells [193]. In another strategy to treat cancer, a polyarginine CPP was coupled with a tumor suppressing p53 protein to inhibit the growth of bladder cancer cells [194]. An interesting approach to build upon transporting anti-cancer proteins has been to use the tumor environment to modulate the function of CPPs, where by controlling the activity of the CPP, more cancer suppressing protein can be delivered to tumors. Fei et al., for example, constructed a CPP that would be active in the acidic environment of tumor tissue by linking the MAP CPP to a pH-sensitive peptide [195]. This approach improved the delivery of glutathione S-transferase to tumor cells in mice while reducing delivery of the protein to other tissues.

CPPs have also been incorporated into gene editing strategies for treat disease. Specifically, CPPs are being used to deliver endonucleases into cells as an approach to remove disease-causing genes. In one recent study, a CPP was used to deliver the Cas9 protein and guide RNA for RNA-guided endonuclease gene editing [196]. Using this method, gene disruption was observed in several cell types. In another study, Liu et al. used polyarginine to transport transcriptor activator-like effector endonuclease (TALEN) protein into cells [197]. The authors showed that the TALEN protein was able to specifically disrupt CCR5 and BMPR1A genes.

As described in several earlier examples, CPPs make it possible to transport enzymes into cells, which can lead to treatments for a wide range of diseases. Enzymes that prevent oxidative damage are just one of several types of enzymes that are of interest for intracellular delivery, which can lead to preventative treatments against ischemic injury. For example, TAT was combined with an enzyme called glyoxalase to prevent oxidative damage of neuronal cells [198]. In another example, antioxidant enzymes catalase and superoxide dismutase were delivered into cells using TAT, which protected the cells from oxidative stress [199, 200]. In an interesting approach to develop a long duration treatment for acute lymphoblastic leukemia, CPPs were used to deliver enzyme into red blood cells [48]. The enzyme L-asparaginase was delivered into functional red blood cells using the LMWP CPP. This offers an innovative strategy to improve the circulation characteristics of proteins and many other types of molecules.

CPPs have been used in several protein delivery applications in which the target cell type was non-mammalian, such as bacteria, fungus, and protozoa. The few brief examples presented here demonstrate the broad penetrating ability of CPPs through cell membranes much different than that used to move proteins into human or mammal cells. Marchione et al., for example, demonstrated that the ZEBRA peptide CPP was able to deliver a green fluorescent protein into a pathogenic fungus [201]. This demonstrates the possibility that other types of protein therapeutics may be delivered into fungal cells. Keller et al. used several different types of CPPs to compare the ability of the CPP to deliver a protein (BSA or β Galactosidase) into a protozoa [202]. The authors noted that this approach could lead to new strategies to study protozoa and inhibit their growth. CPPs have also been used to deliver molecules into other animal cell types, which can

serve as important tools for advancing science as well as benefitting human health. For example, Ma et al. used CPPs to deliver antigens into antigen presenting cells to provide fish immunity against bacterial infection [203], showing that CPPs can be an effective component in the formulation of novel vaccines.

Small Molecules

Similar to the large biomolecules discussed earlier, small hydrophilic molecules can also face difficulties in traversing the hydrophobic cell membrane. In addition, conditions such as cancer, can also prevent effective transport of small molecules across the lipid bilayer. CPPs have been shown to be a practical approach in improving the delivery of small-molecule cytotoxic drugs into cancer cells, while reducing the exposure of non-diseased tissues. In one study, doxorubicin was coupled with polyarginine and found to inhibit tumor growth *in vivo* with fewer side effects compared to doxorubicin alone [204]. The authors noted that the cause behind the accumulation of the drug in the tumor was likely improved by the interaction of the cationic CPP with glycosaminoglycans. Cai et al. used the hydrophobic PFV CPP to increase the delivery of a stealth liposome loaded with doxorubicin into cancer cells [140]. An interesting result in this study was that the hydrophobic CPP modified liposomes caused a reduction in tumor volume and resulted in fewer side effects compared to an unmodified liposome.

Other strategies to improve small molecule drug delivery have focused on introducing new functionalities to CPPs for greater intracellular control of CPP/drug conjugates. Lelle et al. investigated a CPP that was cross-linked with doxorubicin using a reducible disulfide linker [205]. The CPP conjugates were found to be cytotoxic toward

cancer cells with release of the doxorubicin into the cell cytosol. Nasrolahi et al. studied the anticancer activity of doxorubicin conjugated to a CPP in drug resistant cancer cells [206]. The authors observed more antiproliferative activity from the doxorubicin conjugated to the cyclic $W(RW)_4$ CPP compared to the linear $(RW)_4$ CPP. Additionally, they found that the cyclic CPP doxorubicin conjugate had improved trafficking to the nucleus and reduced cellular efflux compared to free doxorubicin.

Other types of small molecules have been delivered by CPPs as part of novel technologies ranging from neutron capture cancer therapy to methods for developing new cell preservation protocols. Although the examples presented here are broad, they show that CPPs have wide utility beyond the delivery of well-studied molecules. As part of an innovative cancer treatment, a CPP attached to a boron compound was delivered into malignant glioma cells for boron neutron capture cancer therapy [207]. The CPP combined with the boron compound was found to improve the killing of cancer cells compared to the boron compound without peptide. CPPs are also being used as part of innovative strategies to preserve cells without cryopreservation. The preservation agent trehalose was delivered into cells using a newly developed CPP, KRKRWHW, with the overall intent to investigate alternative cell preservation by desiccation [132]. The authors demonstrate that the novel CPP enters cells and that the inclusion of the preservation agent is non-toxic. Another example of delivery of a small molecule using CPPs is the conjugation of the Tat CPP to a fluorescent label to photosensitize intracellular vesicles [208]. The label was further used as part of a strategy to damage the lipid membrane upon excitation of the label.

Novel chemotherapy approaches have focused on targeting the activity of anticancer drug-CPP conjugates to tumor tissue. One approach that is growing in popularity is to make the CPP functional only when an enzyme common to the extracellular environment of tumors is present. Olson et al. demonstrated this with a CPP connected to an anionic polyion by a tumor matrix metalloproteinase cleavable linker, allowing the CPP to be activated in tumor tissue [209]. Xia et al. used this strategy to deliver paclitaxel with an activatable LMWP (ALMWP), protected by a polyanionic peptide that would only become active by tumor metalloproteinases removing the polyanion [210]. Another approach to producing activatable CPPs has been to use the acidity of the tumor environment to control the peptide activity. Jin et al. made TAT inactive by converting the lysine amino groups of peptide to succinyl amides [211]. The group found that the acidity of tumor tissue can convert the modified peptide back to the active form of TAT, which caused better accumulation of peptide to the tumor.

Imaging

Imaging is of growing importance in the detection and monitoring of disease markers, which can lead to more effective disease management. CPPs have been coupled with fluorophores, contrast agents, quantum dots, and other readily detectable molecules for visualizing the intracellular environment as well as specific cells. In fact, fluorophores were one of the earliest cargos conjugated to CPPs as a means to study their activity. Since then, CPPs have become important tools in biology for delivering fluorophores and quantum dots for intracellular detection. Earlier studies, such as that by Delehanty et al., demonstrated that quantum dots could be transported across the lipid bilayer using polyarginine [212]. Subsequent work has utilized CPPs to deliver

fluorescent agents into cells for targeted intracellular delivery, which has also proven to be especially useful in cell biology. Liu et al. was recently able to use the HR9 peptide to deliver quantum dots into cells without delivery to a lysosome or other organelles [213]. In other cell biology applications, oxygen sensitive probes have been coupled to CPPs [214]. Using these probes allowed for the study of oxygen use inside cells. New fluorescence strategies using CPPs have also been developed for better diagnosis of diseases over-expressing certain intracellular markers, such as the ubiquitin E3 ligase Smurf1 [215]. Researchers were able to observe Smurf1 binding through a CPP bearing a FITC label, a black hole quencher, and a Smurf1 binding peptide. Changes in peptide confirmation with binding allowed for the group to observe the peptide and protein binding.

CPPs have been designed to activate in certain tissue environments, and this has led to several exciting imaging applications. For example, there is great interest in developing CPPs that will activate in tumors, which can in turn improve the detection of cancer cells and allow for real time imaging so that tumors may be removed more effectively. CPP fluorophore conjugates have been designed to become active in tumors through an anionic domain that may be removed by tumor matrix metalloproteinases, effectively labeling tumor cells [216]. Efforts to better detect cancer metastasis through MRI and to improve the surgical removal of cancer have used activatable CPPs with fluorescent labels and gadolinium. [217, 218]. In another approach, an activatable CPP allowed for Savariar et al. to detect tumors *in vivo* [219]. In this study, a tumor specific protease disrupts the quenching of a label when the CPP is activated, which results in ratiometric detection of tumor metastasis. This approach has also been used for detection

of thrombin activation in which a CPP was made active by thrombin, allowing the CPP to be internalized in nearby cells, which can lead to better treatment of atherosclerosis and strokes [220]. Another exciting approach has been the development of chemically sensitive linkers to produce other novel activatable CPPs. This has led to new possibilities of detecting chemicals through imaging. For example, Weinstain et al., developed a hydrogen peroxide activatable CPP to observe inflammation in the lungs of mice using FRET [221]. This enabled the group to detect oxidative stress both *in vitro* and *in vivo*, which has the potential to be a useful tool to monitor several types of diseases.

2.5 Conclusions

CPPs offer an exciting potential to transport many different types of therapeutic drugs across the cell membrane and into cellular compartments or the cell cytoplasm where a drug can be most effective. While we do not entirely understand, nor can we necessarily predict how a CPP and its cargo will be transported into cells, we are developing the tools and knowledge necessary to harness their ability. Already, there are hundreds of CPPs being explored for the delivery of therapeutic small molecules, peptides, proteins, nucleic acids, and imaging agents. These studies are demonstrating success both *in vitro* and *in vivo*. Successful transition from the laboratory setting to the clinic is only a matter of time.

Acknowledgements: This work was partially supported by the Defense Threat Reduction Agency (DTRA) under Award Number HDTRA1-13-1-0021. This chapter was previously published as: Ramsey, J.D. and N.H. Flynn, *Cell-penetrating peptides transport therapeutics into cells.* Pharmacology & therapeutics, 2015. **154**: p. 78-86.

CHAPTER III

EFFECT OF CATIONIC GRAFTED COPOLYMER STRUCTURE ON THE ENCAPSULATION OF BOVINE SERUM ALBUMIN

3.1 Introduction

One of the most promising methods to improve the controlled delivery of proteins is nano-encapsulation within biocompatible polymers. Although many methods of encapsulating proteins and biomolecules have been discovered, encapsulation using electrostatic interactions is one of the most practical. Encapsulation using electrostatics avoids the use of harsh solvents or direct modification of the protein, which are common with other protein encapsulation techniques and may lead to decreased protein function [222]. The formation of polyion complexes from oppositely charged polymers has been studied extensively, especially for gene delivery [20, 223-225]. In particular, cationic block copolymers of poly-L-lysine (PLL) and polyethylene glycol (PEG) have been widely studied as gene delivery vectors. PLL is a cationic polymer that has been used in many applications in which the polymer associates with negatively charged surfaces and molecules including nucleic acids and proteins [20, 226, 227]. PEG is another widely used polymer which has been found to improve the circulation characteristics and

biocompatibility of many materials introduced *in vivo* [12]. Proteins and other particles coated with PEG are generally less immunogenic, less prone to renal clearance, and more resistant to proteolysis [228]. Additionally, coupling PEG onto cationic polymers has been found to reduce the susceptibility of the resulting complex to aggregation [223, 229]. Charged polymers and copolymers have also found growing applicability in encapsulation of protein-based therapeutics [21, 226, 230-233], where protein polyion complexation has already been demonstrated to be an effective method to encapsulate proteins [27, 231, 234-240]. Additionally, several enzymes complexed with polyions have been shown to retain catalytic activity following encapsulation [231, 234, 241, 242].

Although the characteristics of charged block copolymers that lead to encapsulation of proteins into micelles have been well studied, there have been relatively few investigations into what design parameters are important for the encapsulation of proteins by charged grafted copolymers. The purpose of the present work was to investigate how variations in grafted cationic copolymer architecture affect protein encapsulation and stability. First, nine different PLL-g-PEG copolymers were synthesized to investigate the effect of PEG:PLL grafting ratio and PLL molecular weight on protein encapsulation. Using BSA as a model protein, we saw that the properties of the copolymer affected protein encapsulation and nanoparticle stability while having no detrimental impact on protein function. Moreover, the protein remained functional toward small molecules as a NP, demonstrating that release of the protein was not necessary for protein-small molecule interactions. Together, the results of this study provide insight into how grafted copolymer architecture affects the properties of self-assembled protein

NPs and guides improvements toward the use of grafted cationic copolymers for protein delivery.

3.2 Materials and Methods

Bovine serum albumin (BSA), poly-L-lysine-HBr (PLL) with molecular weights 4-15 kDa, 15-30 kDa, and 30-70 kDa, p-nitrophenyl caprylate, and chymotrypsin from bovine pancreas were purchased from Sigma Aldrich (St. Louis, MO). Polyethylene glycol with 2 and 5 kDa molecular weights and functionalized with a carboxymethyl succinimidyl ester (mPEG-NHS) were purchased from Creative PEGworks. Glutaraldehyde (50% (w/w)), acrylamide/bisacrylamide (37.5:1) and other polyacrylamide gel casting and running materials were purchased from Fisher Scientific (Pittsburgh, PA). DQ Green BSA was purchased from Life Technologies (Grand Island, NY).

3.2.1 PLL-g-PEG Grafted Copolymer Synthesis

PLL-g-PEG was synthesized using the succinimidyl ester leaving group on the PEG to conjugate to the primary amine groups of the PLL. Various masses of 2 kDa and 5 kDa mPEG-NHS (a 50/50 mixture (w/w)) were added to 15 mg of 4-15, 15-30, and 30-70 kDa PLL-HBr dissolved in 200 µL of phosphate buffered saline (PBS). The amounts of PEG required to form each copolymer were pre-determined experimentally by trial and error (data not shown). For 4-15 kDa PLL (defined as “low molecular weight”), 28, 40, and 48 mg of a 50/50 (w/w) mixture of 2 and 5 kDa PEG were added to the dissolved PLL to produce the grafting ratios 2, 10, and 20, respectively. For 15-30 kDa PLL (defined as “medium molecular weight”), 4, 40, and 48 mg of a 50/50 (w/w) mixture of 2

and 5 kDa PEG were added to the dissolved PLL to produce the grafting ratios 2, 10, and 20. For 30-70 kDa PLL (defined as “high molecular weight”), 2, 10, and 18 mg of a 50/50 (w/w) mixture of 2 and 5 kDa PEG were added to the dissolved PLL to produce the grafting ratios 2, 10, and 20, respectively. The mixtures were allowed to react for 2 hours before being washed with ultrapure water in a 10 kDa centrifugal concentrator. After 3 washes, each grafted copolymer was lyophilized and stored at -20°C.

The grafting ratio of each PLL-g-PEG was determined using proton nuclear magnetic resonance spectroscopy (^{1}H NMR). Each grafting ratio was approximated as a distribution of PLL molecular weights was used to synthesize the grafted copolymer. Lyophilized polymer was dissolved in D_2O, and ^{1}H NMR spectroscopy was performed using a Bruker Avance INOVA 400 MHz spectrometer. The grafting ratio, or PEG chains per PLL chain, was determined by integrating the PLL and PEG peaks at 4.3 ppm and 3.7 ppm, respectively. A summary of the copolymers produced is shown in Table 2.1.

3.2.2 BSA Nanoparticle Synthesis

BSA nanoparticles (NPs) were formed through the electrostatic interaction of the cationic backbone of the PLL-g-PEG copolymer and negatively charged BSA. BSA was prepared by dissolving lyophilized BSA in PBS to a concentration of 1 mg/mL. The BSA was then filtered through a 0.2 μm syringe filter to remove larger aggregates. Then the filtered protein concentration was determined by measuring the absorbance of the sample at 280 nm. The filtered BSA solution was further diluted in PBS to produce a 0.27 mg/mL BSA solution.

PLL-g-PEG copolymer was dissolved in PBS at varying concentrations in order to add the same volume of polymer solution to BSA while varying the copolymer-to-protein mass ratio (C:P ratio) when forming NPs. Copolymer-to-protein mass ratios of 1:1, 2:1, 3:1, 7:1, 10:1, and 14:1 were produced to study the effect of copolymer concentration on protein encapsulation. NPs were formed by adding 7.5 μL of copolymer solution to 25 μL of BSA at 0.27 mg/mL under gentle vortexing and allowing the solution to incubate for 1 hour at room temperature, similar to the approach of Gaydess and coworkers [241].

Following NP formation, NPs were stabilized using glutaraldehyde to cross-link amino groups [27]. From a 50% stock solution, glutaraldehyde was diluted in PBS to produce a 0.025% glutaraldehyde solution. After 1 hour of NP formation, 5 μL of 0.025% glutaraldehyde was added to the NP samples followed by incubation for 3 hours at room temperature. The cross-linked NPs were either used immediately or stored at 4°C.

3.2.3 SEM Analysis of BSA Nanoparticles

The morphology and size of the BSA NPs were analyzed with an FEI Quanta 600 scanning electron microscope (SEM) at an accelerating voltage of 20 kV. Samples of BSA were encapsulated using a PLL-g-PEG (15-30 kDa), grafting ratio 10, with a C:P ratio of 7:1, and were deposited onto aluminum SEM stubs using a drop-casting method and allowed to air-dry at room temperature for 24 hours. Dried samples were sputter-coated with gold using a Cressington 108 sputter coater. Average sample size and size

distribution of the NPs were determined by analyzing 117 particles using ImageJ image analysis software.

3.2.4 TEM Analysis of BSA Nanoparticles

The internal structure of BSA NPs was analyzed using transmission electron microscopy (TEM). BSA was encapsulated using PLL-g-PEG (15-30 kDa) with a grafting ratio of 10 and a C:P ratio of 7:1 as described in the NP synthesis section. Following NP synthesis, 30 µL of NPs were placed on a formvar-carbon coated grid and allowed to air-dry at room temperature overnight. The sample was then negatively stained with 30 µL of phosphotungstic acid (pH 7.4), which was wicked off the grid after 1 minute using filter paper. The sample was allowed to dry for 2 hours before observation with a JEOL JEM-2100 electron microscope.

3.2.5 Gel Migration Assay and Encapsulation Efficiency

The extent of BSA encapsulation into NPs was determined using a non-reducing gel retardation assay. Samples containing approximately 2 µg of BSA, BSA exposed to glutaraldehyde, or BSA NPs were loaded onto 8% SDS-PAGE gels. The samples *were not* boiled and sample buffer (61% (v/v) DI water, 13% (v/v) 0.5 M Tris-HCl pH 6.8, 26% (v/v) glycerol, 2.1% (w/v) SDS, and 0.01% (w/v) bromophenol blue) *did not* include a reducing agent. SDS-PAGE gels were run at 200 V on a Bio-Rad tetracell mini gel electrophoresis apparatus until the dye front reached the bottom of the gel. The running buffer (1.5 g/L Tris Base and 7.2 g/L glycine) did not contain SDS. The SDS-PAGE gels were stained with Coomassie G-250 before imaging. The relative band intensity of the

non-encapsulated BSA was compared to the BSA with which copolymer was added to determine the extent of protein encapsulation.

3.2.6 Nanoparticle Size and ζ-Potential

The hydrodynamic diameter and surface charge of NPs were measured using a ZetaPALS Brookhaven Instruments Corporation ζ-potential analyzer. Prior to the measurements, samples were diluted in PBS to a total volume of 750 μL or 1.5 mL and passed through a 0.2 μm syringe filter directly into a disposable cuvette to remove dust from the sample. Dynamic light scattering (DLS) was used to determine the NP hydrodynamic diameter. A total of 5 measurements, lasting 2 minutes per measurement at a 90° angle were used to determine the average size of the NPs by intensity. The ζ-potential, determined by using phase analysis light scattering (PALS), was calculated from the electrophoretic mobility using Smoluchowski's equation [243]. A total of 10 measurements, each lasting 30 seconds, were used to determine the average ζ-potential of the NPs.

3.2.7 Retention of Protein Esterolytic Activity

The effect of encapsulation on protein function was determined by measuring the cleavage of a p-nitrophenyl ester by BSA [244]. Based on the method used by Córdova et al., the ester binding and hydrolysis of encapsulated BSA was measured by monitoring the release of p-nitrophenol spectrophotometrically [245]. To measure esterolytic activity, 5 μL of 6 mM p-nitrophenyl caprylate in isopropanol was added to 100 μL of either non-encapsulated BSA or NPs, and the mixture was allowed to incubate 20 hours

at 37°C before absorbance measurements were taken at 410 nm on a Packard Spectracount plate reader.

3.2.8 Stability of NPs Against Polyanions

The stability of NPs against heparin, a polyanion with a high charge density, was evaluated using the gel retardation assay described above. NPs were produced from low, medium, and high molecular weight (all 10:1 grafting ratio) copolymers at 1:1, 7:1, and 14:1 C:P ratios. The NPs were then incubated with PBS (control) or heparin in PBS at 0.1 mg/mL and 1 mg/mL for 24 hours at 37°C before PAGE.

3.2.9 Stability of NPs Against Protease Degradation

NPs were prepared following the method described above to encapsulate DQ Green BSA, a form of BSA that is so heavily labeled with BODIPY dye that the fluorescence is self-quenched. When degraded by protease, this quenching is relieved as fragments are released, and thus the protein degradation can be measured fluorometrically [246]. For these assays, DQ Green BSA NPs were prepared from low molecular weight grafting ratio 10, medium molecular weight grafting ratio 10, and high molecular weight grafting ratio 10 copolymers and encapsulated at 1:1, 7:1, and 14:1 C:P ratios. The NPs were incubated with chymotrypsin at 0.25 mg/mL at 37°C, and the fluorescence was measured over time (Exc: 485 nm Em: 535 nm) using a Beckman Coulter DTX 880 Multimode Detector.

3.2.10 Statistical Analysis

Statistical analysis was performed in Microsoft Excel using one-way analysis of variance (ANOVA) and pair-wise comparisons by Tukey's *post hoc* test. Data from the protease degradation study were fitted using a one site saturation model in SigmaPlot.

3.3 Results and Discussion

3.3.1 PLL-g-PEG Synthesis

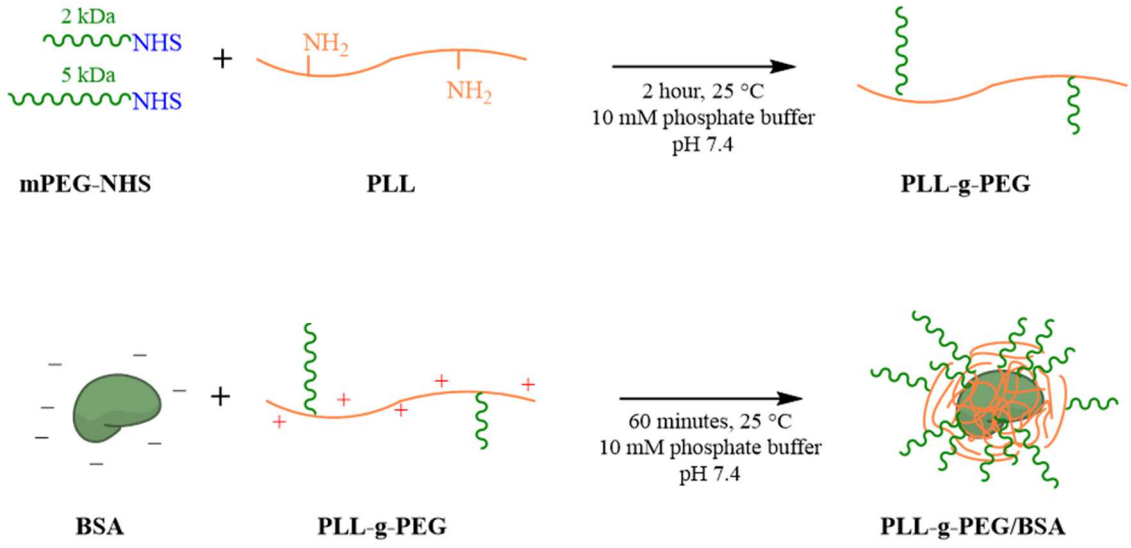

Figure 3.5. Synthesis of PLL-g-PEG Copolymer and Synthesis of BSA NPs. mPEG-NHS (2 and 5 kDa) was grafted onto 4-15 kDa, 15-30 kDa, and 30-70 kDa PLL. Three different grafting ratios (approximately 2, 10, and 20) were produced by varying the mass of PEG added to each PLL. BSA NPs were produced through self-assembly of the negatively charged BSA protein and the cationic PLL-g-PEG copolymer. After one hour of assembly in phosphate buffered saline, the NPs were cross-linked using 0.003% glutaraldehyde.

A library of nine PLL-g-PEG copolymers was synthesized to study the effect of PLL molecular weight and PEG grafting ratio on BSA encapsulation. A mixture of PEG molecular weights were used for the copolymers because a future aim of our work is to develop copolymers functionalized with two different types of ligands at different

distances away from the PLL backbone. The synthesis of PLL-g-PEG was performed as illustrated in Figure 3.1, with greater quantities of PEG added to the PLL to produce higher grafting ratios. The approximate number of PEG chains grafted onto each PLL chain was determined using ^{1}H NMR. The grafting ratio calculation and ^{1}H NMR spectrum may be found as supplementary material (Section S1 of Appendix). A summary of the library used and the results obtained is presented in Table 3.1. All of the copolymers produced had PEG grafting ratios within three PEG chains of the targeted grafting ratio. By producing this nine-copolymer library, we could then proceed to better understand the effect of PEG grafting and PLL molecular weight on association of the grafted copolymer with BSA.

Table 3.1. Summary of PLL-g-PEG Library Produced for BSA Encapsulation. The observed grafting ratios were measured using ^{1}H NMR.

Polymer Nomenclature	PLL Molecular Weight	Targeted PEG Grafting Ratio	Observed PEG Grafting Ratio (±3 of Targeted Grafting Ratio)
LMW 2	Low (4-15 kDa)	2	4.6
LMW 10	Low (4-15 kDa)	10	7.9
LMW 20	Low (4-15 kDa)	20	23.5
MMW 2	Medium (15-30 kDa)	2	4.6
MMW 10	Medium (15-30 kDa)	10	11.0
MMW 20	Medium (15-30 kDa)	20	19.1
HMW 2	High (30-70 kDa)	2	3.6
HMW 10	High (30-70 kDa)	10	11.2
HMW 20	High (30-70 kDa)	20	17.1

3.3.2 BSA Encapsulation Efficiency

To determine the extent of BSA encapsulation, NPs assembled from the copolymer library were characterized by gel retardation assays. Results showed that the BSA exposed to glutaraldehyde migrated slightly faster compared to unmodified BSA (Fig. 3.2, lane 2 of each panel). At low glutaraldehyde and protein concentrations, intramolecular cross-linking of the protein is more likely to occur than intermolecular cross-linking [247]. The results of Figure 3.2 indicate that glutaraldehyde did not cause intermolecular cross-linking of BSA as no additional higher molecular weight aggregates were observed following treatment. The slightly faster migration of BSA through the gel is likely a result of intramolecular cross-linking of the BSA that hindered the ability sodium dodecyl sulfate (SDS) to fully denature the protein. Upon the addition of copolymer, a combination of cross-linking between copolymer chains and between the copolymer and protein occurred. At the 1:1 C:P ratio, some heterogeneous retardation of BSA mobility ("smearing") was apparent on the gel, with a concomitant decrease in band intensity or spreading of the band for the free protein (Fig. 3.2, lane 3 of each panel). In cases at which the free protein band widened at a 1:1 C:P ratio, this appears to be due to a portion of the BSA becoming cross-linked by glutaraldehyde, producing a free protein band that appears to be a mixture of what is observed in lanes 1 and 2. The migration of BSA decreased as the C:P ratio was increased above 1:1, with markedly reduced BSA migration being apparent at higher C:P ratios for all of the copolymers. At C:P ratios between 3:1 and 7:1, high molecular weight copolymers retarded the mobility of

effectively all of the BSA molecules (Fig. 3.2, row 1, lane 6), indicating that encapsulation or loading of the protein into the NPs was 100%.

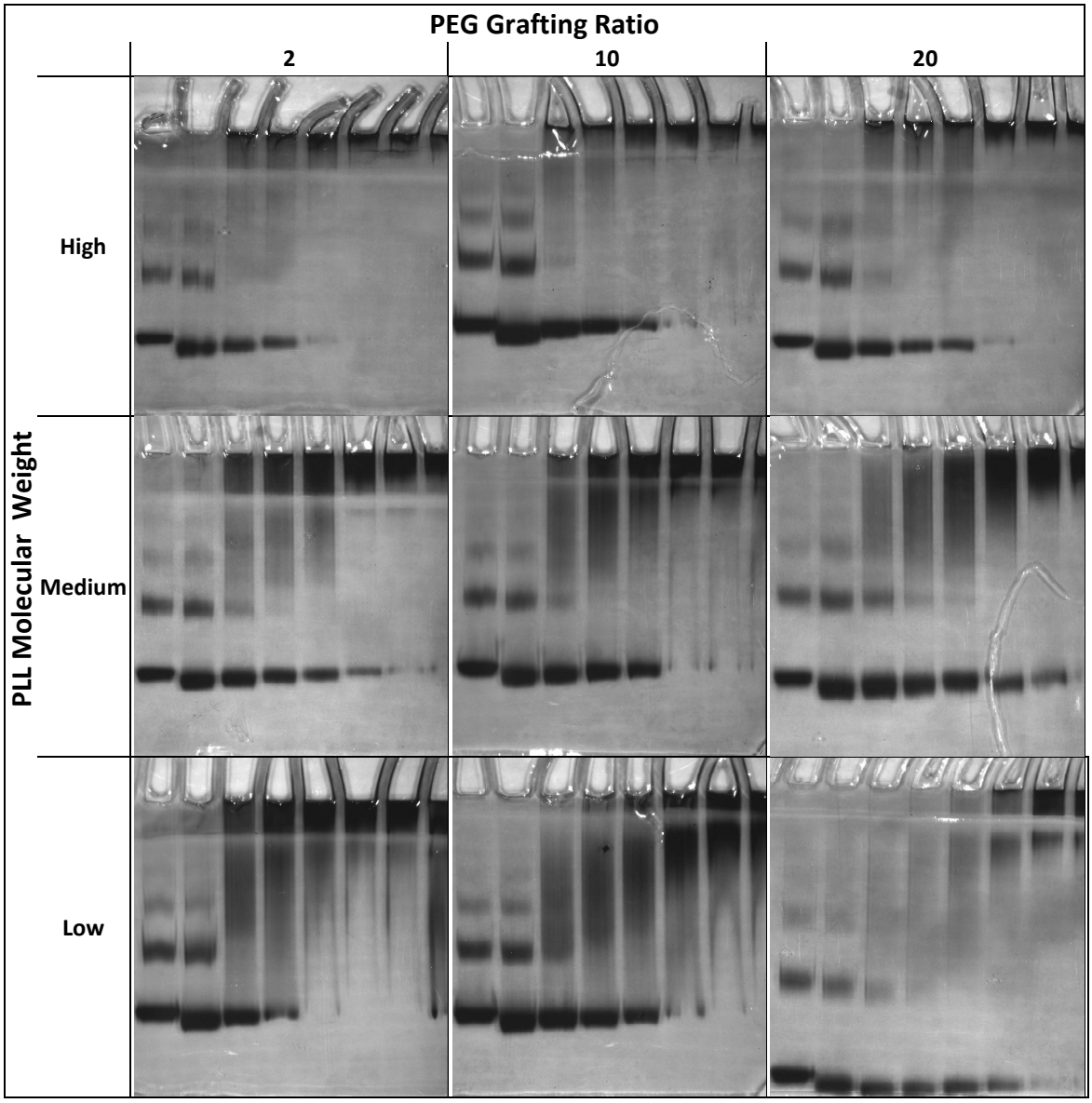

Figure 3.2. Encapsulation Efficiency of BSA with high, medium, and low molecular weight PLL-g-PEG copolymers with grafting ratios 2, 10, and 20. Each column corresponds to the mPEG grafting ratio for the copolymer. The row corresponds to the PLL molecular weight, with high, medium, and low being 30-70 kDa, 15-30 kDa, and 4-15 kDa PLL, respectively. In each panel, the sample in each lane is as follows with the NP lanes differentiated by C:P ratio: Lane 1: BSA; Lane 2: BSA incubated with glutaraldehyde; Lane 3 1:1 NP; Lane 4: 2:1 NP; Lane 5: 3:1 NP; Lane 6: 7:1 NP; Lane 7: 10:1 NP; Lane 8: 14:1 NP. The extent of BSA encapsulation was determined by comparing the relative band density of the BSA monomer for each C:P ratio to the non-encapsulated protein.

When the C:P ratio was increased even further, all of the protein was retained in the stacking gel, which also suggested complete loading of the protein into NPs. These results demonstrated a direct relationship between C:P ratios and BSA encapsulation.

The molecular weight of the copolymer PLL chain also had a substantial effect on protein encapsulation. For most of the copolymers, higher C:P ratios were required to effectively encapsulate BSA with the LMW and MMW copolymers compared to the HMW copolymers. For the MMW copolymers, a C:P ratio of at least 7:1 was required for protein migration to be fully retarded. Similarly, the LMW copolymers were generally the least effective in retarding migration. The LMW 2 copolymer was one exception with this copolymer associating effectively with BSA. Due to a higher number of copolymer chains relative to the MMW 2 and HMW 2, the LMW 2 copolymer may have been able to form glutaraldehyde crosslinks between multiple copolymer chains better than the other copolymers, leading to more efficient encapsulation. Generally though, the higher the molecular weight of the PLL portion of the copolymer, the more efficiently the copolymer associates with the protein.

The larger molecular weight PLL copolymers encapsulated BSA at lower C:P ratios compared to the smaller molecular weight copolymers. This is similar to higher PLL molecular weights improving DNA condensation through improved ion pairing [248, 249]. This decrease in C:P ratio required for efficient encapsulation was likely a result of the differences in the electrostatic charge of the copolymers. Because the grafted copolymer was synthesized by conjugating PEG to the amine groups that give the PLL

polymer its positive charge, higher grafting ratios result in copolymers with fewer amine groups and a lower charge. Similarly, for a fixed grafting ratio (mol:mol), high molecular weight PLL has a greater number of positively charged amine groups per PLL chain than the medium or low molecular weight PLL. This leaves the high molecular weight copolymers with more charge overall, and enables them to more easily associate with the BSA. In contrast, medium and low molecular weight copolymers have more PLL amine groups substituted by PEG. Thus, the low and medium molecular weight copolymers have had more of the PLL charge neutralized, leading to the observed higher quantities of copolymer needed to effectively associate with the BSA. Although using high amounts of copolymer to encapsulate a protein is not necessarily desirable for most efficient use of the copolymer, using copolymers with a large number of PEG chains is likely to be beneficial *in vivo* for reducing serum protein opsonization and clearance [250]. Therefore, there is a need to balance efficient encapsulation with sufficient PEGylation.

Together, the results of Figure 3.2 indicate that copolymer molecular weight, C:P ratio, and grafting ratio all impact the encapsulation of BSA. For a fixed PLL molecular weight, increasing the amount of grafted PEG generally led to a decrease in the amount of protein encapsulated for a given C:P ratio. PEG grafting onto PLL, however, is important in the formation of micelle-like nanoparticles rather than large aggregates commonly formed from cationic polymers and negatively charged biomolecules [22, 248]. To limit the number of particles further characterized, the PLL molecular weight and the C:P ratio (1:1, 7:1, and 14:1) were varied while the grafting ratio was held constant (10:1) for the remainder of the study.

3.3.3 NP Structure and Morphology

In addition to the gel retardation assay, electron microscopy was used to confirm the formation of BSA NPs. BSA NPs were observed in Figures 3.3 and 3.4, using scanning (SEM) and transmission electron microscopy (TEM). SEM results for the encapsulation of BSA with MMW 10 and a C:P ratio of 7:1 show NPs that were typically ellipsoids but often had irregular morphologies, Figure 3.3. The size of the BSA NPs based on SEM ranged from about 20 – 100 nm, with an average of 50 nm (Figure 3.4). This was similar to the diameter of other protein polyion complexes that have been previously characterized with sizes under 100 nm [234, 241].

TEM was used to determine the internal structure of the NPs. The TEM micrograph in Figure 3.3 (Panel B) shows NPs produced from MMW 10 with a C:P ratio of 7:1 that ranged from approximately 20-100 nm in diameter. The interior of the NPs had a punctate appearance with a bright outline. The white outline surrounding each particle is consistent with the formation of a PEG corona, which is similar to that observed around other PEGylated NPs [251]. This contrasts with BSA that had been encapsulated with MMW PLL alone (Panel C) in which only a thin dark outline surrounded these particles, which were typically much larger than 100 nm. The layering of the light outer region over the punctate interior suggests that the PEGylated NPs had a core/shell structure. A core-shell structure is consistent with the observations of others that have produced polyion complexes [225, 252]. This is likely due to steric effects of the hydrophilic PEG favoring placement at the outer surface of the particle and the cationic component of the polymer favoring association with negatively charged carboxylic groups on the BSA surface.

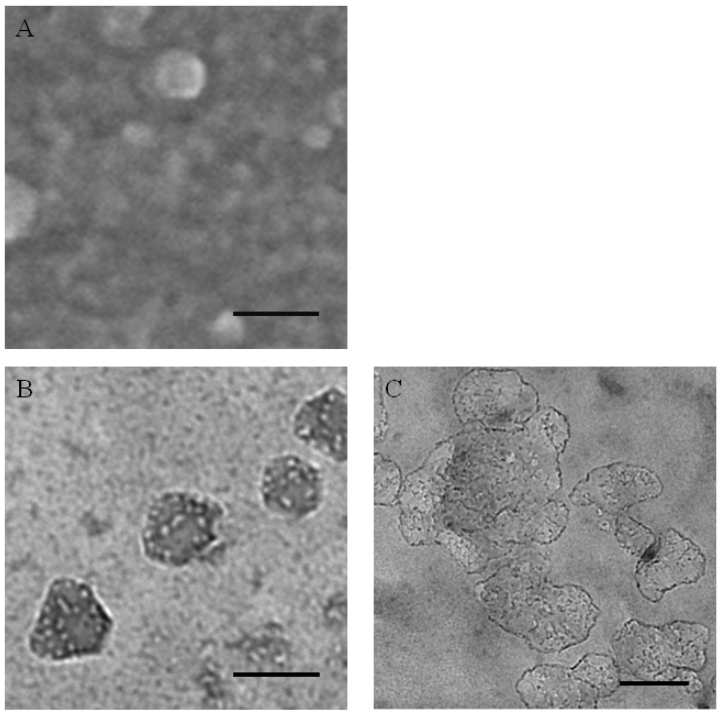

Figure 3.3. Electron Microscopy of BSA NPs. The formation of BSA NPs was confirmed using SEM (A) and TEM (B). A TEM micrograph of BSA complexed with unPEGylated 15-30 kDa PLL was used as a control (C). The NPs in the above micrographs were produced using BSA and medium molecular weight PLL, PEG grafting ratio 10 with a 7:1 C:P ratio. The SEM and TEM scale bar lengths are 100 nm.

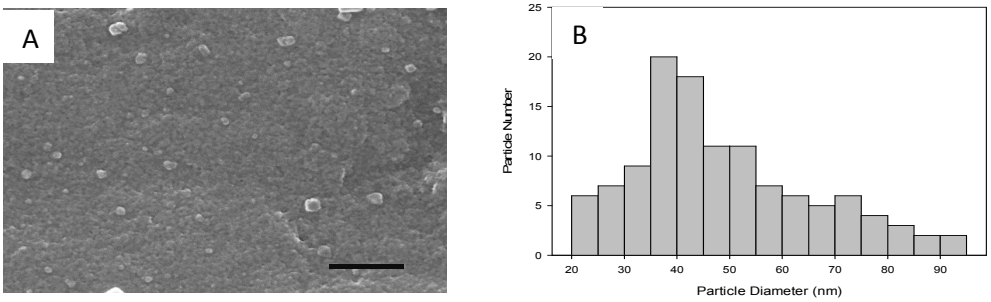

Figure 3.4. NP Size Distribution. The size distribution of MMW 10 7:1 NP was determined from multiple the SEM micrographs with a representative one shown above (A). The scale bar length is 500 nm. To determine the size distribution, NPs were treated as spherical particles and the particle diameter was determined using Image J (B). The size distribution was determined from 117 NPs. The mean particle size was approximately 50 nm with particles ranging in size between 20-100 nm.

3.3.4 NP Physicochemical Properties

Dynamic light scattering and PALS were used to determine the size and ζ-potential of NPs formed from LMW 10, MMW 10, and HMW 10 copolymers at a 7:1 C:P ratio (Table 3.2). The particle size, when measured using dynamic light scattering, indicated that NPs were approximately 20 nm in diameter for all three copolymers tested. Light scattering indicated that a distribution of NPs was formed, with some NPs slightly smaller than 20 nm and other NPs up to 100 nm in diameter (data not shown). All three techniques indicate that a distribution of nanoparticle sizes was formed with a size ranging from approximately 20-100 nm. The low contrast of the NPs when observed under SEM favors larger particles to be more easily observed and differentiated from the background, which may skew the average particle size. Additionally, differences in sample preparation may contribute to the differences observed.

Table 3.2 Physicochemical Characterization of BSA NPs. The average hydrodynamic diameter for LMW 10, MMW 10, and HMW 10 7:1 NPs was determined using dynamic light scattering. The ζ-potential or surface charge of the NPs was measured using Phase Analysis Light Scattering (PALS). The results shown are the mean and standard deviation of three replicates.

	LMW 10 NP	**MMW 10 NP**	**HMW 10 NP**
Diameter (nm)	24±0.6	18.8±3.4	23.5±3.2
ζ-Potential (mV)	-2.3±4.3	-12.4±1.2	5.3±2.5

To learn how the copolymers affected the NP surface charge, the ζ-potential, a measurement of surface charge, was determined for NPs formed from LMW 10, MMW 10, and HMW 10. In contrast to particle size, each of the three copolymers produced NPs with different ζ-potentials. The NPs produced from the HMW 10 copolymer were positive in charge. This was expected as the HMW 10 has the fewest number of

positively charged amine groups substituted by PEG of the three copolymers tested, resulting in particles with a positive charge.

NPs produced from the MMW 10 copolymer had the most negative charge of the three measured. A negative surface charge may suggest the presence of protein as well as PEG near the particle surface. Given there was a small amount of free BSA at this C:P ratio based on the gel retardation assay, it is possible that some free protein was associated with the NP surface which may have resulted in the non-linear relationship between the ζ-potential and the copolymer molecular weight. Even though a small amount of free protein was observed on the PAGE gels for the other two copolymers, it is conceivable that the charge density of the MMW 10 copolymer and the extent that the polymer was PEGylated made this effect more prevalent compared to the other two copolymers. The lower charge density of the MMW 10 copolymer, relative to the HMW 10 copolymer, may have allowed for a combination of PEG and small quantities of protein to be located at the particle surface.

The LMW 10 NPs had a charge close near neutral, which was expected from NP produced from the most PEGylated of the three copolymers because PEG is a neutrally charged polymer. The more highly PEGylated LMW 10 NPs, however, may prevent any free protein adsorption to the NP surface from occurring The higher degree of PEGylation may cause the PEG to become densely packed and prevent any protein binding near the particle surface. Overall, the ζ-potential of the NPs tested were near 0 mV, which could be a positive characteristic for minimizing non-specific interactions with strongly anionic biomolecules such as serum proteins and cell surface proteoglycans.

3.3.5 Retention of Protein Esterolytic Activity

To examine the effect of encapsulation on protein function, the esterolytic activity of BSA toward a p-nitrophenyl ester was measured. Albumin can bind to and hydrolyze ester substrates [253]. Results showed that the ability of BSA to bind and cleave a p-nitrophenyl ester was not adversely affected by encapsulation or cross-linking (Fig. 3.5); esterolytic activity of the encapsulated BSA was similar to that of the non-encapsulated BSA. When BSA was encapsulated with the medium or high molecular weight copolymers, the activity of the protein was slightly higher than the non-encapsulated protein. Although significant compared to the free protein, the C:P ratio had a relatively minimal effect on protein activity within individual copolymer PLL molecular weights, with higher C:P ratio NPs showing slightly higher esterolytic activity.

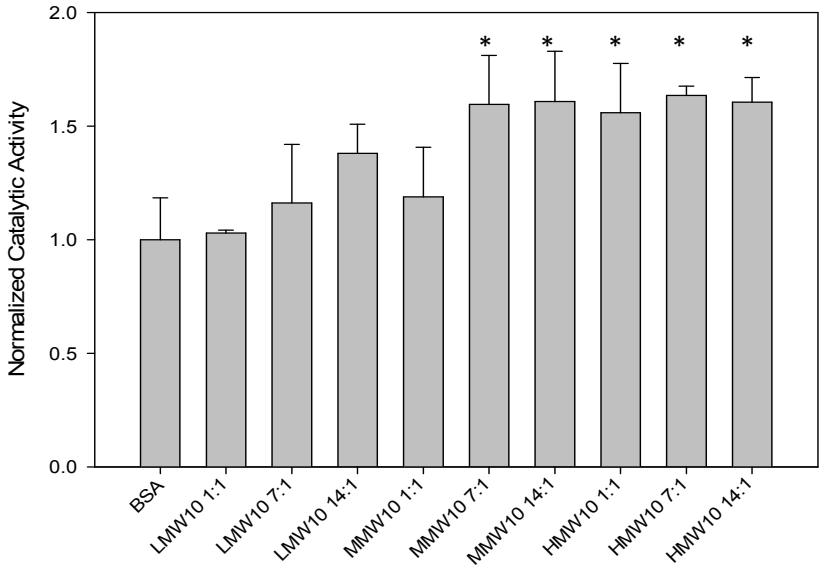

Figure 3.5. Retention of BSA Esterolytic Activity. BSA catalytic activity was measured by monitoring the hydrolysis of p-nitrophenyl caprylate with absorbance values taken at 410 nm after approximately 20 hours. Activity was normalized to that of the non-encapsulated BSA. The data is the mean and standard deviation of three replicates. * indicates $p<0.05$ between BSA and the indicated NP.

Our finding that encapsulation slightly enhances BSA esterolytic activity is consistent with previous observations that the catalytic activity of lysozyme toward a p-nitrophenol ester was enhanced following encapsulation with a polyaspartate-PEG copolymer [254]. Those authors suggested that the enhanced activity was likely due to accumulation of the hydrophobic substrate in the micelle, leading to a higher concentration of substrate near the protein than in the surroundings of the micelle. This explanation is also consistent with the observation that increasing the C:P ratio led to an increase in protein catalytic activity. Others have similarly seen an increase in apparent enzyme activity following encapsulation of catalase into polyion complex micelles, which could also be attributed to an increase in substrate concentration within the micelle [234].

3.3.6 Stability of NPs Against Polyanions

Many serum proteins and heparin sulfate proteoglycans have an overall negative charge, which may cause dissociation of polyion complexes *in vivo*. To learn how susceptible the copolymer NPs are to negatively charged molecules the stability of LMW 10, MMW 10, and HMW 10 NPs to polyanions was evaluated using heparin (Figure 3.6). Generally, the NPs were resistant to the effects of heparin, with most of the protein remained associated with the NPs after co-incubation. Although very little dissociation of the encapsulated protein was observed, increasing heparin concentration led to protein release from the NP. The LMW10 copolymer had the lowest stability against polyanions, as more BSA was released from these NPs compared to MMW10 and HMW10 copolymers. This may be due to the low molecular weight copolymer having the lowest

charge density among the three copolymers tested. The low molecular weight copolymers have the fewest cationic amine groups per copolymer chain making them more susceptible to disassociation by a polyanion. For all three copolymers tested, the 7:1 C:P ratio showed the greatest stability against heparin at 1 mg/ml compared to the 1:1 and 14:1 ratios. At the 1:1 C:P ratio, the protein is not fully encapsulated, making the amount of free protein detected in the presence of heparin already high. The 14:1 C:P ratio in particular was among the least stable of the NPs. NPs with high C:P ratios (14:1) may be more susceptible to dissociation by polyanions due to less organization between copolymer and BSA layers, reducing the efficiency of glutaraldehyde cross-linking. At the 7:1 C:P ratio, glutaraldehyde cross-linking of NPs completely encapsulating the protein is most efficient relative to the 1:1 and 14:1 C:P ratios.

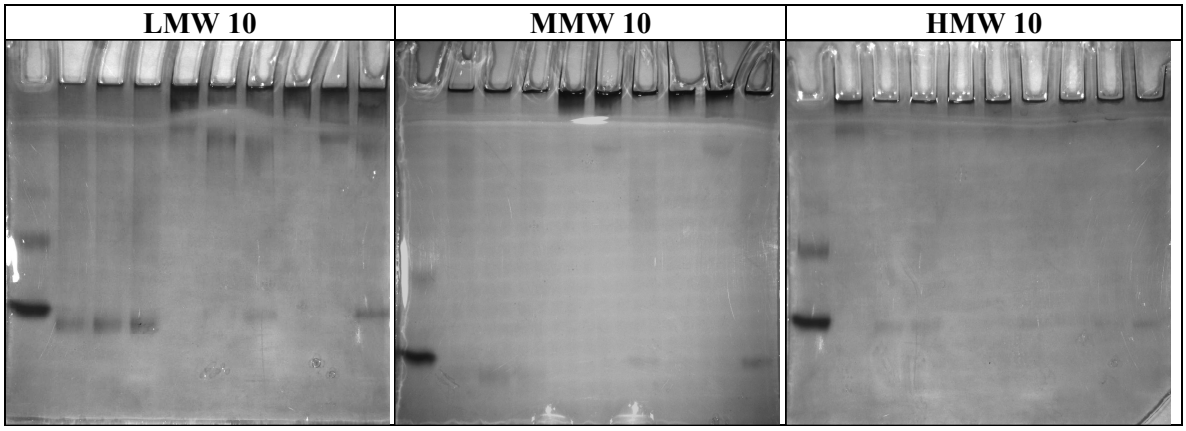

Figure 3.6. NP Polyion Stability after Incubation with Heparin. NPs were incubated with heparin at 37°C for 1 day. Lane 1: BSA; Lane 2: 1:1 NP, 0 mg/ml heparin; Lane 3: 1:1 NP 0.1 mg/ml heparin; Lane 4: 1:1 NP 1 mg/ml heparin, Lane 5: 7:1 NP 0 mg/ml heparin; Lane 6: 7:1 NP 0.1 mg/ml heparin; Lane 7: 7:1 NP 1 mg/ml heparin; Lane 8: 14:1 NP 0 mg/ml heparin; Lane 9: 14:1 NP 0.1 mg/ml heparin; Lane 10: 14:1 NP 1 mg/ml heparin.

3.3.7 Stability of NPs Against Proteolysis

Proteolysis is a major cause of inactivation of pharmaceutically relevant proteins in clinical settings. In order to determine if our NP could protect BSA from proteolysis,

the effect of encapsulation was evaluated using chymotrypsin as a model protease [255, 256]. These assays used BSA that was heavily labeled with a self-quenching BODIPY fluorescent dye, with degradation of the BSA being observed as an increase in fluorescence [246]. Results showed that the non-encapsulated BSA was rapidly degraded by chymotrypsin, as indicated by the increase in fluorescence over the first 24 hours of the study (Fig. 3.7, filled circles). Cross-linking the BSA with glutaraldehyde reduced the maximal degree of proteolysis (Fig 3.7, open circles). Encapsulation provided additional protection from the protease, with the BSA NPs releasing only 25% of the fluorescence relative to the free protein after 48 hours of exposure to chymotrypsin. Although the extent of chymotrypsin protection was found to be relatively similar for all of the copolymers, the high molecular weight copolymer appeared to offer slightly lesser protection. Additionally, the C:P ratio had little effect on protecting against BSA degradation. These results indicated that glutaraldehyde cross-linking and copolymer complexation can markedly reduce the susceptibility of a protein to protease-mediated degradation.

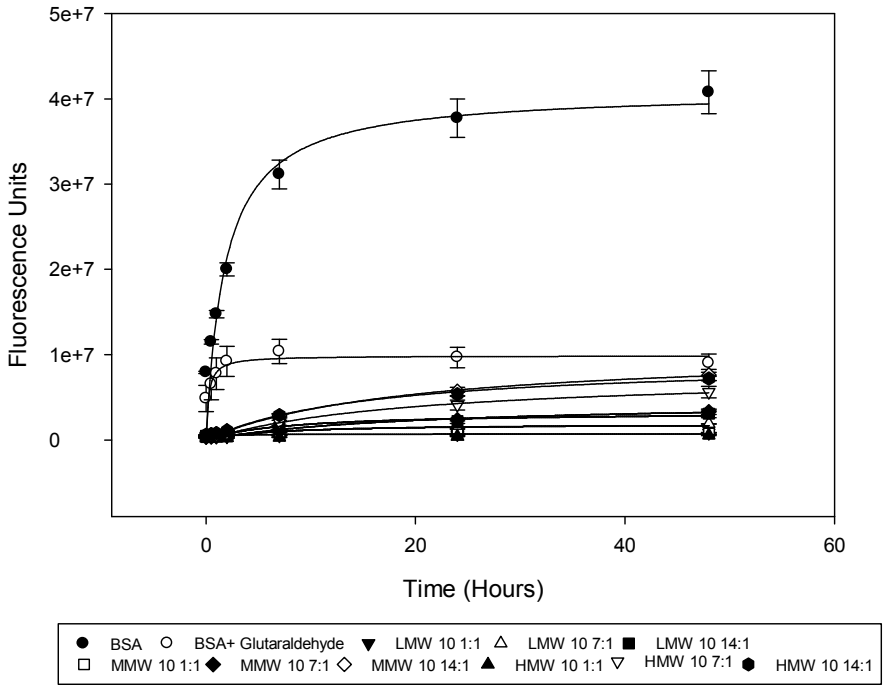

Figure 3.7. Stability of NPs to Protease Degradation. DQ Green BSA was encapsulated to form LMW 10, MMW 10, and HMW 10 NPs at 1:1, 7:1, and 14:1 C:P ratios. NPs were exposed to chymotrypsin (0.25 mg/ml) at 37°C over 48 hours. Proteolysis was monitored fluorometrically. Each data point represents the mean of three replicates and the error bars represent the standard deviation.

Glutaraldehyde cross-linking as well as other cross-linking strategies have been commonly used to enhance the stability of proteins and polyion complexes against proteases and other forms of degradation [31, 247]. The increased stability of proteins modified by cross-linkers, such as glutaraldehyde, has been attributed to an increase in protein rigidity due to intramolecular and/or intermolecular cross-linking between proteins and polymers [257]. Chymotrypsin has preferential activity at aromatic amino acid residues [258]. Intramolecular cross-linking of BSA likely affected conformational changes of the protein and reduced the access of chymotrypsin to the hydrophobic residues the protease preferentially cleaves.

Similarly, the formation of rigid, intermolecular cross-links by glutaraldehyde between copolymer chains as well as between the copolymer and BSA could be expected to further prevent access of the chymotrypsin to the protein. Additionally, PEGylation of the copolymers can sterically hinder interactions between the chymotrypsin and the protein NPs. Similar results were observed by others who found that encapsulation of DNA into polyplexes by PLL-g-PEG reduced the susceptibility of the DNA to degradation by nucleases [10, 259]. Protection as a result of PEGylation is consistent with the observation that the HMW 10 copolymer provided the least protection against proteolysis of the three NPs. The HMW 10 copolymer had the fewest PEG chains capable of protecting the protein compared to the low and medium molecular weight copolymers (at a given C:P ratio).

3.4 Conclusions

Protein encapsulation into polyion complexes is a promising approach to improve protein delivery. Very little systematic investigation, however, has been done into how characteristics of grafted cationic copolymers affect the encapsulation and stability of protein polyion complexes. The approach taken in this study found that PLL molecular weight, PEG grafting ratio, and C:P ratio all affect encapsulation of BSA. Protein catalytic activity was retained through the encapsulation process and even showed increased levels of activity at high C:P ratios for the medium and high molecular weight copolymers. Over a constant grafting ratio of 10, the medium and high molecular weight copolymers showed more resistance to polyanions than the low molecular weight copolymer. The low and medium molecular weight copolymer provided more protection for the protein from proteolysis compared to the high molecular weight copolymer.

Overall, a medium molecular weight PLL backbone with a grafting ratio of approximately 10 PEG:PLL effectively balanced protein association with the copolymer and NP stability. Future studies that focus on protein delivery under physiological conditions will undoubtedly provide additional framework for the design of an efficient protein delivery system.

Acknowledgements: This work was funded by contract HDTRA1-13-1-0021 from the Defense Threat Reduction Agency (DTRA) and the Oklahoma State University Interdisciplinary Toxicology Program.

This chapter was previously published as: Flynn, N., et al., *Effect of cationic grafted copolymer structure on the encapsulation of bovine serum albumin.* Materials Science and Engineering: C, 2016. **62**: p. 524-531.

CHAPTER IV

ALBUMIN DENATURATION IMPACTS MACROPHAGE UPTAKE OF CPP FUNCTIONALIZED PLL-G-PEG/GOX COMPLEXES.

4.1 Introduction

Since the discovery of the first cell-penetrating peptide (CPP) derived from the HIV Tat protein, CPPs have garnered significant interest as vehicles for delivering therapeutic agents into the intracellular space [109, 260]. While CPPs are capable of transporting themselves across the membrane of most cell types, they are also capable of transporting many types of cargo into the cell interior, including small molecule drugs, dyes, quantum dots, proteins, viruses, and many types of nanoparticles that would otherwise be unable to reach the cell interior [49]. Many types of CPPs contain several arginine residues, making them highly cationic in physiological conditions [261]. This cationic property is believed to drive the binding of CPPs to negatively charged cell surface proteoglycans, such as glycosaminoglycans, before they are internalized [262, 263]. CPPs are then internalized by a variety of pathways, which can include direct translocation and various forms of endocytosis [49]

While much has been learned about how CPPs function and their ability to deliver a wide range of therapeutic cargos has been demonstrated, CPPs have significant challenges to their use as delivery vectors. One of several important limitations to CPP-mediated therapeutic delivery is poor cell and tissue specificity [260]. Because CPPs are capable of traversing the membrane of most cell types, delivery of the CPP and its cargo to targeted cells is reduced when non-target cells take them up. Additionally, nanoparticle and nanoscale conjugates that could potentially utilize CPPs as part of their delivery are also prone to untargeted delivery, due to uptake and removal by macrophage cells which rapidly remove most nanoscale delivery agents from circulation [65, 264]. Therefore, identifying factors that contribute to off-target uptake of CPP-nanoscale conjugates could potentially provide avenues to reduce the delivery of CPP-functionalized conjugates to non-targeted macrophage cells.

While the interaction between CPP-functionalized conjugates and cell surfaces has been subject to significant study, the interactions that CPPs have with proteins in the extracellular environment have received considerably less attention. Recently, Cedervall et al. discovered that the surface of nanoparticles become coated by a dynamic layer of proteins or "protein corona" [51]. This protein corona has been shown to be a significant player in the biological outcomes of nanoparticles, with distinct proteins in the corona being implicated in the toxicity, uptake, and other physiological responses to nanoparticles [54, 58, 265]. Nanoparticles functionalized with CPPs are also likely to form a protein corona which may impact cellular uptake. CPPs are known to interact with negatively charged proteins due to electrostatic interactions, but the consequences of these interactions on the delivery of the CPP cargo is not well known [266].

Understanding how CPPs and CPP-functionalized nanoparticles interact with proteins in the biological medium is important to better utilize CPPs toward therapeutic delivery.

While the composition of the nanoparticle protein corona impacts nanomaterial interactions with cells, the conformation of the proteins of the corona are also important in nanoparticle interactions with cells. Fleischer and Payne recently found that amine-functionalized polystyrene nanoparticles denature the albumin present in their protein corona, and this denaturation leads to significant association of the particles to BS-C-1 monkey kidney epithelial cells through scavenger receptors [60]. Likewise, Yan et al. found that polymethacrylic acid nanoparticles denature albumin, which leads to uptake of the particles by differentiated THP-1 macrophage cells through the scavenger receptor [57]. These results demonstrate that charged polymeric nanoparticles denature albumin, which makes them susceptible to increased uptake by macrophages and potentially other cell types, but it is unclear if this may also extrapolate to other types of cationic nanoscale complexes. Because macrophages are known to preferentially uptake denatured proteins [267, 268], we predict that CPP-functionalized nanoparticles with a corona of denatured proteins are more likely to be taken up by macrophage than those that induce less protein denaturation.

In this work, we aimed to understand if CPPs cause denaturation of serum albumin, and if this denaturation could contribute to uptake by macrophage cells. We first synthesized nanoscale complexes functionalized with a small library of model CPPs. Poly-l-lysine grafted with polyethylene glycol (PLL-g-PEG) and the protein glucose oxidase (GOX) were used to synthesize a model nanoscale complex to serve as a base for CPP functionalization. PLL-g-PEG/GOX complexes were then functionalized with the

CPPs Tat, Pen, and LMWP [45, 113, 269]. Once the CPP-PLL-g-PEG/GOX groups were synthesized, an albumin protein corona was formed around each complex. CPP functionalized complexes were found to produce alteration in albumin protein structure. Albumin denaturation was found to potentially significantly impact the uptake of CPP functionalized complexes by macrophage cells.

4.2. Materials and Methods

Fluorescein isothiocyanate (FITC), glucose oxidase (GOX), albumin, FITC-albumin conjugate, Ellman Reagent, amiloride (cat.# A7410), chlorpromazine (cat.# C8138), genestein (cat.# G6649), and poly-l-lysine (15-30 kDa) (cat.# P7890) were purchased from Sigma Aldrich (St. Louis, MO). Cell penetrating peptides Tat (YGRKKRRQRRRC), Pen (RQIKIWFQNRRMKWKKC), and LMWP (CVSRRRRRRGGRRRR) were custom synthesized at greater than 95% purity by EZBiolab (Carmel, IN). Polyethylene glycol functionalized with succinimidyl ester (2kDa mPEG-NHS) and heterobifunctional polyethylene glycol with succinimidyl ester and maleimide (5 kDa Mal-PEG-NHS) were purchased from CreativePEGworks (Durham, NC). All other chemicals including DQ Green BSA (cat.#12050), those for polyacrylamide gel electrophoresis and cell culture, such as DMEM and fetal bovine serum (FBS), were purchased from Fisher Scientific (Pittsburgh, PA). RAW 264.7 mouse macrophage cells were purchased from ATCC (Manasses,VA).

4.2.1 PLL-g-PEG Grafted Copolymer Synthesis

PLL-g-PEG was synthesized by methods previously used [9]. A 50/50 (w/w) mixture of 40 mg of 2 kDa mPEG-NHS and 5 kDa Mal-PEG-NHS was added to 15 mg

of 15-30 kDa PLL in phosphate buffered saline (PBS, pH 7.4) and allowed to react for 2 hours. Unreacted PEG was then removed using a Pierce protein 10kDa concentrator. The grafted copolymer was then air-dried before storage at -20°C. H^1-NMR was used to measure the extent of PEG grafting onto PLL, by dissolving an aliquot of the copolymer in D_2O and using a Bruker Avance INOVA 400 MHz spectrometer. Peaks corresponding to the H of the α carbon of each lysine monomer at 4.2 ppm and H corresponding to the PEG conjugation to ϵ-amino groups at 2.55 ppm were integrated to determine the grafting ratio [270].

4.2.2 CPP-PLL-g-PEG/GOX Complex Formation

PLL-g-PEG/GOX complex formation was adapted from previous methods, using electrostatic interactions to drive association between PLL-g-PEG and GOX [9, 30, 36]. PLL-g-PEG (50 µl, 14 mg/ml, in PBS) was added to GOX (50 µl, 2 mg/ml, in PBS) while vortexing, and then allowed to incubate for one hour. After incubating, PLL-g-PEG/GOX complexes were crosslinked using glutaraldehyde (0.003%) for 3 hours to stabilize the complexes. Following crosslinking, the complexes were functionalized with either Tat, Pen, or LMWP (Table 4.1) by adding 7×10^{-2} µmols of each of the peptides to the complexes and allowing thiol-reactive maleimide groups on PLL-g-PEG to react with the peptide cysteine thiol groups for 30 minutes. The extent of peptide conjugation was determined using Ellman's reagent to measure the extent of unreacted peptide before and after conjugation [271]. The Ellman assay was performed following the manufacturers' suggested protocol. The complexes were then washed using a 10 kDa centrifugal concentrator before use or storage at 4°C.

4.2.3 CPP-PLL-g-PEG/GOX Complex Characterization

To confirm that each of the copolymers completely encapsulated GOX, a gel migration assay was used to measure association of the protein with the copolymer as previously described by our group [9]. Following synthesis, a 5 µl aliquot of each of the complexes was added to non-reducing SDS-PAGE sample buffer and loaded onto 8% SDS-PAGE gels. An equivalent loading of un-encapsulated GOX was used as a control for a non-encapsulated sample. The gel was then run at 200 V on a Bio-Rad Mini-PROTEAN Tetracell and stained using Coomassie G250 following completion. The intensity of the protein band corresponding to any non-encapsulated GOX was compared to the free GOX control to determine the extent GOX associated with each of the complexes.

In order to characterize size and surface charge of the CPP-PLL-g-PEG/GOX complexes, the hydrodynamic diameter and ζ-potential were measured using dynamic light scattering (DLS) and phase analysis light scattering (PALS). A Brookhaven Instrument Corporation ZetaPALS ζ-potential analyzer was used for both measurements. Briefly, a 60 µl aliquot of CPP-PLL-g-PEG/GOX complexes were loaded into a cuvette that was placed into the instrument for DLS. Triplicate measurements consisting of at least five runs per measurement, with each run lasting one minute were used to determine the hydrodynamic diameter and polydispersity of the complexes. The surface charge of the CPP-PLL-g-PEG/GOX complexes were measured using PALS. CPP-PLL-g-PEG/GOX complexes, synthesized as described above, were diluted to a volume of 1.5 ml using PBS (pH 7.4) and loaded into a cuvette that was placed in the instrument. The ζ-potential of the complexes was then calculated from their mobility using Smoluchowski's

equation [243]. The measurements were made in triplicate, with each measurement consisting of 10 runs, each lasting one minute.

4.2.4 Albumin Protein Corona Formation and Denaturation

To determine if albumin forms a protein corona around CPP-PLL-g-PEG/GOX complexes, non-denaturing native PAGE was used to determine if albumin becomes bound to CPP-PLL-g-PEG/GOX complexes. Non-denaturing agarose gel electrophoresis has been similarly used to detect the formation of a protein corona around dendrimers and separate them from unbound protein [272]. CPP-PLL-g-PEG/GOX complexes were prepared as described above. A 5 µg aliquot of each CPP-PLL-g-PEG/GOX complex (by GOX concentration) was combined with bovine serum albumin (BSA) for a final albumin concentration of 5 µg/µl. The resulting BSA/CPP-PLL-g-PEG/GOX complexes were then allowed to incubate for 30 minutes at 37°C. A 1 µg aliquot of albumin- PLL-g-PEG-CPP/GOX complexes (by GOX concentration) were then loaded onto 8% non-denaturing PAGE gels and run at 200V on a Bio-Rad Mini- PROTEAN Tetracell before staining with Coomassie G-250. The extent to which albumin binds to the complexes was compared to a control in which an equivalent amount of albumin was loaded onto the gel without complexes. Reductions in albumin migration compared to the control was used to evaluate albumin binding to the complexes.

To determine the extent to which CPP-PLL-g-PEG/GOX complexes denature albumin that associates with the complexes as part of a protein corona, a fluorescence quenching assay with DQ Green BSA was used to detect changes in albumin structure. DQ Green BSA is an albumin which has been heavily labeled with BODIPY dye so that

its fluorescence has been self-quenched. Self-quenching fluorophores and other fluorescence based assays have been previously used to detect changes in protein structure [273]. CPP-PLL-g-PEG/GOX complexes were prepared as described above. An albumin protein corona was then formed, as described above, by incubating 5 µg aliquots of CPP-PLL-g-PEG/GOX complexes with DQ Green BSA at a final concentration of 5 µg/µl. After either 30 or 60 minutes at 37°C, the fluorescence of the mixture was then measured (ex: 485 nm/ em: 535 nm) using a Beckman Coulter DTX 880 Multimode Detector. The extent of albumin denaturation was normalized (equation below) to DQ Green BSA that had not been incubated with complexes (negative control) and DQ Green BSA which had been boiled (positive control).

$$Normalized\ Fluorescence\ (\%) = \frac{\left(BSA_{CPP-PLL-g-PEG/GOX} - BSA_{non-boiled}\right)}{\left(BSA_{boiled} - BSA_{non-boiled}\right)} \times 100$$

4.2.5 CPP-PLL-g-PEG/GOX and BSA/CPP-PLL-g-PEG/GOX Complex-Macrophage Cell Association

To determine the extent to which CPP-PLL-g-PEG/GOX and BSA/CPP-PLL-PEG/GOX complexes associate with macrophage cells, fluorescence microscopy was used to visualize interaction of the complexes with macrophage cells. GOX was labeled with FITC, according to the manufacturer's protocol, and was encapsulated in CPP-PLL-g-PEG/GOX complexes. A mouse macrophage cell line, RAW 264.7 cells ,were first cultured in DMEM supplemented with 10% fetal bovine serum (FBS) and maintained in an incubator maintained at 37°C and 5% CO_2. Approximately 24 hours prior to visualizing the cells, 1×10^5 RAW 264.7 cells were seeded on polylysine-coated glass microscope coverslips. On the following day, CPP-PLL-g-PEG/GOX and BSA/CPP-

PLL-g-PEG/GOX encapsulating FITC-GOX (10 μg by GOX concentration) were added to the cells in serum free DMEM. After 30 minutes of incubation at 37°C, the cells were washed with PBS and fixed with 4% formaldehyde. The coverslips were then mounted with ProLong Gold antifade mounting medium onto microscope slides before imaging with a Nikon Eclipse TE2000-U fluorescence microscope.

4.2.6 Inhibition of Macrophage Uptake Pathways

To better understand how albumin attachment to CPP-PLL-g-PEG/GOX complexes affects their uptake, pharmacological inhibitors were used to inhibit various forms of endocytosis (phagocytosis, macropinocytosis, caveolin dependent endocytosis, and clathrin mediated endocytosis) [274]. Prior to beginning the uptake studies, the cytotoxicity of each inhibitor was assessed using the Cell Titer Blue cell viability assay to ensure cell viability would be maintained above 90% [274, 275]. For uptake studies, RAW 264.7 cells were cultured, as described, before seeding on 96-well plates at 1×10^4 cells/well. After one day, the medium of the cells was replaced with serum free DMEM. One hour before the experiment, amiloride (to inhibit phagocytosis and macropinocytosis), cholorpromazine (to inhibit clathrin mediated endocytosis), or genestein (to inhibit caveolae mediated endocytosis) were added to the cells for final concentrations of 4.5 μg/ml, 8 μg/ml, and 26 μg/ml, respectively. After one hour, 1 μg (by GOX mass) of FITC-labeled CPP-PLL-g-PEG/GOX or BSA/CPP-PLL-g-PEG/GOX were added to the cells. After 30 minutes at 37°C, Trypan Blue was added to the cells to quench any FITC fluorescence associated with non-internalized complexes [276, 277]. The fluorescence intensity was then measured (ex: 485 nm/em: 535 nm) using a Beckman Coulter DTX 880 Multimode Detector.

4.2.7 CPP-PLL-g-PEG/GOX Albumin Denaturation and Macrophage Uptake

To determine if RAW 264.7 cells take up denatured albumin differently than non-denatured albumin, RAW 264.7 macrophage cells were cultured and seeded on 96-well plates at 1×10^4 cells/well as described above. FITC-albumin and boiled (denatured) FITC-albumin were added (5 μg) to RAW 264.7 cells in serum-free medium. Trypan Blue was then added to the cells to quench the fluorescence not associated with internalized protein, as described above. The fluorescence intensity was then measured at ex. 485 nm/em. 535 nm using a Beckman Coulter DTX 880 Multimode Detector.

To understand the effect of albumin denaturation on uptake of CPP-PLL-g-PEG/GOX complexes by macrophage cells, non-complex bound denatured albumin was used to partially saturate the uptake of the albumin bound complexes. CPP-PLL-g-PEG/GOX complexes, with FITC GOX, were prepared as described above. The complexes were then incubated with either albumin or denatured albumin at 5 μg/μl at 37°C for 30 minutes as also described above. The albumin/CPP-PLL-g-PEG/GOX complexes (1 μg by GOX concentration) were then added to the RAW 264.7 cells in serum-free medium. The cells were allowed to incubate for 30 minutes at 37°C before Trypan Blue was added to quench FITC fluorescence of complexes in the medium or bound to the cell surface.

This experiment was also similarly performed to detect the cytotoxic activity of GOX, using 5 μg of albumin/CPP-PLL-g-PEG/GOX, by rinsing the cells with PBS following a 30 minute incubation with the complexes, and assessing cell viability using the Cell Titer Blue cell viability assay following the manufacturer's protocol.

4.2.8 Data Analysis

Each measurement was determined by taking the mean of the results of triplicate, biological replicate, samples. The error associated with the measurement was evaluated by determining the standard deviation from the mean. Statistical analysis were performed using the Student's t-test, with a p-value of less than 0.05 to describe significant differences between two groups.

4.3. Results

4.3.1 CPP-PLL-g-PEG/GOX NP Formation and Characterization

PLL-g-PEG-Mal was synthesized as previously described, resulting in approximately 10 PEG chains grafted onto each PLL backbone, as determined by H^1 NMR (Figure S1 in Appendix) [9]. Following synthesis of PLL-g-PEG-Mal, electrostatic interactions were used to complex PLL-g-PEG-Mal with GOX, as illustrated in line 1 of the synthesis scheme in Figure 4.1A. CPPs were conjugated through their cysteine thiol reacting with the PEG-maleimide. An Ellman assay indicated that approximately 7×10^{-2} μmols of each CPP conjugated to the PLL-g-PEG/GOX complexes, representing conjugation of CPPs to nearly all available maleimide groups of the copolymer. Using SDS-PAGE, electrostatic association of the PLL-g-PEG copolymer to GOX and crosslinking of the complexes was confirmed through hindered migration of GOX through the gel (Figure 4.1B, Lane 4). Functionalization of PLL-g-PEG/GOX complexes with Pen, Tat, and LMWP CPPs showed similarly hindered migration of GOX during SDS-PAGE (lanes 5-7).

Table 4.1. Summary of CPPs Conjugated to PLL-g-PEG/GOX Complexes

CPP	CPP Sequence	Est. CPP Net Charge	R#
Penetratin (Pen)	RQIKIWFQNRRMKWKKC	+7	3
HIV Tat 47-57 (Tat)	YGRKKRRQRRRC	+9	6
Low molecular weight protamine (LMWP)	CVSRRRRRRGGRRRR	+10	10

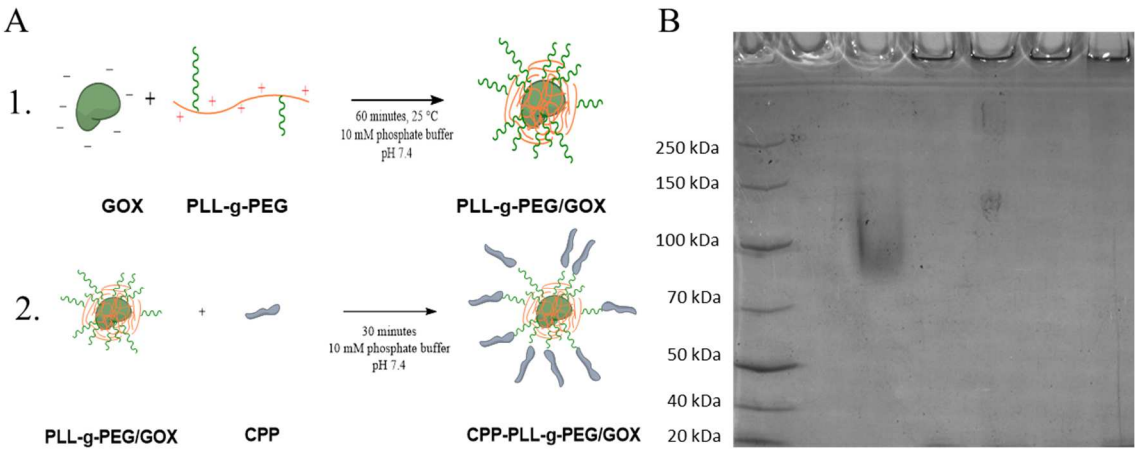

C

	PLL-g-PEG/GOX	Pen-PLL-g-PEG/GOX	Tat-PLL-g-PEG/GOX	LMWP-PLL-g-PEG/GOX
Diameter (nm)	13.5±0.8	16.4±0.7	17.5±4.1	21.1±6.9
PDI	0.345±0.107	0.291±0.007	0.254±0.024	0.216±0.057
ζ-potential (mV)	4.84±1.69	8.62±1.28	9.46±0.77	10.45±1.40

Figure 4.1. Synthesis and Characterization of CPP-PLL-g-PEG/GOX Complexes. A: Synthesis schematic of CPP-PLL-g-PEG/GOX complexes; 1. PLL-g-PEG associates with GOX through electrostatic interaction. 2: PLL-g-PEG/GOX complexes were then functionalized with either the Pen, Tat, or LMWP CPPs. B: SDS-PAGE was used to determine the extent GOX remained associated with each of the complexes under denaturing conditions. Lane 1: Ladder; Lane 2: Empty; Lane 3: GOX; Lane 4: PLL-g-PEG/GOX; Lane 5: Pen-PLL-g-PEG/GOX; Lane 6: Tat-PLL-g-PEG/GOX; Lane 7: LMWP-PLL-g-PEG/GOX. C: Physicochemical characteristics (particle size, polydispersity index (PDI), and ζ-potential) were determined using DLS and PALS.

Following synthesis, DLS and PALS were used to determine that the size and surface charge of the CPP-PLL-g-PEG/GOX complexes (Table 4.1C). PLL-g-PEG/GOX complexes were approximately 14 nm in diameter while functionalization with CPPs

resulted in complexes ranging in size from 14 -20 nm in diameter. PLL-g-PEG complexation with GOX resulted in complexes with a near neutral to slightly positive surface charge of 5 mV. The addition of CPPs increased the surface charge to 8.6, 9.5, and 10.5 mV for Pen, Tat, and LMWP functionalized complexes, respectively.

4.3.2 Albumin Association to CPP-PLL-g-PEG/GOX Complexes

To evaluate the extent to which albumin associates with CPP-PLL-g-PEG/GOX complexes, non-denaturing native PAGE was used to visualize changes in albumin migration down the gel (Figure 4.2A). Association of albumin to the complexes was determined by detecting changes in free albumin migration down the gel following incubation with the complexes compared to a control (lane 1) in which no complexes had been added. For all of the complexes, most of the albumin added to the samples remained unbound to the complexes, but slight changes in albumin migration were, nevertheless, observed. Upon the addition of PLL-g-PEG/GOX complexes to albumin (lane 2), a slight decrease in intensity of albumin that migrated down the gel was observed compared to the control. A similar decrease in albumin band intensity was also observed for Pen-PLL-g-PEG/GOX complexes (lane 3). Much greater decreases in the intensity of the middle and lowest albumin bands were observed for Tat-PLL-g-PEG/GOX and LMWP-PLL-g-PEG/GOX complexes (lanes 4 and 5), indicating that less albumin was able to freely migrate down the gel when incubated with these complexes.

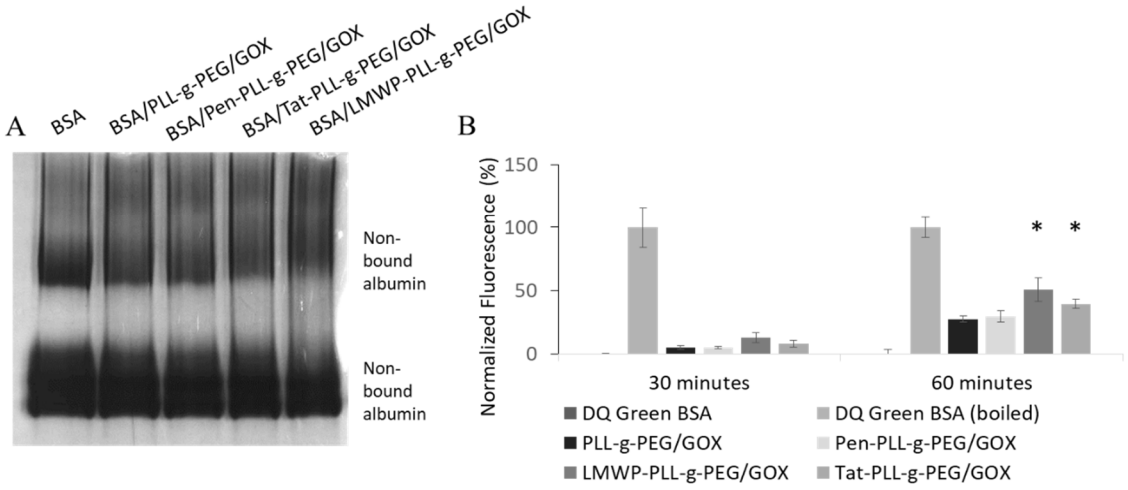

Figure 4.2. Serum Albumin Forms a Protein Corona Around CPP-PLL-g-PEG/GOX Complexes. Panel A: Native PAGE of albumin/CPP-PLL-g-PEG/GOX complexes. Equivalent amounts of albumin were loaded with and without CPP-PLL-g-PEG/GOX complexes. Lane 1: Albumin (BSA); Lane 2: BSA/PLL-g-PEG/GOX; Lane 3: BSA/Pen-PLL-g-PEG/GOX; Lane 4: BSA/Tat-PLL-g-PEG/GOX; Lane 5: BSA/LMWP-PLL-g-PEG/GOX. Panel B: DQ Green BSA Fluorescence Quenching Assay. The fluorescence associated with DQ Green BSA following incubation with CPP-PLL-g-PEG/GOX complexes was evaluated after 30 and 60 minutes. DQ Green BSA (negative control) and boiled DQ Green BSA (positive control) were used as controls. * indicates $p<0.05$ when comparing differences between CPP-PLL-g-PEG/GOX with PLL-g-PEG/GOX as determined by the Student's t-Test.

To monitor changes in albumin structure when in contact with CPP-PLL-g-PEG/GOX complexes, a fluorescence quenching assay was used to observe perturbations in albumin structure (Figure 4.2B). Increases in fluorescence were associated with alteration in albumin structure. CPP-PLL-g-PEG/GOX complexes were incubated with non-denatured heavily labeled DQ Green BSA, and fluorescence measurements were taken after 30 and 60 minutes of incubation at 37°C. All results were normalized to DQ Green BSA alone (negative control) and boiled DQ Green BSA (positive control). PLL-g-PEG/GOX and Pen-PLL-g-PEG/GOX complexes showed minor denaturation after 30 minutes, which increased to approximately 25% of the positive control after 60 minutes. Tat-PLL-g-PEG/GOX complexes showed higher fluorescence associated with reduced fluorescence quenching compared to PLL-g-PEG/GOX and Pen-PLL-g-PEG/GOX

complexes. LMWP-PLL-g-PEG/GOX showed the greatest increase in fluorescence intensity, with the most fluorescence detected after both 30 and 60 minutes, compared to the other groups. After 60 minutes, the change in fluorescence of DQ Green BSA when incubated with Tat and LMWP functionalized PLL-g-PEG/GOX complexes was significantly different compared to that of the unmodified complexes. These results indicate that Tat and LMWP cause 25% of the denaturation of the positive albumin control after 60 minutes.

4.3.3 Uptake of Albumin/CPP-PLL-g-PEG/GOX Complex by Macrophage Cells

To determine if CPP-PLL-g-PEG/GOX and BSA/CPP-PLL-g-PEG/GOX complexes associate with macrophage cells, fluorescence microscopy was used to visualize the complexes following incubation with RAW 264.7 macrophage cells (Figure 4.3). CPP-PLL-g-PEG/GOX and albumin bound CPP-PLL-g-PEG/GOX (BSA/CPP-PLL-g-PEG/GOX) complexes encapsulating FITC-labeled GOX became bound and/or internalized within macrophage cells after 30 minutes. LMWP-PLL-g-PEG/GOX complexes showed the greatest extent of association with macrophages, regardless of the presence of albumin. The other Pen and Tat modified complexes showed relatively similar extents of association with macrophages, which appeared to be slightly higher than that of the unmodified complexes. Complexes that had been incubated with albumin prior to addition to the cells generally resulted in similar association with macrophage cells as for unmodified complexes. LMWP-PLL-g-PEG/GOX complexes that had been pre-incubated with albumin tended to show slightly greater association with the macrophage cells than the other complexes.

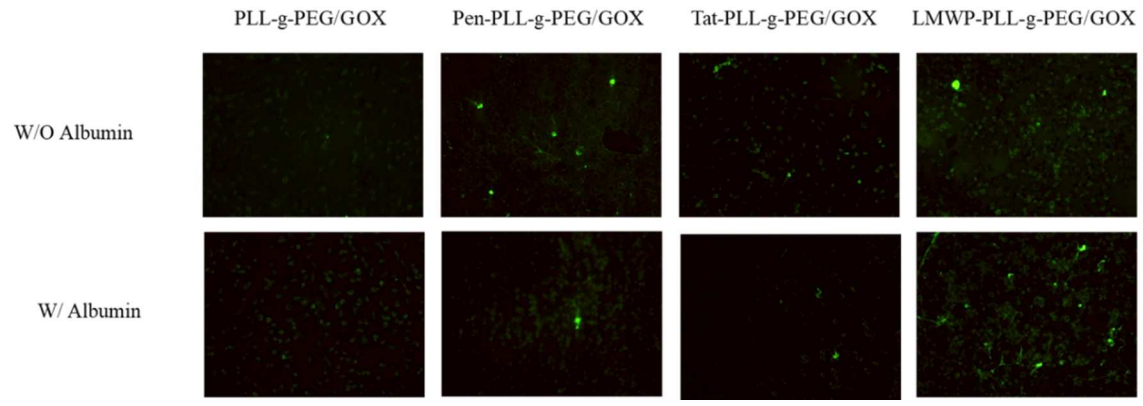

Figure 4.3. CPP-PLL-g-PEG/GOX and Albumin/CPP-PLL-g-PEG/GOX Associate with Macrophage Cells. CPP-PLL-g-PEG/GOX and albumin/CPP-PLL-g-PEG/GOX complexes, encapsulating FITC labeled GOX, were allowed to incubate with RAW 264.7 mouse macrophage cells for 30 minutes. Fluorescence microscopy was used to observe association of the complexes with the cells.

4.3.4 Albumin/CPP-PLL-g-PEG/GOX Complex Uptake Pathway by Macrophage Cells

After determining that CPP-PLL-g-PEG/GOX complexes associate with macrophage cells, pharmacological inhibitors were used to evaluate the uptake mechanism of the complexes. By using Trypan Blue to quench the fluorescence of surface bound complexes, uptake of CPP-PLL-g-PEG/GOX and BSA/CPP-PLL-g-PEG/GOX complexes was evaluated fluorometrically (Figure 4.4). PLL-g-PEG/GOX complexes showed a reduction in uptake in the presence of chlorpromazine and genestein, indicating that they are primarily taken up by clathrin and caveolae-mediated endocytosis (Figure 4.4A). When PLL-g-PEG complexes were associated with albumin, the uptake of the complexes were significantly reduced when caveolae-mediated endocytosis was inhibited by genestein. The other CPP-PLL-g-PEG/GOX complexes also showed a reduction in fluorescence when the cells had been incubated in the presence of chlorpromazine, suggesting uptake by clathrin-mediated endocytosis (Figure 4.4B-D). When the albumin bound CPP-PLL-g-PEG/GOX complexes were added to the

macrophages, however, significant reductions ($p<0.05$) in fluorescence were observed when the cells were treated with genestein compared to other pharmacological inhibitors. The reduced fluorescence for cells treated with genestein suggests that albumin complexed with CPP-PLL-g-PEG/GOX complexes were more favorably taken up by macrophages by a caveolae- mediated endocytosis uptake pathway.

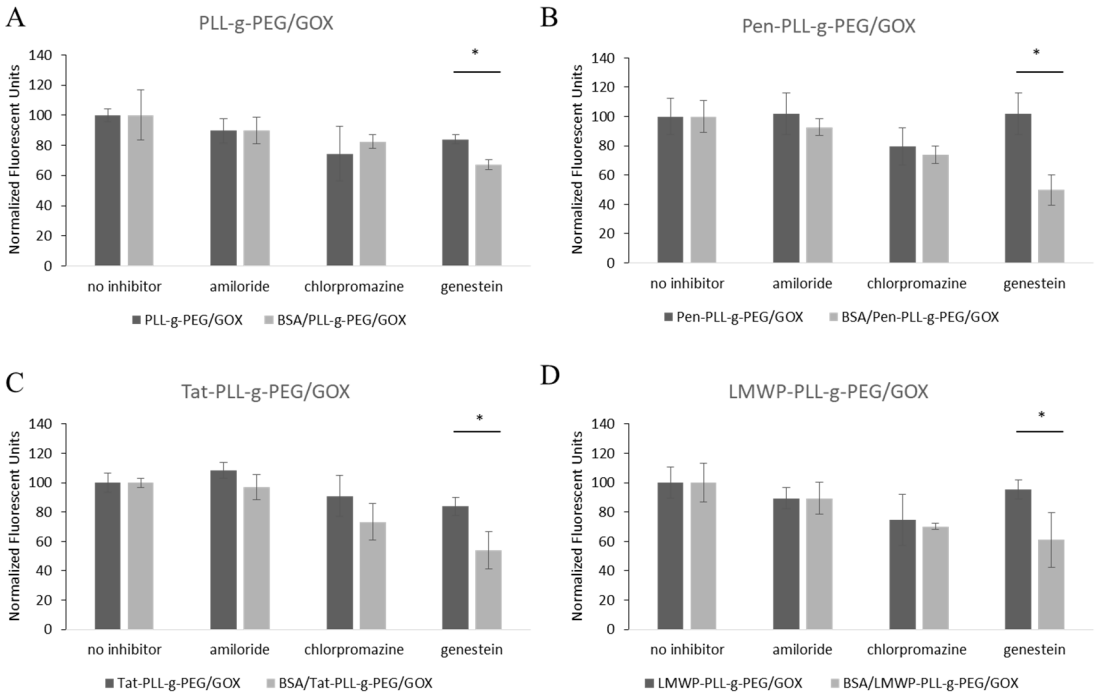

Figure 4.4. Macrophage Uptake Pathway of CPP-PLL-g-PEG/GOX and Albumin/CPP-PLL-g-PEG/GOX Complexes. To evaluate how macrophages take up CPP-PLL-g-PEG/GOX and albumin/CPP-PLL-g-PEG/GOX complexes, amiloride, chlorpromazine, and genestein were used to inhibit phagocytosis and macropinocytosis, clathrin-mediated endocytosis, and caveolae-mediated endocytosis, respectively. A: PLL-g-PEG/GOX and BSA/PLL-g-PEG/GOX; B: Pen-PLL-g-PEG/GOX and BSA/Pen-PLL-g-PEG/GOX; C: Tat-PLL-g-PEG/GOX and BSA/PLL-g-PEG/GOX; D: LMWP-PLL-g-PEG/GOX and BSA/LMWP-PLL-g-PEG/GOX. * indicates that complexes with and without albumin, when treated with the same pharmacological inhibitor, have a difference with a $p<0.05$, determined by the Student's T-test.

4.3.5 CPP-PLL-g-PEG/GOX Albumin Denaturation on Macrophage Uptake

To determine if albumin denaturation within the protein corona of CPP-PLL-g-PEG/GOX complexes influences the uptake of the complexes by macrophages, an excess of denatured albumin (5 mg/ml, in which most of the albumin would remain unbound to the complexes) and complexes were added to macrophage cells. If denatured albumin reduces the uptake of the complex, this would suggest that a receptor for denatured albumin participates in the uptake of CPP-PLL-g-PEG/GOX complexes. First, to verify that RAW 264.7 cells preferentially take up denatured albumin compared to albumin in its native state, the uptake of FITC-albumin was compared to FITC-albumin that had been boiled (Figure 4.5A). After 30 and 60 minutes, the uptake of denatured FITC-albumin was approximately 10% and 80% higher compared to that of non-denatured FITC-albumin.

Next, the impact of albumin on the internalization of CPP-PLL-g-PEG/GOX complexes by macrophage cells was determined (Figure 4.5B). All albumin-bound complexes were susceptible to uptake by macrophages, with the greatest fluorescence being detected for the Tat- and LMWP-functionalized complexes. When the complexes were pre-incubated with an excess of denatured albumin, however, the uptake of the complexes slightly decreased, but this was only statistically significant for LMWP-PLL-g-PEG/GOX complexes.

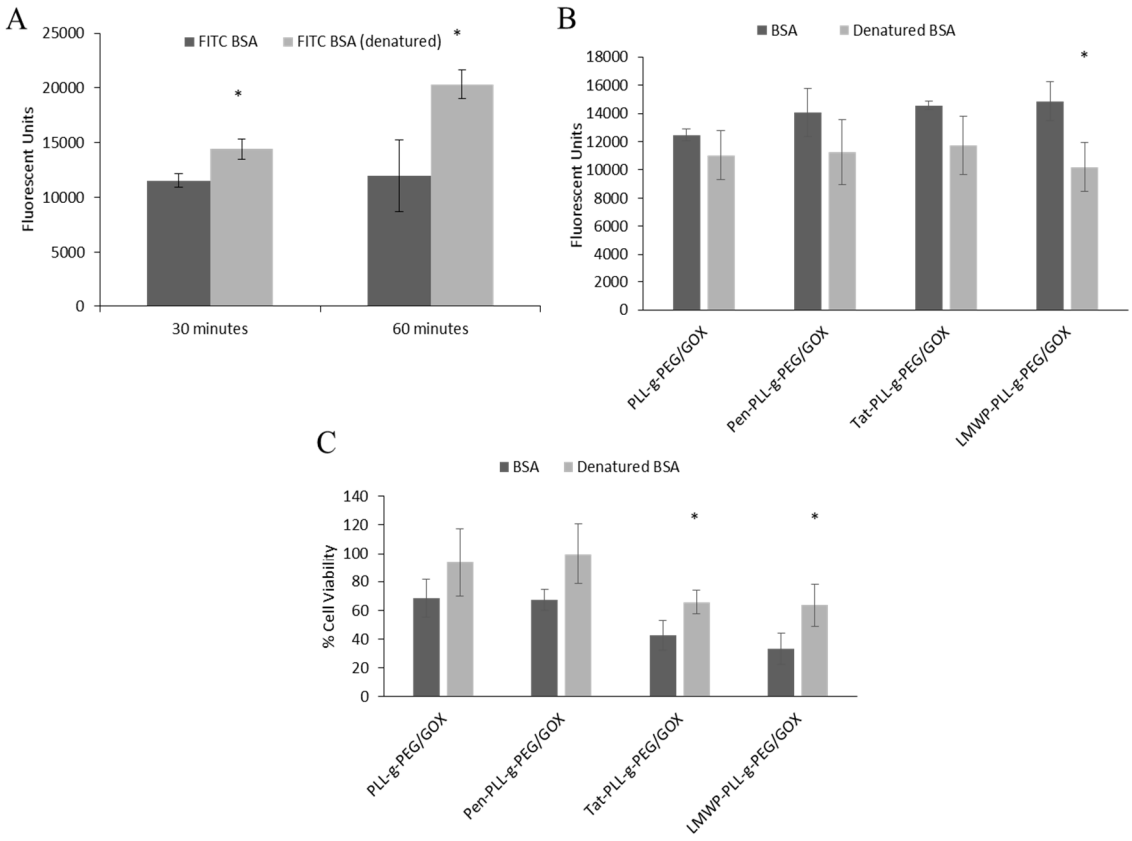

Figure 4.5. Impact of Albumin Denaturation on Macrophage Uptake of CPP-PLL-g-PEG/GOX Complexes. A. Evaluation of RAW 264.7 uptake of FITC labeled albumin and denatured (boiled) FITC albumin after 30 and 60 minutes. Trypan Blue was used to quench extracellular fluorescence. B. Evaluation of RAW 264.7 uptake of CPP-PLL-g-PEG/GOX and albumin/CPP-PLL-g-PEG/GOX complexes, encapsulating FITC GOX, in the presence of cell culture concentrations of albumin or denatured albumin. Trypan Blue was used to quench extracellular fluorescence. C. Cell viability of RAW 264.7 cells after 30 minute incubation with CPP-PLL-g-PEG/GOX in the presence of excess albumin and denatured albumin. The Cell Titer Blue cell viability assay was used to determine cell viability. * indicates a difference between two groups with $p<0.05$ as determined by the Student's T-test.

Additionally, as GOX is a cytotoxic protein, we expected that if the uptake of GOX could be blocked by saturating the uptake of the complexes with denatured albumin, the viability of the macrophage cells could be improved by adding an excess of denatured albumin to the cells with the complexes (Figure 4.5C). All CPP-PLL-g-PEG/GOX complexes showed significant cytotoxicity to macrophage cells in the presence of albumin. The largest reduction of cell viability occurred for macrophages

treated with Tat- and LMWP-functionalized CPP-PLL-g-PEG/GOX complexes. When an excess of denatured albumin was added to the cells with the CPP-PLL-g-PEG/GOX complexes, the viability of the macrophage cells improved, with the most significant denatured albumin protection occurring for the Tat- and LMWP-functionalized complexes. This suggests that an excess of denatured albumin reduced the ability of the macrophage cells to take up the complexes, indicating that albumin denaturation plays a role in uptake.

4.4. Discussion

CPPs are emerging as promising carriers to facilitate the transport of biomacromolecules and nanoparticles into the cell interior [49]. Understanding what CPP characteristics tend to lead to off-targeted uptake will be important in the design of CPP-functionalized nanocarriers which avoid macrophage uptake. Macrophages are an important part of the immune system that remove damaged cells, cellular components, and harmful pathogens from the body [278]. Although they play this important role, they are also a barrier toward the application of novel nanomedicines *in vivo* due to their role in removal of nanomedicines from circulation [71]. In this work, we aimed to better understand how macrophages take up nanocarriers that are functionalized with CPPs, and the role that albumin may play in this uptake.

In this work, we used GOX as part of a model CPP-functionalized delivery system to study the interaction of CPPs with albumin, and the effect of CPP interaction with albumin on macrophage uptake. When combined with PLL-g-PEG, GOX associated with the copolymer into nanoscale complexes, as determined by the decrease in GOX

mobility in PAGE as well as an increase in particle size to from approximately 9 nm to 20 nm (Figure 4.1). This is a similar increase in particle size from that observed in earlier works by our group and others in which complexation of bovine serum albumin and buturylcholinesterase resulted in nanoscale complexes of about 20-30 nm in size [9, 36, 37, 43]. Additionally, the particle size is similar to that of when Kawamura et al. used GOX to form nanoscale complexes with another cationic polymer, polyethylene glycol-grafted-poly(allyl amine) for potential use in glucose sensors [279]. With the formation of PLL-g-PEG/GOX, the complexes were functionalized with several CPPs in order to understand how CPP characteristics affect the interaction of these complexes with albumin and what effect this interaction has on macrophage uptake.

Albumin binds to CPP-PLL-g-PEG/GOX complexes which results in albumin denaturation. Incubation of CPP-PLL-g-PEG/GOX with BSA resulted in albumin binding to the complexes (Figure 4.2). Albumin in the protein corona of nanoparticles has been found to be subject to changes in conformation, with highly charged cationic or anionic particles leading to denaturation of the protein. This was observed by Fleischer and Payne for cationic polystyrene nanoparticles and by Yan et al. for anionic polymethacrylic acid nanoparticles [57, 60]. We similarly observed that CPPs also cause denaturation of albumin (Figure 4.2). The extent of albumin denaturation induced by CPPs tended to increase with arginine content of the CPPs, with Pen (three arginine residues) denaturing albumin the least and LMWP (ten arginine residues) denaturing albumin the most. The increase in albumin denaturation with increasing charge and arginine content is consistent with the work of others that observed albumin denaturation when bound to cationic nanoparticles [57, 60].

CPP-PLL-g-PEG/GOX and BSA/CPP-PLL-g-PEG/GOX complexes were taken up by macrophage cells (Figures 4.3 and 4.4). Uptake pathway studies showed that the CPP functionalized complexes tended to follow either a clathrin- or caveolae-mediated uptake pathways, depending on which CPP was used to functionalize the complexes. Non-endocytic uptake of the complexes were also possible. The addition of albumin, as part of the protein corona of the complexes, tended to shift this uptake pathway to more strongly favor caveolae-mediated endocytosis. Caveolae-mediated endocytosis is associated with the endocytosis of several types of receptor-ligand interactions [280]. This suggests the possibility that the uptake of the BSA/CPP-PLL-g-PEG/GOX complexes are internalized by macrophages using a receptor for denatured albumin.

Others have found that albumin denaturation as part of a nanoparticle protein corona was associated with uptake by scavenger receptors, through inhibition with poly-inosinic acid [57, 60]. Although scavenger receptor uptake is often associated with phagocytosis, scavenger receptors have been shown to participate in other routes of endocytosis as well, including caveolae-mediated endocytosis [281, 282]. This suggest that scavenger receptors potentially play a role in the uptake of albumin bound CPP-PLL-g-PEG/GOX complexes.

Macrophage uptake of CPP-PLL-g-PEG/GOX complexes through albumin denaturation occurred if the CPP caused sufficient albumin denaturation. To determine the involvement of albumin denaturation of BSA/CPP-PLL-g-PEG/GOX complexes in their uptake by macrophages, excess denatured albumin was used to saturate receptors associated with the uptake of the denatured protein to inhibit uptake of the albumin bound complexes (Figure 4.5). Albumin denatured on its own was found to be taken up to a

greater extent than non-denatured albumin. This is in agreement with earlier studies that showed that phagocytic cells take up denatured albumin more than non-denatured albumin [267]. When an albumin protein corona was formed around CPP-PLL-g-PEG/GOX complexes, a slight, non-statistically significant, increase in the uptake of most of the complexes was observed, but the overall uptake was largely comparable to that in albumin-free medium. The uptake of the complexes by macrophage cells tended to decrease, however, when an excess of denatured albumin was present along with the CPP-PLL-g-PEG/GOX complexes. This effect was only significant, however, for LMWP-functionalized complexes ($p<0.05$), which were also observed to cause the greatest extent of albumin denaturation of the CPPs compared to non-functionalized complexes ($p<0.05$). The ability to inhibit the uptake the complexes with denatured albumin suggest that albumin denaturation could contribute to the uptake of CPP-PLL-g-PEG/GOX complexes by macrophage cells if sufficient denaturation occurs.

The uptake of the complexes and the denaturation of albumin appears to be correlated to arginine content of the CPPs. Arginine content, within CPPs, is known to play an important role in the ability of the peptide to become internalized [283]. The number of arginine residues, and likely overall charge of the peptide, may also affect how the peptide interacts with multiple amino acids within albumin and cause changes in protein structure. Additional investigation is needed to more clearly separate the effect of charge and arginine content on protein denaturation. While this study only investigated the effect of CPP-functionalized complexes on albumin denaturation, it is likely that CPPs have the potential to denature other proteins that would form a protein corona around the complexes as well. Nanoparticles have been shown to induce denaturation of

other proteins, besides albumin, such as γ-globulin and insulin [74]. Additionally, complement proteins, such as C3, have been demonstrated to preferentially bind to denatured plasma proteins, resulting in their clearance from plasma [284]. This suggest that denaturation of albumin bound to CPP-PLL-g-PEG/GOX could potentially initiate the binding of complement type proteins, in addition to other proteins that may form a protein corona, and this denaturation could also contribute to clearance of the complexes by the immune system in an *in vivo* environment. Additional studies will be needed in subsequent work to better understand how CPP-induced albumin denaturation could contribute to the binding of other serum proteins to the complexes. Although the denaturation of albumin by CPP-PLL-g-PEG/GOX complexes was shown to alter how the complexes interact with immune cells *in vitro*, the effect of albumin denaturation on other aspects of the immune response and clearance of the complexes *in vivo* are also needed in future work.

4.5. Conclusions

The CPPs Pen, Tat, and LMWP were used to functionalize PLL-g-PEG/GOX complexes, which were then used to better understand how CPPs interact with albumin. Each of the CPP-PLL-g-PEG/GOX complexes were found to denature albumin, with greater denaturation of albumin occurring with increasing charge and arginine content of the CPP. Albumin denaturation by CPPs resulted in uptake of CPP-PLL-g-PEG/GOX complexes by macrophages, primarily through caveolae-mediated endocytosis. Excess denatured albumin was found to inhibit uptake of the CPP-PLL-g-PEG/GOX complexes, suggesting receptor-mediated uptake of the complexes through the binding of denatured albumin, which is likely mediated through scavenger receptors. These results indicate

that CPPs with high charge or arginine content could be more likely to be taken up by macrophage cells. Although a wide variety of factors should contribute to selection and design of CPPs for the delivery of nanotherapeutics, the ability to avoid macrophage uptake and to have reduced impact on serum proteins should play an important role in the selection of CPPs for therapeutic delivery applications.

CHAPTER V

INTRACELLULAR DELIVERY OF GLUCOSE OXIDASE FOR ENHANCED CYTOTOXICITY TO PSMA EXPRESSING PROSTATE CANCER CELLS.

5.1 Introduction

Hydrogen peroxide and other reactive oxygen species (ROS), although naturally occurring as part of mammalian cell metabolic processes, are also potently cytotoxic [285]. ROS causes cytotoxicity through oxidative damage to biomolecules essential to normal cellular function, such as proteins, lipids, and DNA [78, 286-288]. Due to the cytotoxicity of ROS, the delivery of ROS or similar oxidative therapies has long been investigated in efforts to broaden and improve the strategies available to treat cancer [79-81, 289, 290].

Although ROS has been of interest as an anticancer agent, the delivery of ROS to cancer cells and tumors is not trivial. Previous work has found that the delivery of ROS generators, rather than ROS itself, is the most practical approach to cause oxidative damage to cancer cells [80]. This approach was pioneered by Nathan & Cohn and Ben-Yoseph & B.D. Ross in which microspheres containing glucose oxidase (GOX) and PEGylated GOX, respectively, were previously used as peroxide generators in order to

inhibit the growth of tumors in mice [79, 80]. GOX catalyzes the oxidation of β-D-glucose, forming gluconic acid and hydrogen peroxide as products [291]. Ben-Yoseph & Ross found that PEGylated GOX was effectively cytotoxic to cancer cells *in vivo*, but due to the ubiquitous presence of glucose throughout the body, the use of antioxidant enzymes were also required to counter systemic toxicity [79].

Recent work has emphasized the importance of localizing peroxide formation to the tumor tissue. To better control the delivery of peroxide formers, Fang et al. locally administered D-proline after i.v. injection of PEGylated D-amino acid oxidase, the substrate for another peroxide forming enzyme, where significant improvements in survival were demonstrated in mice bearing tumors of S-180 sarcoma cells [292]. Fan et al. used organosilica particles loaded with GOX and L-arginine to co-generate nitrous oxide and hydrogen peroxide to inhibit tumor growth [293]. Although GOX and other oxidases have been found to show strong potential to inhibit tumor growth when PEGylated or loaded into particles near cancer cells or within a tumor, it is unclear if the oxidase cytotoxicity could be further enhanced if the enzyme were taken up by cancer cells, rather than delivered locally to the cells. To determine if binding and intracellular delivery of GOX and other oxidases can potentially enhance their cytotoxicity, alternative strategies to deliver these cytotoxic proteins are needed.

Cationic polymers, such as polylysine, polyethyleneimine, and polyamidoamine, have been used to modify and package numerous biomacromolecules, including nucleic acids and proteins [21, 294]. Charged copolymers and polyethylene glycol (PEG) have been found to be capable of electrostatic self-assembly with nucleic acids and proteins into nanoscale complexes [27, 295]. Complexation with PEGylated cationic copolymers

has been shown to improve aspects of delivery, including resistance to heat denaturation, protease degradation, stimuli-responsive delivery, as well as the ability functionalize proteins and DNA without covalent modifications, which are potentially deactivating [36, 43, 296]. This approach has been successfully applied toward the encapsulation of proteins such as bovine serum albumin, butyrylcholinesterase, lysozyme, insulin, superoxide dismutase and others to modify how these proteins are delivered [9, 31, 36, 297]. PEGylated cationic copolymers have been shown to permit proteins, as well as DNA, to cross the cell membrane, enabling delivered proteins to have activity within the intracellular space [29, 298].

In this study, we aimed to enhance the cytotoxicity of GOX by delivering it intracellularly to prostate cancer cells expressing the prostate specific membrane antigen (PSMA). Prostate cancer cells express higher amounts of PSMA compared to healthy prostate cells [299-301]. PSMA is expressed at even higher levels when prostate cancer becomes androgen independent and the risk of metastasis increases [299]. Therefore, PSMA may be exploited to preferentially deliver a therapeutic, such as GOX or other drugs, to prostate cancer cells compared to healthy cells by using an anti-PSMA antibody [302]. We hypothesize that binding and internalization of oxidase enzymes directly to prostate cancer cells can potentially enhance the cytotoxicity of ROS-forming enzymes because the peroxides generated are likely cause more oxidative damage within the intracellular space. In this study, conditions were first identified that lead to effective association of GOX to the cationic copolymer poly-L-lysine-g-polyethylene glycol (PLL-g-PEG), while retaining maximum enzyme activity. The PLL-g-PEG copolymer was then functionalized with monoclonal anti-PSMA monoclonal antibody to improve PLL-g-

PEG/GOX binding and internalization into PSMA expressing cancer cells. The ability of anti-PSMA-PLL-g-PEG/GOX to generate ROS and cause cytotoxicity was then compared to unmodified GOX *in vitro* to determine if strategies to enhance binding and internalization of ROS- generating enzymes can be used to enhance their potency.

5.2. Materials and Methods

Glucose oxidase from *Aspergillus Niger* (cat.# G7141), poly-l-lysine (PLL) (15-30 kDa) (cat.# P7890), dithiothreitol (DTT), 2',7' dichlorofluorescein diacetate (DCFHDA), fluorescein isothiocyanate (FITC) and the anti-PSMA monoclonal antibody clone 3A/12 (cat.# MABC291) were purchased from Sigma Aldrich (St. Louis, MO). Polyethylene glycol (2 kDa mPEG-NHS and 5 kDa, maleimide-PEG-NHS) was purchased from Creative PEGworks (Winston Salem, NC). Pierce centrifugal concentrators (10 kDa and 100 kDa), D-glucose, RPMI-1640 cell culture medium, Kaighn's F-12K cell culture medium, fetal bovine serum, acrylamide and other chemicals needed for electrophoresis were purchased from Fisher Scientific (Hampton, NH). LNCaP and PC-3 cells were purchased from ATCC (Manasses, VA). Cell Titer Blue was purchased from Promega Corporation (Madison, WI). Phosphate buffered saline (PBS, pH 7.4) was made in-house.

5.2.1 Copolymer Synthesis

Poly-l-lysine-grafted-polyethylene glycol was synthesized using previously described methods [9]. Briefly, 15 mg of PLL was dissolved in 200 ul of PBS. Next, 40 mg of a 50/50 (w/w) mixture of 2kDa mPEG-NHS and 5kDa maleimide-PEG-NHS was added to the dissolved PLL. The mixture was allowed to incubate for one hour before a 10 kDa Pierce centrifugal concentrator was used to wash unreacted polymer from the PLL-g-

PEG-maleimide. The polymer was then dried and stored at -20°C until use. H^1-NMR was used to determine the PEG grafting ratio onto the PLL backbone. An aliquot of polymer was dissolved in D_2O and H^1-NMR spectroscopy was performed on a Bruker INOVA 400 NMR spectroscope. The PEG:PLL grafting ratio was then determined by integrating the peaks of the PEG linkage to PLL ε-amino groups at 2.55 ppm and the H-peak of PLL α- carbons at 4.2 ppm [270]. The ratio of the two integrated peaks was then used to calculate grafting ratio.

5.2.2 Formation of Anti-PSMA-PLL-g-PEG/GOX

PLL-g-PEG/GOX complexes were formed using previous methods to associate cationic copolymers with proteins [9]. Varying concentrations of PLL-g-PEG (25µl) were slowly added to GOX dissolved in PBS (2 mg/ml, 25 µl), while gently vortexing. The mixture was allowed to incubate for one hour at room temperature before the complexes were cross-linked to aid in their stability. To cross-link PLL-g-PEG/GOX, various concentrations of glutaraldehyde (5 µl) were added to the complexes and allowed to incubate for three hours at room temperature. PLL-g-PEG/GOX was then functionalized with partially reduced anti-PSMA monoclonal antibody as described below.

Using methods described by Mahmoud et al., anti-PSMA monoclonal antibody was partially reduced using DTT to generate free thiol groups to enable conjugation of the antibody to PLL-g-PEG/GOX [303]. DTT was added to 50 µg of the anti-PSMA monoclonal antibody to a final concentration of 20 mM and allowed to incubate at 37°C for 30 minutes. For conjugation, the antibody was added to PLL-g-PEG/GOX complexes at a 1:1 mass ratio and allowed to incubate 30 minutes before washing with a 100 kDa

centrifugal concentrator. The complexes were then either used immediately or stored at 4°C overnight before use.

5.2.3 Association of PLL-g-PEG to GOX

To determine if PLL-g-PEG associates with GOX, unmodified GOX and non-crosslinked PLL-g-PEG/GOX (5 μg) were applied to non-denaturing 8% PAGE gels, and electrophoresis was performed on a Bio-Rad Mini-PROTEAN Tetracell gel electrophoresis system at 200V. After approximately 45 minutes, the non-denaturing gels were stained with Coomassie G-250 to visualize protein migration.

SDS-PAGE (denaturing) was used to identify cross-linking conditions that would result in complexes resistant to protein release. Unmodified GOX and PLL-g-PEG/GOX cross-linked with varying concentrations of glutaraldehyde were applied to the gel (5 μg), and electrophoresis was performed on a Bio-Rad Mini-PROTEAN Tetracell gel electrophoresis system at 200V. After approximately 45 minutes, the SDS-PAGE gels were stained with Coomassie G-250 to visualize protein migration. SDS-PAGE was also used, following the same methods, to determine the size of antibody fragments (after the DTT reduction described above).

5.2.4 PLL-g-PEG/GOX Enzymatic Activity

The retention of GOX activity following PLL-g-PEG/GOX formation was evaluated with 2',7' dichlorofluorescein diacetate (DCFHDA) as a fluorescent indicator of the generation ROS, using methods from the work of LeBel et al. [304]. A stock solution of DCFHDA was first dissolved in ethanol (1 mM) before being further diluted in water (0.2 mM) and allowed to incubate 30 minutes in the dark. DCFHDA solution (5 μM), $FeSO_4$

(10 μM) and glucose (10 mM) were then combined in PBS as a substrate solution for the assay. The substrate mixture was then added to GOX or PLL-g-PEG/GOX complexes (50 μg/ml normalized to GOX), and allowed to incubate 30 minutes in the dark. Fluorescence intensity (ex: 495 nm/ em: 535 nm) corresponding to ROS production was then measured using a Beckman Coulter DTX880 Multimode Detector.

5.2.5 Anti-PSMA-PLL-g-PEG/GOX Physicochemical Characterization

The physicochemical properties of PLL-g-PEG/GOX were determined using dynamic light scattering (DLS) to determine the complex size, and phase analysis light scattering (PALS) to determine the surface charge [9]. A Brookhaven Instrument Corporation ZetaPALS ζ-potential analyzer was used for both measurements. Briefly, a 60 μl aliquot of PLL-g-PEG/GOX was loaded into the instrument. Triplicate measurements consisting of at least five runs per measurement, with each run lasting 2 minutes, were used to determine the hydrodynamic diameter and polydispersity of the complexes. The surface charge of the complexes was measured using PALS. PLL-g-PEG/GOX complexes were diluted to a volume of 1.5 ml using PBS (pH 7.4). The ζ-potential was calculated from mobility using Smoluchowski's equation [243]. Measurements were taken in triplicate, with each measurement consisting of 10 runs and each run lasting one minute.

5.2.6 Prostate Specific Membrane Antigen (PSMA) Targeting

Anti-PSMA-PLL-g-PEG/GOX cytotoxicity against PSMA expressing LNCaP cells and non-PSMA expressing PC-3 cells was used evaluate the effect of PSMA receptor targeting. LNCaP and PC-3 cells were cultured in RPMI 1640 and Kaighn's F-12K medium supplemented with 10% fetal bovine serum (FBS), respectively, at 37°C

and 5% CO_2 before use. For experiments, LNCaP and PC-3 cells (1×10^4 cells/well) were cultured on 96-well plates one day before beginning the experiment. The LNCaP and PC-3 cells (60% confluency) were then treated with GOX, PLL-g-PEG/GOX, or antiPSMA-PLL-g-PEG/GOX at 10 μg/ml for 30 minutes in serum containing medium. The cells were then washed and their medium replaced before they were incubated another 24 hours. The cell viability was determined using the Cell Titer Blue assay following the manufacturer's suggested protocol.

5.2.7 Anti-PSMA-PLL-g-PEG/GOX Cytotoxicity in Serum

To determine how the presence of serum affects anti-PSMA-PLL-g-PEG/GOX cytotoxicity toward PSMA-expressing LNCaP cells, cell viability was assed using the Cell Titer Blue cell viability assay. LNCaP cells were grown to approximately 70% confluency in RPMI 1640 with 10% FBS in 5% CO_2 before seeding on a 96-well plate at a density of 1×10^4 cells/well. After approximately 24 hours of incubation, the LNCaP cells were treated with PLL-g-PEG/GOX or anti-PSMA-PLL-g-PEG/GOX (5 μg/ml) in RPMI 1640 medium with either 0% or 10% FBS. The cells were exposed to the complexes for 30 minutes before they were removed, then the cells washed and the medium replaced with fresh RPMI 1640 medium with FBS. The cells were allowed to incubate for 2, 4, and 24 hours before Cell Titer Blue was used to assess cell viability following the manufacturer's suggested protocol.

5.2.8 Anti-PSMA-PLL-g-PEG/GOX Generation of ROS

To determine if anti-PSMA-PLL-g-PEG/GOX cause oxidative damage to LNCaP cells, a DCFHDA assay was used to measure the intracellular generation of ROS. LNCaP

cells were grown to approximately 70% confluency in RPMI 1640 with 10% FBS in 5% CO_2 before seeding on a 96-well plate at a density of 1×10^4 cells/well. After 24 hours, the cells were treated with 10 μM DCFHDA using methods described by Eruslanov et al. for detection of ROS [305]. DCFHDA was first dissolved in DMSO (10 mM) to produce a stock solution. Working concentrations of DCFHDA were produced by further dissolving DCFHDA stock solution in serum-free RPMI medium (10 μM). The LNCaP cell medium was then replaced with the RPMI medium with DCFHDA. After 30 minutes of incubation at 37°C, the DCFHDA was removed, the cells were washed, and fresh medium containing serum was added to the cells. Then the cells were treated with PLL-g-PEG/GOX and antiPSMA-PLL-g-PEG/GOX for 30 minutes. The complexes were then removed, the cells washed, and the medium replaced with fresh medium. Trypan blue (0.1%) was added to the cells to quench extracellular fluorescence before measurements [276, 277]. The generation of ROS was detected fluorometrically over 24 hours using a Beckman Coulter DTX880 Multimode Detector (ex: 495 nm/em: 535 nm).

5.2.9 Visualization of Anti-PSMA-PLL-g-PEG/GOX Uptake

Fluorescence microscopy was used to visualize anti-PSMA-PLL-g-PEG/GOX uptake into LNCaP cells. Prior to complex synthesis, GOX was labeled with FITC using the manufacture's recommended protocol. The FITC-labeled GOX was used make PLL-g-PEG/GOX and anti-PSMA-PLL-g-PEG/GOX complexes as earlier described. LNCaP cells (2×10^5 cells) were seeded onto polylysine coated glass coverslips in 6-cm cell culture dishes. After incubating 24 hours, FITC-labeled GOX, PLL-g-PEG/GOX, and anti-PSMA-PLL-g-PEG/GOX (5 μg/ml) were then added to the cells in serum-free medium and allowed to incubate for 30 minutes at 37°C. Following 30 minutes of

exposure, the cell culture medium was removed and the cells washed with PBS to remove unbound complexes. The treated cells were then either fixed immediately or were allowed to incubate for 4 or 24 hours before fixation. The cells were treated with 4% formaldehyde for 15 minutes for fixation before a second wash with PBS. The glass coverslips were mounted using DAPI ProLong Gold antifade mounting medium (Life Technologies) on glass microscope slides. The cells were imaged with a Nikon Eclipse TE2000-U fluorescent microscope.

5.2.10 Anti-PSMA-PLL-g-PEG/GOX Uptake Pathway

To better understand how anti-PSMA-PLL-g-PEG/GOX is internalized by LNCaP cells, the mechanism of uptake of by the complexes was evaluated using pharmacological inhibitors with methods described by Keswani et al. [274]. LNCaP cells were grown to approximately 70% confluency in RPMI 1640 supplemented with 10% FBS before being seeded on 96-well plates at a density of 1×10^4 cells/well. Prior to uptake studies, the cytotoxicity of each inhibitor toward LNCaP cells was determined in order to treat the cells with the maximum amount of inhibitor without reducing cell viability below 90% [274]. The maximum concentration of inhibitor tolerable to the cells was then used for uptake studies. Approximately 24 hours after seeding LNCaP cells, the cell medium was replaced with serum-free RPMI 1640, two hours before addition of anti-PSMA-PLL-g-PEG/GOX. To inhibit macropinocytosis, clathrin-dependent endocytosis, and caveolae-dependent endocytosis, LNCaP cells were treated with amiloride (2.5 μg/ml), chlorpromazine (3 μg/ml), and genestein (1.7 μg/ml), respectively, one hour prior to the addition of the NP complexes [280]. Anti-PSMA-PLL-g-PEG/GOX (5 μg/ml) was then allowed to incubate with the cells for 30 minutes, then the cells were washed, and the

medium was replaced with fresh RPMI 1640 medium containing serum. The uptake of antiPSMA-PLL-g-PEG/GOX was determined through their cytotoxic activity toward the LNCaP cells, with the Cell Titer Blue assay being used to determine cell viability 24 hours after addition of the complexes.

5.3. Results

5.3.1Anti-PSMA-PLL-g-PEG/GOX Formation

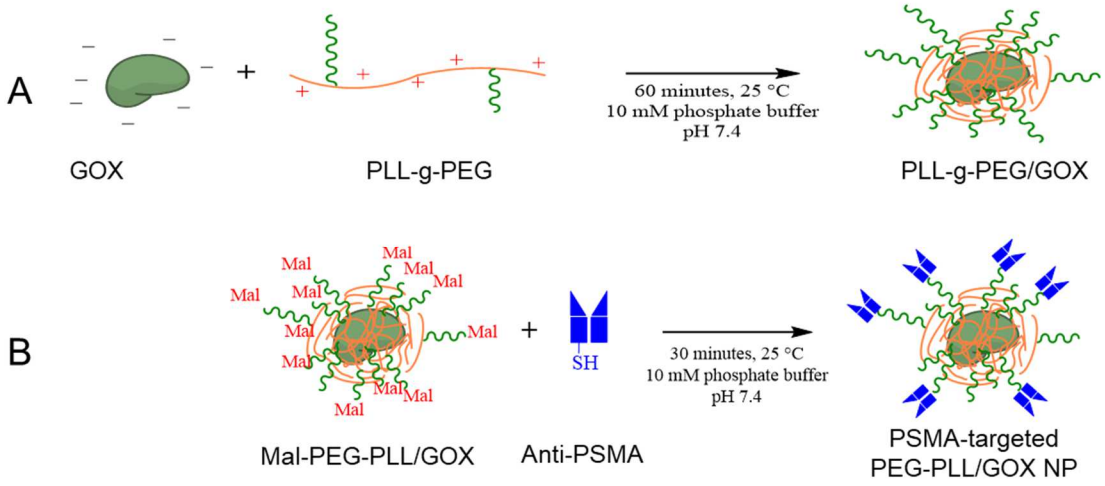

Figure 5.1 Anti-PSMA-PLL-g-PEG/GOX Synthesis Scheme. A. Electrostatic interaction was used to associate PLL-g-PEG to GOX. PLL-g-PEG/GOX was then crosslinked with glutaraldehyde. B. PLL-g-PEG GOX was then functionalized with anti-PSMA monoclonal antibody through conjugation of the reduced antibody with cysteine groups with maleimide groups of the PLL-g-PEG.

PLL-g-PEG-Mal was first synthesized in preparation for producing anti-PSMA-PLL-g-PEG/GOX. H^1 NMR spectroscopy (Appendix, S1) confirmed PEG conjugation onto PLL, with a grafting ratio of approximately 10 PEG chains to each PLL chain. PLL-g-PEG was then able to be complexed with GOX as described in Figure 5.1A through electrostatic attraction between PLL ϵ-amino groups and negatively charged residues on GOX. To determine an effective range at which PLL-g-PEG associates with GOX, PLL-g-PEG was added to the enzyme at different copolymer to protein (C:P) ratios. Native PAGE (non-denaturing) was then used to evaluate association of the polymer with the

protein through the lack of protein migration into the gel. In Figure 5.2A, the protein corresponding to GOX disappeared upon addition of PLL-g-PEG at a 1:1 C:P ratio. GOX was also unable to migrate through the gel at higher C:P, indicating that PLL-g-PEG associates with GOX at C:P ratios from 0.37:1-7:1. We proceeded with a C:P ratio of 7:1 to reduce the number of potential samples for later studies.

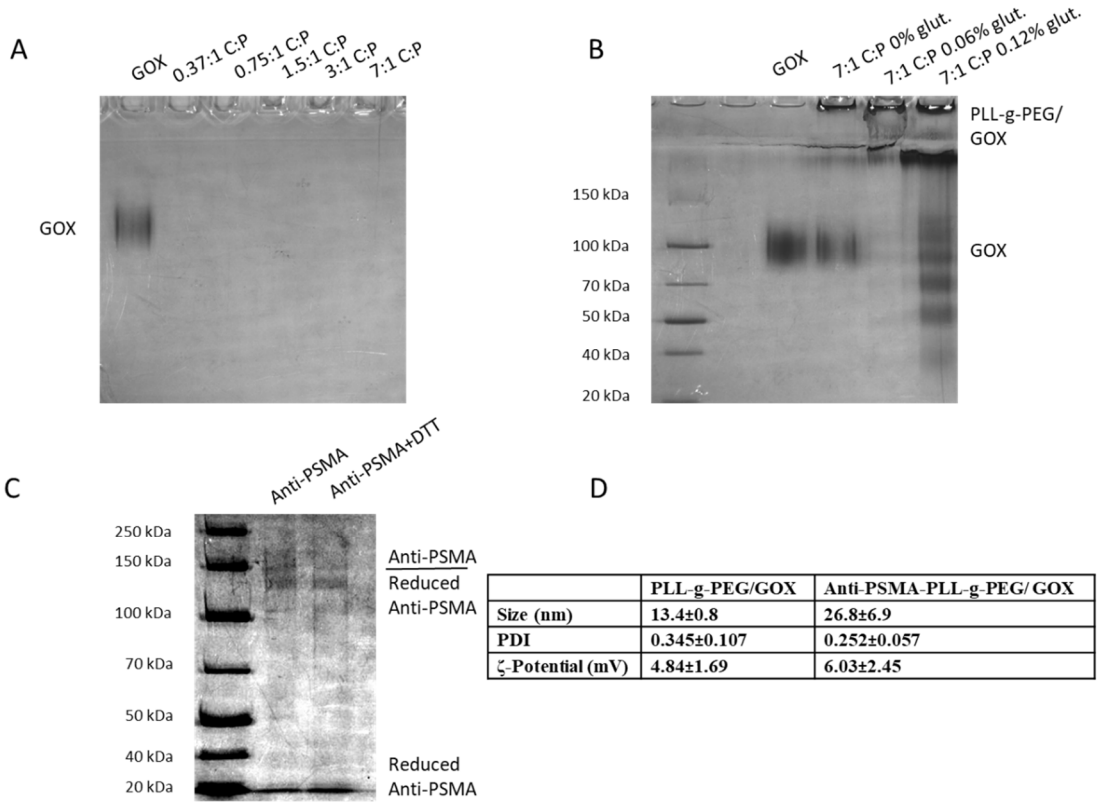

	PLL-g-PEG/GOX	Anti-PSMA-PLL-g-PEG/ GOX
Size (nm)	13.4±0.8	26.8±6.9
PDI	0.345±0.107	0.252±0.057
ζ-Potential (mV)	4.84±1.69	6.03±2.45

Figure 5.2. Characterization of AntiPSMA-PLL-g-PEG GOX. A. Native PAGE of GOX combined with PLL-g-PEG. Lane 1: Free GOX; Lane 2: 0.37:1 C:P PLL-g-PEG/GOX; Lane 3: 0.75:1 C:P PLL-g-PEG/GOX; Lane 4: 1.5:1 C:P PLL-g-PEG/GOX; Lane 5: 3:1 C:P PLL-g-PEG/GOX; Lane 6: 7:1 C:P PLL-g-PEG/GOX. B. SDS- PAGE of GOX combined with PLL-g-PEG. Lane 1: Ladder; Lane 2: Empty; Lane 3: Free GOX; Lane 4: 7:1 C:P PLL-g-PEG/GOX with 0% glutaraldehyde; Lane 5: 7:1 C:P PLL-g-PEG/GOX with 0.06% glutaraldehyde; Lane 6: 7:1 C:P PLL-g-PEG/GOX with 0.12% glutaraldehyde. C. AntiPSMA antibody sulfydryl reduction using DTT after 37°C for 30 minutes. Lane 1: Ladder; Lane 2: AntiPSMA antibody; Lane 3: Reduced antiPSMA antibody. D. Physicochemical properties of antiPSMA PLL-g-PEG/ GOX determined using DLS and PALS.

After identifying conditions at which PLL-g-PEG would associated to GOX, PLL-g-PEG/GOX was cross-linked with glutaraldehyde to make them resistant to protein release under physiological conditions. SDS-PAGE was used to determine the cross-linking conditions at which PLL-g-PEG would remain associated with glucose oxidase (GOX) under denaturing conditions (Figure 5.2B). Under denaturing conditions, non-crosslinked GOX was unable to remain fully associated with PLL-g-PEG as a protein band of similar density migrated the same distance as unmodified GOX (lane 4). Upon addition of 0.06% glutaraldehyde, GOX was able to remain fully associated the PLL-g-PEG (lane 5).

5.3.2 Anti-PSMA-PLL-g-PEG/GOX Characterization

Once conditions were identified that would lead to effective encapsulation of GOX to form PLL-g-PEG/GOX, the complexes were functionalized with the anti-PSMA antibody to enhance the binding and uptake of the complex by LNCaP cells. Anti-PSMA was partially reduced to expose free sulfhydryl groups within the antibody. DTT reduction resulted in antibody fragments of approximately 130 kDa, 100 kDa, and 20 kDa (Figure 5.2C). FITC labeling of the antibody indicated that typically one antibody was conjugated per eight GOX enzymes prepared as PLL-g-PEG/GOX (not shown).

DLS and PALS were used to determine particle size and ζ- potential of anti-PSMA-PLL-g-PEG/GOX (Table 5.2D). Using DLS, the size of the enzyme was found to be 9 nm, PLL-g-PEG/GOX was 15 nm, and anti-PSMA-PLL-g-PEG/GOX was 30 nm. The ζ- potential of PLL-g-PEG/GOX and anti-PSMA-PLL-g-PEG/GOX were found to be near neutral with a slightly positive charge.

5.3.3 Retention of GOX Activity Following PLL-g-PEG/GOX Association

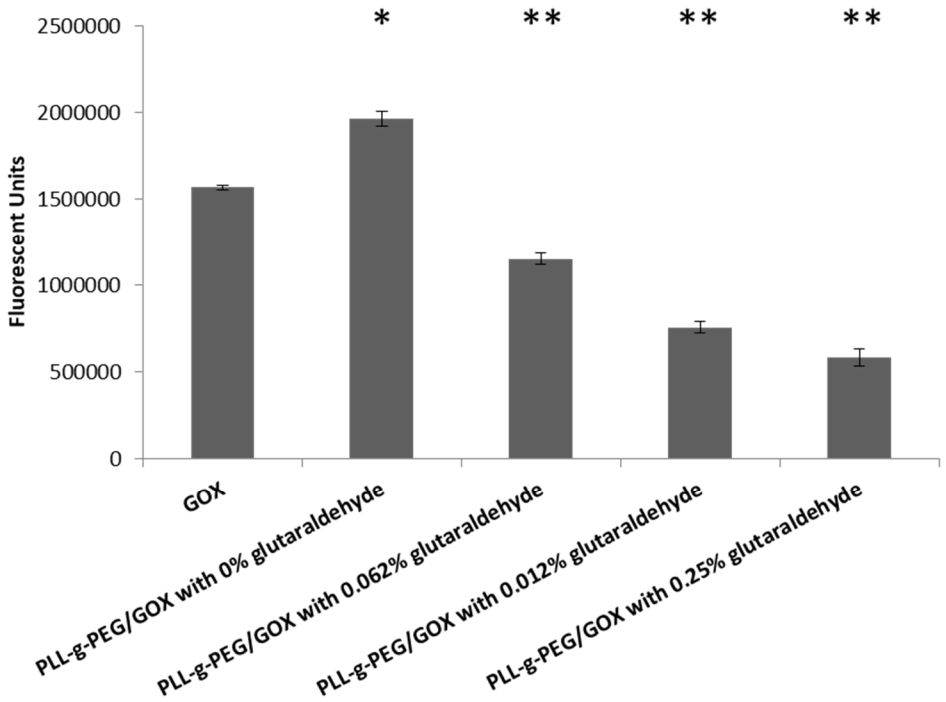

Figure 5.3. Effect of Glutaraldehyde Treatment on PLL-g-PEG/GOX Activity. The complexes were incubated with 10mM glucose as a substrate. * indicates that GOX and PLL-g-PEG/GOX with 0% glutaraldehyde had a $p<0.05$ when a Student's t-Test was used to compare differences between the groups. ** indicates that PLL-g-PEG/GOX with 0% glutaraldehyde and PLL-g-PEG/GOX with other concentrations of glutaraldehyde had a $p<0.05$ when a Student's t-Test was used to compare differences between the two groups.

To determine how PLL-g-PEG association with GOX affected the activity of the enzyme, the generation of H_2O_2 was detected using a DCFHDA assay (Figure 5.3). Association of the GOX with PLL-g-PEG was not found to negatively impact enzyme activity, as no observable reduction in fluorescence occurred. The addition of 0.06% glutaraldehyde, however, was found to reduce enzyme activity to 80% relative to the unmodified enzyme. Further increasing the amount of glutaraldehyde was found to further reduce enzymatic activity. Because effective association of the enzyme was retained under denaturing conditions with 0.06% glutaraldehyde, this concentration was used for all subsequent synthesis of GOX complexes.

5.3.4 Cytotoxicity of Anti-PSMA-PLL-g-PEG/GOX

To determine if functionalization of PLL-g-PEG with anti-PSMA alters GOX cytotoxicity toward cancerous cells, the cell viability of PSMA-expressing LNCaP and non-PSMA-expressing PC-3 prostate cancer cells was evaluated after treatment with GOX, PLL-g-PEG/GOX, and anti-PSMA-PLL-g-PEG/GOX (Figure 5.4). GOX alone did not show any significant cytotoxicity when incubated with both cells lines at a concentration of between 0.1-10 ug/ml. When GOX was combined with PLL-g-PEG, PLL-g-PEG/GOX either had no effect or only slightly reduced the viability of both cell types. When PLL-g-PEG/GOX was functionalized with anti-PSMA antibody, the viability of LNCaP cells was significantly reduced to ~35% viability ($p<0.05$) after a 30 minute exposure to the anti-PSMA-PLL-g-PEG/GOX complexes at 10 µg/ml. In contrast, PC-3 cells only had a 20% reduction in cell viability relative to the untreated cells under the same conditions.

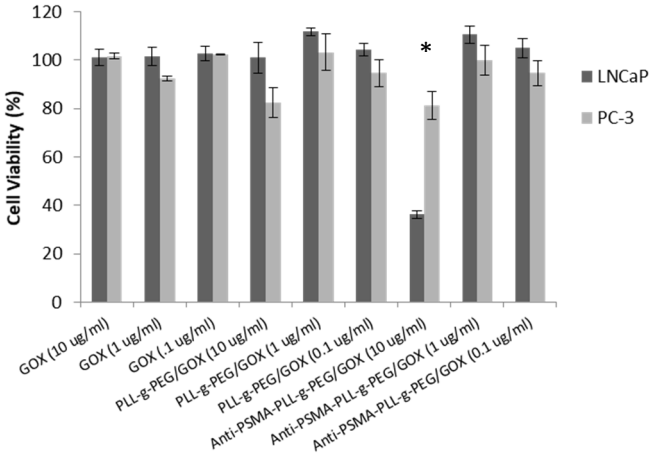

Figure 5.4. Cell viability of LNCaP (PSMA +) and PC-3 cells (PSMA -) after a 30 minute treatment with GOX, PLL-g-PEG/GOX, and Anti-PSMA-PLL-g-PEG/GOX. Each cell type was treated with either 10, 1, or 0.1 µg/ml (by GOX concentration) of each sample type. After 30 minutes, the medium over the cells was removed, washed and replaced with fresh medium. The cell viability was normalized to cells that were untreated (negative control) and cells treated with isopropanol (positive control). * indicates that differences between LNCaP and PC-3 cells had a $p<0.05$ determined by the Student's t-Test, n=3.

5.3.5 Anti-PSMA Reactive Oxygen Species Formation and Cytotoxicity

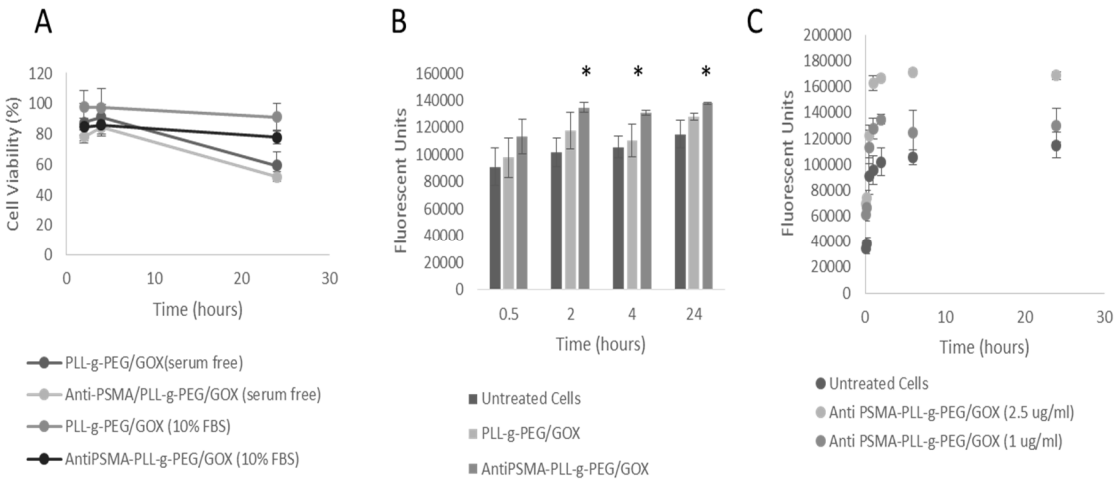

Figure 5.5. Anti-PMA-PLL-g-PEG/GOX Cytotoxicity and Generation of Reactive Oxygen Species. A. The cytotoxicity of PLL-g-PEG/GOX and anti-PSMA-PLL-g-PEG/GOX (5 µg by GOX concentration) toward LNCaP cells was evaluated over 24 hours in the presence and absence of serum, using the Cell Titer Blue cell viability assay. B. The generation of intracellular ROS within LNCaP cells after incubation with PLL-g-PEG/GOX and anti-PSMA-PLL-g-PEG/GOX (1µg by GOX concentration) was evaluated by the DCFDA assay over 24 hours. * indicates a difference with a $p<0.05$ between untreated LNCaP cells and cells treated with anti-PSMA-PLL-g-PEG/GOX, determined by the Student's t-Test. C. The generation of intracellular ROS in LNCaP cells over 24 hours by anti-PSMA-PLL-g-PEG/GOX at GOX concentrations of 1 µg/ml, and 2.5 µg/ml.

To determine if serum impacts the ability of anti-PSMA-PLL-g-PEG/GOX to induce cytotoxicity in LNCaP cells, the viability of the cells was evaluated in the presence and absence of serum (Figure 5.5A). When LNCaP cells were treated with the complexes in serum-free medium, the viability of LNCaP cells was reduced to approximately 60% after 2 hours. The viability further reduced to approximately 40% after 24 hours compared to untreated cells. The cytotoxicity of both PLL-g-PEG/GOX and anti-PSMA-PLL-g-PEG/GOX were similar to one another in serum-free conditions, with the anti-PSMA complexes being only slightly more cytotoxic (Figure 5.5A). When LNCaP cells were treated with PLL-g-PEG/GOX and anti-PSMA-PLL-g-PEG/GOX in

serum-containing medium, the cytotoxicity of both types of complexes was significantly reduced relative to serum-free conditions. PLL-g-PEG/GOX had only negligible cytotoxicity (90-100% cell viability), while anti-PSMA-PLL-g-PEG/GOX significantly reduced ($p<0.05$) cell viability compared to control cells. This suggest that, although serum prevents some of the interactions of PLL-g-PEG/GOX that induces LNCaP cytotoxicity, the anti-PSMA antibody was able to prevent a complete loss of activity of the complexes toward the LNCaP cells.

To determine if ROS are formed within the time-course that anti-PSMA-PLL-g-PEG/GOX causes cytotoxicity, a DCFDA assay was used to detect changes in ROS formation in LNCaP cells. Upon incubation with anti-PSMA-PLL-g-PEG/GOX, an increase in fluorescence associated with ROS formation was detected almost immediately after incubation compared to untreated cells (Figure 5.5B). Additionally, elevated ROS levels were detected over a similar time-course as cytotoxic effects were observed (Figure 5.5C). These results suggest that anti-PSMA-PLL-g-PEG generated intracellular ROS in conjunction with losses in cell viability.

5.3.6 Visualization of Binding and Uptake of Anti-PSMA-PLL-g-PEG/GOX

The binding and uptake of anti-PSMA-PLL-g-PEG/GOX was observed using fluorescence microscopy. In Figure 5.6A, the fluorescence of PLL-g-PEG/GOX, anti-PSMA-PLL-g-PEG/GOX were compared to unmodified GOX after four hours. LNCaP cells treated with PLL-g-PEG/GOX and anti-PSMA-PLL-g-PEG/GOX had much more FITC fluorescence compared to unmodified GOX. Anti-PSMA-PLL-g-PEG/GOX showed comparable FITC fluorescence to PLL-g-PEG/GOX, but the fluorescence was

slightly more distributed among the cells. These results demonstrate that anti-PSMA-PLL-g-PEG/GOX and PLL-g-PEG/GOX associate with LNCaP cells.

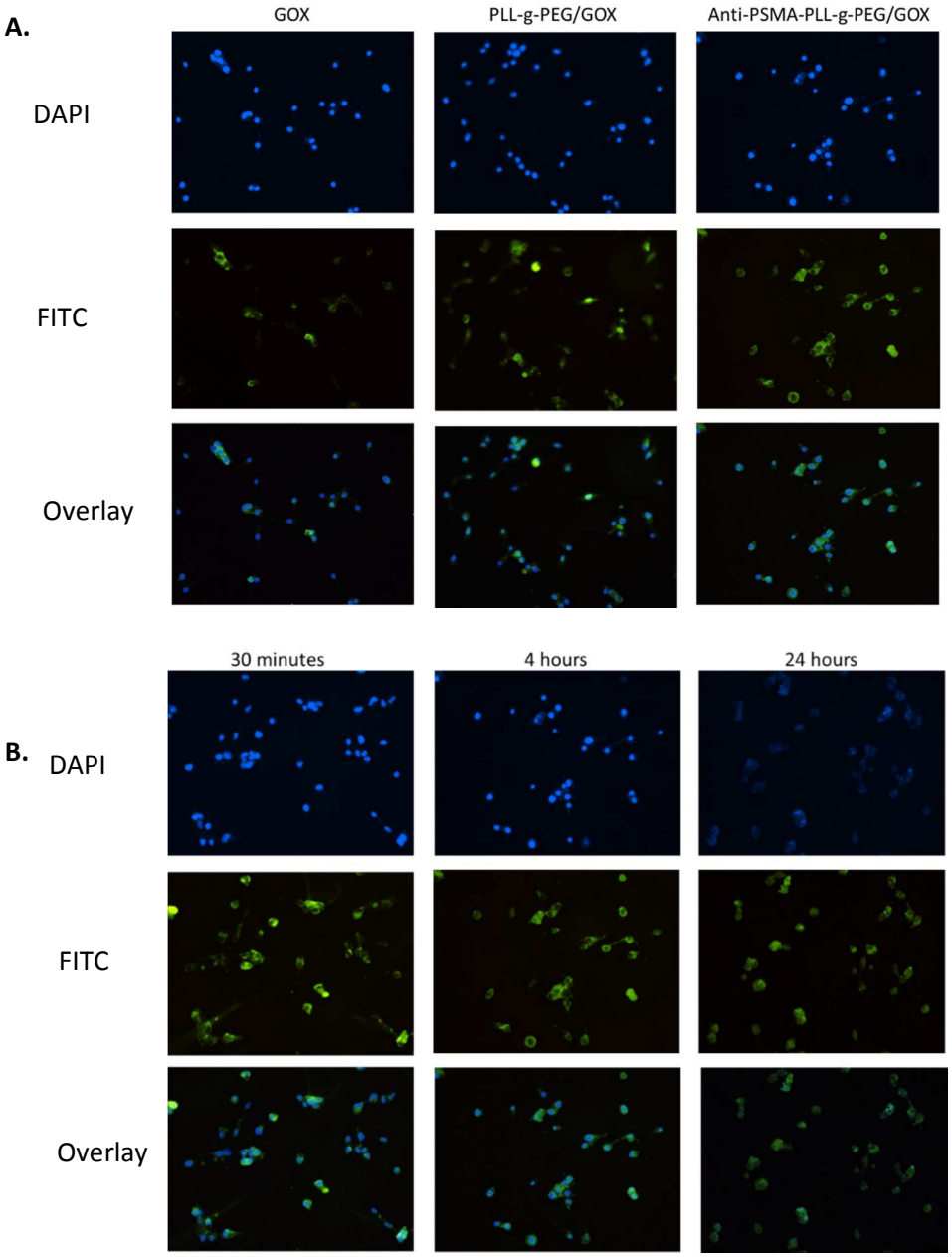

Figure 5.6. Visualization of Anti-PSMA-PLL-g-PEG/GOX Association with LNCaP Cells. Fluorescence microscopy was used to observe anti-PSMA-PLL-g-PEG/GOX association with LNCaP cells. LNCaP cell nuclei were statined with DAPI (top rows). GOX and GOX encapsulated within PLL-g-PEG/GOX and anti-PSMA-PLL-g-PEG/GOX were stained with FITC (middle rows). The third rows are an overlay of DAPI and FITC for each group. A. A comparison of association between GOX, PLL-g-PEG/GOX, and anti-PSMA-PLL-g-PEG/GOX with LNCaP cells after 4 hours. B. Association of anti-PSMA-PLL-g-PEG/GOX with LNCaP cells after 30 minutes, 4 hours, and 24 hours.

In Figure 5.6B, anti-PSMA-PLL-g-PEG/GOX was incubated with LNCaP cells, and the cells were fixed at different time points after addition of the complexes. At 30 minutes, cell nuclei were small and distinct while FITC fluorescence showed signs of being both diffuse and punctate within the cells, suggesting that the complexes localize within endosomes. After four hours, cell nuclei were still distinct and FITC fluorescence was more diffuse in the cell than after 30 minutes, indicating that the complexes were likely released into the cytosol. Additionally, much of the FITC fluorescence was found near cell nuclei as opposed to the 30 minute time point. After 24 hours, DAPI staining of the nuclei showed more indistinct nuclei with almost all of the FITC fluorescence co-localized as opposed to what was seen at earlier time points. These images suggests that internalized anti-PSMA-PLL-g-PEG/GOX eventually co-localize with the nucleus once internalized in LNCaP cells.

5.3.7 Mechanism of Anti-PSMA-PLL-g-PEG/GOX Cellular Uptake

The mechanism of anti-PSMA-PLL-g-PEG/GOX uptake was assessed using pharmacological inhibitors, followed by evaluating the cytotoxic activity of the complexes (Figure 5.7). LNCaP cells had significantly improved viability when incubated with chlorpromazine (10%) ($p<0.05$) and genestein (20%) ($p<0.01$), but not with amiloride. The improved viability after incubation with chlorpromazine and genestein suggests that caveolae-mediated endocytosis plays an important role in the uptake of anti-PSMA-PLL-g-PEG/GOX, with clathrin-mediated endocytosis also having a role in the uptake.

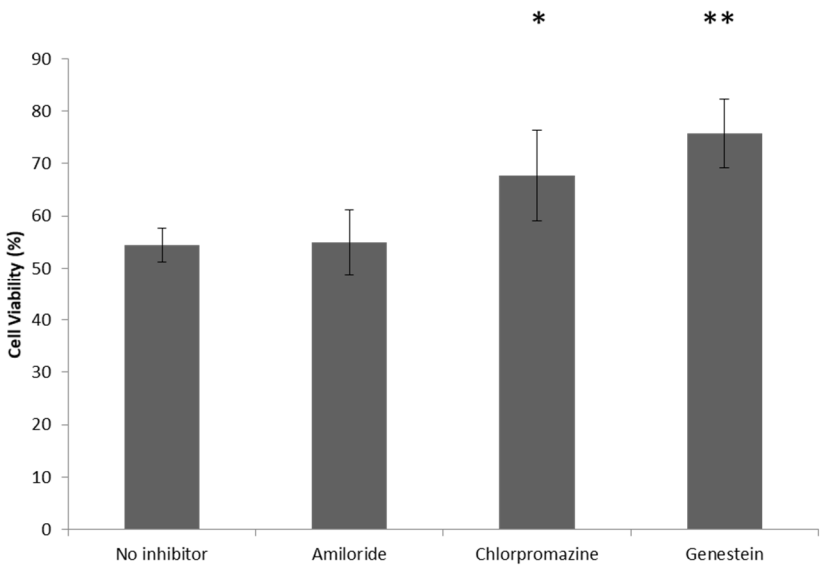

Figure 5.7. Effect of endocytosis inhibitors on Anti-PSMA-PLL-g-PEG/GOX cytotoxicity to LNCaP cells. LNCaP cells were treated with amiloride, chlorpromazine, and genestein to inhibit macropinocytosis, clathrin mediated endocytosis, and caveolae mediated endocytosis prior to addition of anti-PSMA-PLL-g-PEG/GOX. * indicates $p<0.05$ and ** indicates $p<0.01$ when the Student's t-Test was used to compare differences between the untreated group and treated groups.

5.4. Discussion

Prostate cancer is a significant health burden on society, affecting 11.6% of all men at some point in their lifetime [306]. Glucose is important for tumors to remain viable and grow, which was first identified by Warburg over 90 years ago [307]. Several types of cancer, including prostate cancer, have been found to be susceptible to metabolic stress, with glucose depletion resulting in the formation of excessive cytotoxic mitochondrial ROS [308]. A novel approach toward cancer treatment is to deliver cytotoxic hydrogen peroxide to the cancer while simultaneously reducing the amount of glucose available for cancer cell metabolism [81]. High levels of hydrogen peroxide and others forms of ROS can result in nuclear and mitochondrial DNA damage, protein carbonylation, and lipid peroxidation, which in turn results in multiple cell signaling pathways that lead to apoptosis [309]. This suggests that prostate cancer and other types

of cancer can be treated if subjected to glucose depletion in conjunction with generation of high levels of ROS.

The feasibility of this approach was first demonstrated by Nathan & Cohn, by i.p. injection of GOX conjugated to latex microspheres; they delivered a peroxide generator that was able to prolong the survival of mice treated with P388 lymphoma cells [80]. Ben-Yoseph & B.D. Ross similarly found that intratumorally administered PEGylated GOX could be used to inhibit the growth of solid tumors in mice formed from 9L glioma cells [79]. Although PEGylated GOX was demonstrated to reduce tumor volume in conjunction with a reduction in intratumoral ATP, a lack of retention of the enzyme in the tumor tissue required that SOD and catalase anti-oxidant enzymes be administered to the mice to prevent systemic toxicity. These early studies show that, although GOX is effective at inhibiting the growth of multiple types of cancer cells and tumors, ensuring that GOX is locally delivered is critical for the enzyme to be effective and not to cause toxicity to other tissues.

The potential of GOX to deprive tumors of glucose while generating hydrogen peroxide has recently received renewed interest. Zhao et al. developed poly (FBMA-co-OEGMA) nanogels entrapping GOX to form 800 nm particles as a novel treatment for melanoma [310]. After intratumoral injection in mice, the authors observed significant antitumor activity from the GOX nanogels with no observable damage to the kidney, liver, or heart of the mice. In another recent example, Fan et al. conjugated GOX to the surface of arginine-loaded hollow mesoporous silica nanoparticles to form 180 nm particles, which co-generated NO and H_2O_2. [293]. Tumor-bearing mice that received treatment with the GOX nanoparticles survived significantly longer than untreated mice

or mice that received nanoparticles without the surface bound GOX. These recent studies likewise demonstrate that disruption of glucose metabolism in parallel with peroxide formation is an effective treatment for several types of tumors and causes little toxicity if delivered near the tumor.

Although GOX and other peroxide generators have shown significant promise in prolonging the survival of mice with several types of tumors, controlling the delivery of GOX so that it has proximity to tumor tissue is important for it to be safe while effectively cytotoxic. In this study, we aimed to demonstrate that GOX could be made to be more cytotoxic toward PSMA-expressing prostate cancer cells if they were delivered in a way that enhanced the cell binding and internalization of the enzyme. If the enzyme can be delivered directly into cancer cells, smaller quantities of enzyme would be needed to induce cancer cell cytotoxicity, making the delivery of GOX more safe and effective.

Our approach aimed to further improve the delivery of GOX by selectively delivering the enzyme intracellularly by forming using PLL-g-PEG and an anti-PSMA monoclonal antibody to form anti-PSMA-PLL-g-PEG/GOX complexes. GOX readily associated with PLL-g-PEG into nanoscale complexes (Figure 5.2). GOX retained enzymatic activity toward glucose, which was evident by the release of H_2O_2 while associated with the copolymer (Figure 5.3). This is consistent with others who have found that small molecule substrates are accessible to enzymes within similar complexes without severely compromising activity [37, 311].

We further functionalized the GOX complexes by producing antibody fragments from a monoclonal antibody, which had previously been developed and shown to bind effectively to PSMA-expressing prostate cancer cells and used for the delivery of

imaging agents and nanoparticles [302, 312]. Improvements in the cell binding of DNA polyplexes through the use of antibodies have been observed by others and were expected to produce the same benefit to PLL-g-PEG/GOX [313].

Anti-PSMA-PLL-g-PEG/GOX was found to be significantly more cytotoxic toward LNCaP cells than unmodified GOX at equivalent concentrations of the enzyme (Figure 5.4). PLL-g-PEG/GOX also demonstrated significant cytotoxicity, but this effect was negated by the presence of serum proteins (Figure 5.5A). Serum and other proteins are known to bind to the surfaces of nanoparticles as a "protein corona" which likely reduces the ability of PLL-g-PEG/GOX to interact as effectively with the cells [51]. Functionalizing PLL-g-PEG/GOX with the anti-PSMA antibody was found to restore part of the cytotoxicity of GOX complexes in the presence of serum (Figure 5.5A). This suggest that the delivery of PLL-g-PEG/GOX can be controlled to cell types of interest through the use of ligands, such as antibodies.

To determine if the greater cytotoxicity can be attributed to better binding and/or internalization of GOX when modified as anti-PSMA-PLL-g-PEG/GOX, fluorescence microscopy was used to visualize GOX interaction with LNCaP cells (Figure 5.6). Fluorescence associated with anti-PSMA-PLL-g-PEG/GOX and PLL-g-PEG/GOX was observed to be much greater than that of unmodified GOX in serum-free conditions, indicating that PLL-g-PEG and anti-PSMA improve localization of the protein to the cells. In the presence of serum, however, anti-PSMA functionalization maintained uptake of the PLL-g-PEG/GOX complexes, while uptake of non-functionalized complexes was reduced (Figure 5.5A). Over the course of 24 hours, anti-PSMA-PLL-g-PEG/GOX showed increased co-localization with LNCaP nuclei, which is consistent with the

behavior of PLL-g-PEG when complexed with DNA as a gene delivery vector [314]. Co-localization of anti-PSMA-PLL-g-PEG/GOX with the nuclei suggest the superior cytotoxicity could potentially be due to increased peroxide generation near nuclear DNA, resulting in more oxidative DNA damage and increased cytotoxicity.

Anti-PSMA-PLL-g-PEG/GOX internalization by LNCaP cells is primarily mediated by clathrin- and caveolae-mediated endocytosis (Figure 5.7). Uptake by a caveolae endocytosis pathway may be beneficial for the complexes to induce cytotoxicity, as endosomes formed along these pathways are not expected to further develop into lysosomes, which may better protect the enzyme from proteolytic degradation.

ROS generation is consistent with GOX conversion of glucose into H_2O_2 and gluconic acid [291]. The intracellular generation of ROS was higher for anti-PSMA-PLL-g-PEG/GOX compared to untreated control cells (Figure 5.5C). PLL-g-PEG/GOX showed higher ROS generation than untreated control cells as well, but the increase was not significant (Figure 5.5B). The elevated generation of ROS and subsequent cytotoxicity for LNCaP cells treated with anti-PSMA-PLL-g-PEG/GOX, suggests that GOX is more cytotoxic to LNCaP cells when delivered into the cell interior.

5.5 Conclusions

Cytotoxic proteins have the potential provide additional means to treat cancer, but aspects of their delivery have limited their use. One of the biggest challenges to the use of peroxide-forming cytotoxic proteins, as with other chemotherapy drugs, is controlling delivery so as to deliver sufficient amounts of the enzyme to be toxic but cause minimal oxidative stress toward untargeted cells. In this proof-of-concept study, we sought to

improve one aspect of peroxide-forming protein delivery by delivering them into the intracellular space.

We found that GOX cytotoxicity could be enhanced to PSMA-expressing prostate cancer cells by modifying the enzyme with the cationic copolymer PLL-g-PEG and an anti-PSMA antibody. These modifications enabled enhanced binding and uptake of the enzyme in PSMA-expressing LNCaP cells compared to similar cells that lacked the PSMA receptor. Ultimately, concentrations of unmodified GOX that were non-toxic to LNCaP cells were cytotoxic once administered as an anti-PSMA-PLL-g-PEG/GOX complex. These results demonstrate that a practical means to enhance the cytotoxicity of GOX and potentially other peroxide forming proteins is to deliver them intracellularly. The modular design of the complexes also makes it possible for antibodies targeting other cancer cell markers to be utilized to facilitate intracellular delivery of a protein. Further optimization of anti-PSMA-PLL-g-PEG/GOX and assessing the performance of the complexes *in vivo* are planned in our future work to better develop GOX and other peroxide formers as cancer therapeutics.

CHAPTER VI

CONCLUSIONS

Proteins are large biomolecules that are capable of performing a wide range of biochemical reactions. The ability of proteins to accomplish a diverse range of biochemical tasks needed for cell survival makes many of them a member of an important group of potential therapeutics. In order for proteins to be effective therapeutics, however, they must be able to reach the location they are needed while also avoiding uptake by the immune system.

In this work, the copolymer PLL-g-PEG and other materials were used to alter the characteristics of proteins in order to improve aspects of their delivery. Using albumin as a model protein, structural characteristics of PLL-g-PEG were found to not only alter the ability of the copolymer to associate with the protein but to also impact the stability of PLL-g-PEG NP complexes. A 7:1 copolymer to protein ratio worked best for completely associating the protein with the copolymer and for producing stable NP complexes. Moreover, proteins encapsulated in PLL-g-PEG NP complexes were found to retain

their activity toward small molecule substrates.

The PLL-g-PEG NP complexes were then functionalized with CPPs. CPPs are short, typically cationic peptides, that are capable of transporting a wide variety of cargos across the cell membrane. As CPPs are highly cationic and likely to interact with serum proteins on their route to deliver PLL-g-PEG NP complexes, we studied the effect that CPPs have on albumin and macrophage uptake. CPPs, as part of PLL-g-PEG NP complexes, denature albumin with increasing charge and arginine content. Albumin was shown to participate in the uptake of CPP PLL-g-PEG NPs by macrophages, likely through a scavenger receptor.

The use of targeting ligands can improve the selectivity at which PLL-g-PEG NP complexes are delivered to particular cell types. This was demonstrated by functionalizing PLL-g-PEG NP complexes with an anti-PSMA monoclonal antibody to deliver the cytotoxic protein, GOX, to PSMA-expressing cancer cells. GOX was found to produce ROS within PSMA-expressing LNCaP cells, leading to the cytotoxicity of the PLL-g-PEG NP complexes. This work suggests that intracellular delivery of ROS-producing enzymes make the enzyme more cytotoxic to LNCaP cancer cells and potentially other types of targeted cancer cells as well.

While this work demonstrates that protein encapsulation within PLL-g-PEG NPs can be used to modify how proteins interact with cells and other proteins in the biological environment, additional future work is needed to make PLL-g-PEG NPs better protein delivery vectors. A few key topics of future potential research to improve PLL-g-PEG NP complexes are listed below:

- PLL-g-PEG NP complexes are unable to release the protein they encapsulate. While this is a strength for encapsulating proteins that interact with small molecule substrates, this may hinder other proteins that interact with larger biomacromolecules. Identifying ways to release the encapsulated protein, in a controlled manner, could broaden the utility of PLL-g-PEG NP complexes.
- PLL-g-PEG NPs cause denaturation of albumin in their protein corona. Identifying means to reduce the binding and denaturation of corona proteins could reduce non-specific uptake of the PLL-g-PEG NPs. Additionally, identifying other proteins that bind to the NPs, both as part of the protein corona or as a result of albumin denaturation, would better characterize how these NPs interact with the biological environment. Determining how PLL-g-PEG NPs interact with a broader array of cell types would also aid in better understanding the behavior of these NPs in the physiological environment.
- Further characterizing the immunogenicity of PLL-g-PEG NPs would also guide in the design of NPs that more effectively deliver proteins. While the uptake of CPP-functionalized PLL-g-PEG NPs by macrophages was described, characterizing the cytokine response of the macrophages to the NPs could also provide more insight into their immunogenicity.

PLL-g-PEG NPs are capable of modifying proteins that change how they interact with cells and the biological environment. By better engineering how polymers and other materials interact with and deliver therapeutic proteins, novel protein delivery carriers

will be developed, which advance the efficiency of protein therapeutics and as well as improve human health.

REFERENCES

1. Leader, B., Q.J. Baca, and D.E. Golan, *Protein therapeutics: a summary and pharmacological classification.* Nature Reviews Drug Discovery, 2008. **7**: p. 21.

2. Schellekens, H., *Bioequivalence and the immunogenicity of biopharmaceuticals.* Nature reviews Drug discovery, 2002. **1**(6): p. 457.

3. Bolhassani, A., B.S. Jafarzade, and G. Mardani, *In vitro and in vivo delivery of therapeutic proteins using cell penetrating peptides.* Peptides, 2017. **87**: p. 50-63.

4. Etheridge, M.L., et al., *The big picture on nanomedicine: the state of investigational and approved nanomedicine products.* Nanomedicine: Nanotechnology, Biology and Medicine, 2013. **9**(1): p. 1-14.

5. Mishra, B., B.B. Patel, and S. Tiwari, *Colloidal nanocarriers: a review on formulation technology, types and applications toward targeted drug delivery.* Nanomedicine: Nanotechnology, Biology and Medicine, 2010. **6**(1): p. 9-24.

6. Doane, T.L. and C. Burda, *The unique role of nanoparticles in nanomedicine: imaging, drug delivery and therapy.* Chemical Society Reviews, 2012. **41**(7): p. 2885-2911.

7. Min, Y., et al., *Clinical Translation of Nanomedicine.* Chemical Reviews, 2015. **115**(19): p. 11147-11190.

8. Zhou, J., et al., *Octa-functional PLGA nanoparticles for targeted and efficient siRNA delivery to tumors.* Biomaterials, 2012. **33**(2): p. 583-591.

9. Flynn, N., et al., *Effect of cationic grafted copolymer structure on the encapsulation of bovine serum albumin.* Materials Science and Engineering: C, 2016. **62**: p. 524-531.

10. Rimann, M., et al., *Characterization of PLL-g-PEG-DNA nanoparticles for the delivery of therapeutic DNA.* Bioconjugate chemistry, 2008. **19**(2): p. 548-557.

11. Torrice, M., *Does nanomedicine have a delivery problem?* 2016, ACS Publications.

12. Veronese, F.M., *Peptide and protein PEGylation: a review of problems and solutions.* Biomaterials, 2001. **22**(5): p. 405-417.

13. Holle, L.M., *Pegaspargase: An Alternative?* Annals of Pharmacotherapy, 1997. **31**(5): p. 616-624.

14. Harris, J.M. and R.B. Chess, *Effect of pegylation on pharmaceuticals.* Nat Rev Drug Discov, 2003. **2**(3): p. 214-221.

15. Reddy, K.R., M.W. Modi, and S. Pedder, *Use of peginterferon alfa-2a (40 KD)(Pegasys®) for the treatment of hepatitis C.* Advanced Drug Delivery Reviews, 2002. **54**(4): p. 571-586.

16. Pelaz, B., et al., *Surface Functionalization of Nanoparticles with Polyethylene Glycol: Effects on Protein Adsorption and Cellular Uptake.* ACS Nano, 2015. **9**(7): p. 6996-7008.

17. Rausch, K., et al., *Evaluation of Nanoparticle Aggregation in Human Blood Serum.* Biomacromolecules, 2010. **11**(11): p. 2836-2839.

18. Gref, R., et al., *'Stealth'corona-core nanoparticles surface modified by polyethylene glycol (PEG): influences of the corona (PEG chain length and surface density) and of the core composition on phagocytic uptake and plasma protein adsorption.* Colloids and Surfaces B: Biointerfaces, 2000. **18**(3): p. 301-313.

19. Carr Jr, M.E., R. Cromartie, and D.A. Gabriel, *Effect of homo poly (L-amino acids) on fibrin assembly: role of charge and molecular weight.* Biochemistry, 1989. **28**(3): p. 1384-1388.

20. Harada, A. and K. Kataoka, *Formation of polyion complex micelles in an aqueous milieu from a pair of oppositely-charged block copolymers with poly (ethylene glycol) segments.* Macromolecules, 1995. **28**(15): p. 5294-5299.

21. Pack, D.W., et al., *Design and development of polymers for gene delivery.* Nature reviews Drug discovery, 2005. **4**(7): p. 581-593.

22. Wolfert, M. and L. Seymour, *Atomic force microscopic analysis of the influence of the molecular weight of poly (L) lysine on the size of polyelectrolyte complexes formed with DNA.* Gene therapy, 1996. **3**(3): p. 269-273.

23. Toncheva, V., et al., *Novel vectors for gene delivery formed by self-assembly of DNA with poly(l-lysine) grafted with hydrophilic polymers.* Biochimica et Biophysica Acta (BBA) - General Subjects, 1998. **1380**(3): p. 354-368.

24. Cai, X., et al., *Effective Gene Delivery Using Stimulus-Responsive Catiomer Designed with Redox-Sensitive Disulfide and Acid-Labile Imine Linkers.* Biomacromolecules, 2012. **13**(4): p. 1024-1034.

25. Cai, X., et al., *Reversible PEGylation and Schiff-base linked imidazole modification of polylysine for high-performance gene delivery.* Journal of Materials Chemistry B, 2015. **3**(8): p. 1507-1517.

26. Gao, S., et al., *A non-viral suicide gene delivery system traversing the blood brain barrier for non-invasive glioma targeting treatment.* Journal of Controlled Release, 2016. **243**: p. 357-369.

27. Harada, A. and K. Kataoka, *Novel polyion complex micelles entrapping enzyme molecules in the core: preparation of narrowly-distributed micelles from lysozyme and poly (ethylene glycol)-poly (aspartic acid) block copolymer in aqueous medium.* Macromolecules, 1998. **31**(2): p. 288-294.

28. Lee, Y., et al., *Charge□Conversional Polyionic Complex Micelles—Efficient Nanocarriers for Protein Delivery into Cytoplasm.* Angewandte Chemie, 2009. **121**(29): p. 5413-5416.

29. Lee, Y., et al., *Efficient delivery of bioactive antibodies into the cytoplasm of living cells by charge□conversional polyion complex micelles.* Angewandte Chemie International Edition, 2010. **49**(14): p. 2552-2555.

30. Gaydess, A., et al., *Visualization of exogenous delivery of nanoformulated butyrylcholinesterase to the central nervous system.* Chemico-biological interactions, 2010. **187**(1): p. 295-298.

31. Klyachko, N.L., et al., *Cross-linked antioxidant nanozymes for improved delivery to CNS.* Nanomedicine: nanotechnology, biology and medicine, 2012. **8**(1): p. 119-129.

32. Jiang, Y., et al., *SOD1 nanozyme salvages ischemic brain by locally protecting cerebral vasculature.* Journal of Controlled Release, 2015. **213**: p. 36-44.

33. Lockridge, O., *Review of human butyrylcholinesterase structure, function, genetic variants, history of use in the clinic, and potential therapeutic uses.* Pharmacology & Therapeutics, 2015. **148**: p. 34-46.

34. Hirayama, K., et al., *Rapid confirmation and revision of the primary structure of bovine serum albumin by ESIMS and frit-FAB LC/MS.* Biochemical and Biophysical Research Communications, 1990. **173**(2): p. 639-646.

35. Malamud, D. and J.W. Drysdale, *Isoelectric points of proteins: a table.* Analytical biochemistry, 1978. **86**(2): p. 620-647.

36. Pope, C., et al., *In vitro characterization of cationic copolymer-complexed recombinant human butyrylcholinesterase.* Biochemical pharmacology, 2015. **98**(3): p. 531-539.

37. Hester, K., et al., *Polyionic complexes of butyrylcholinesterase and poly-l-lysine-g-poly (ethylene glycol): Comparative kinetics of catalysis and inhibition and in*

vitro inactivation by proteases and heat. Chemico-biological interactions, 2017. **275**: p. 86-94.

38. Vinogradov, S., et al., *Polyion Complex Micelles with Protein-Modified Corona for Receptor-Mediated Delivery of Oligonucleotides into Cells.* Bioconjugate Chemistry, 1999. **10**(5): p. 851-860.

39. Kontos, S. and J.A. Hubbell, *Improving protein pharmacokinetics by engineering erythrocyte affinity.* Molecular pharmaceutics, 2010. **7**(6): p. 2141-2147.

40. Doshi, N., et al., *Red blood cell-mimicking synthetic biomaterial particles.* Proceedings of the National Academy of Sciences, 2009. **106**(51): p. 21495-21499.

41. Kontos, S., et al., *Engineering antigens for in situ erythrocyte binding induces T-cell deletion.* Proceedings of the National Academy of Sciences, 2013. **110**(1): p. E60-E68.

42. Sahoo, K., et al., *Molecular and biocompatibility characterization of red blood cell membrane targeted and cell penetrating peptide-modified polymeric nanoparticles.* Molecular Pharmaceutics, 2017.

43. Sahoo, K., et al., *Nanoparticle Attachment to Erythrocyte Via the Glycophorin A Targeted ERY1 Ligand Enhances Binding without Impacting Cellular Function.* Pharmaceutical research, 2016. **33**(5): p. 1191-1203.

44. Lutolf, M., et al., *Systematic modulation of Michael-type reactivity of thiols through the use of charged amino acids.* Bioconjugate chemistry, 2001. **12**(6): p. 1051-1056.

45. Park, Y.J., et al., *Nontoxic membrane translocation peptide from protamine, low molecular weight protamine (LMWP), for enhanced intracellular protein delivery: in vitro and in vivo study.* The FASEB journal, 2005. **19**(11): p. 1555-1557.

46. He, H., et al., *Cell-penetrating peptides meditated encapsulation of protein therapeutics into intact red blood cells and its application.* Journal of Controlled Release, 2014. **176**: p. 123-132.

47. Choi, Y.-S., et al., *The systemic delivery of siRNAs by a cell penetrating peptide, low molecular weight protamine.* Biomaterials, 2010. **31**(6): p. 1429-1443.

48. Kwon, Y.M., et al., *L-Asparaginase encapsulated intact erythrocytes for treatment of acute lymphoblastic leukemia (ALL).* Journal of Controlled Release, 2009. **139**(3): p. 182-189.

49. Ramsey, J.D. and N.H. Flynn, *Cell-penetrating peptides transport therapeutics into cells.* Pharmacology & therapeutics, 2015. **154**: p. 78-86.

50. Cedervall, T., et al., *Understanding the nanoparticle–protein corona using methods to quantify exchange rates and affinities of proteins for nanoparticles.* Proceedings of the National Academy of Sciences, 2007. **104**(7): p. 2050-2055.

51. Cedervall, T., et al., *Detailed identification of plasma proteins adsorbed on copolymer nanoparticles.* Angewandte Chemie International Edition, 2007. **46**(30): p. 5754-5756.

52. Vroman, L., et al., *Interaction of high molecular weight kininogen, factor XII, and fibrinogen in plasma at interfaces.* Blood, 1980. **55**(1): p. 156-159.

53. Aggarwal, P., et al., *Nanoparticle interaction with plasma proteins as it relates to particle biodistribution, biocompatibility and therapeutic efficacy.* Advanced Drug Delivery Reviews, 2009. **61**(6): p. 428-437.

54. Lundqvist, M., et al., *Nanoparticle size and surface properties determine the protein corona with possible implications for biological impacts.* Proceedings of the National Academy of Sciences, 2008. **105**(38): p. 14265-14270.

55. Monopoli, M.P., et al., *Biomolecular coronas provide the biological identity of nanosized materials.* Nat Nano, 2012. **7**(12): p. 779-786.

56. Lynch, I. and K.A. Dawson, *Protein-nanoparticle interactions.* Nano today, 2008. **3**(1): p. 40-47.

57. Yan, Y., et al., *Differential roles of the protein corona in the cellular uptake of nanoporous polymer particles by monocyte and macrophage cell lines.* ACS nano, 2013. **7**(12): p. 10960-10970.

58. Tenzer, S., et al., *Rapid formation of plasma protein corona critically affects nanoparticle pathophysiology.* Nat Nano, 2013. **8**(10): p. 772-781.

59. Barrán-Berdón, A.L., et al., *Time evolution of nanoparticle–protein corona in human plasma: relevance for targeted drug delivery.* Langmuir, 2013. **29**(21): p. 6485-6494.

60. Fleischer, C.C. and C.K. Payne, *Secondary structure of corona proteins determines the cell surface receptors used by nanoparticles.* The Journal of Physical Chemistry B, 2014. **118**(49): p. 14017-14026.

61. Caracciolo, G., et al., *Selective targeting capability acquired with a protein corona adsorbed on the surface of 1, 2-dioleoyl-3-trimethylammonium propane/DNA nanoparticles.* ACS applied materials & interfaces, 2013. **5**(24): p. 13171-13179.

62. Monopoli, M.P., et al., *Physical− chemical aspects of protein corona: relevance to in vitro and in vivo biological impacts of nanoparticles.* Journal of the American Chemical Society, 2011. **133**(8): p. 2525-2534.

63. Muthusamy, B., et al., *Plasma Proteome Database as a resource for proteomics research.* PROTEOMICS, 2005. **5**(13): p. 3531-3536.

64. Schöttler, S., K. Landfester, and V. Mailänder, *Controlling the Stealth Effect of Nanocarriers through Understanding the Protein Corona.* Angewandte Chemie International Edition, 2016. **55**(31): p. 8806-8815.

65. Owens, D.E. and N.A. Peppas, *Opsonization, biodistribution, and pharmacokinetics of polymeric nanoparticles.* International journal of pharmaceutics, 2006. **307**(1): p. 93-102.

66. Leroux, J.-C., et al., *An investigation on the role of plasma and serum opsonins on the evternalization of biodegradable poly (D, L-lactic acid) nanoparticles by human monocytes.* Life Sciences, 1995. **57**(7): p. 695-703.

67. Mirshafiee, V., et al., *Protein corona significantly reduces active targeting yield.* Chemical communications, 2013. **49**(25): p. 2557-2559.

68. Salvati, A., et al., *Transferrin-functionalized nanoparticles lose their targeting capabilities when a biomolecule corona adsorbs on the surface.* Nature nanotechnology, 2013. **8**(2): p. 137-143.

69. Caracciolo, G., et al., *Surface adsorption of protein corona controls the cell internalization mechanism of DC-Chol–DOPE/DNA lipoplexes in serum.* Biochimica et Biophysica Acta (BBA)-Biomembranes, 2010. **1798**(3): p. 536-543.

70. Ritz, S., et al., *Protein corona of nanoparticles: distinct proteins regulate the cellular uptake.* Biomacromolecules, 2015. **16**(4): p. 1311-1321.

71. Wilhelm, S., et al., *Analysis of nanoparticle delivery to tumours.* Nature Reviews Materials, 2016. **1**: p. 16014.

72. Saha, K., et al., *Regulation of Macrophage Recognition through the Interplay of Nanoparticle Surface Functionality and Protein Corona.* ACS Nano, 2016. **10**(4): p. 4421-4430.

73. Schöttler, S., et al., *Protein adsorption is required for stealth effect of poly (ethylene glycol)-and poly (phosphoester)-coated nanocarriers.* Nature nanotechnology, 2016. **11**(4): p. 372-377.

74. Lacerda, S.H.D.P., et al., *Interaction of Gold Nanoparticles with Common Human Blood Proteins.* ACS Nano, 2010. **4**(1): p. 365-379.

75. Walkey, C.D., et al., *Protein corona fingerprinting predicts the cellular interaction of gold and silver nanoparticles.* ACS nano, 2014. **8**(3): p. 2439-2455.

76. Caracciolo, G., et al., *Evolution of the Protein Corona of Lipid Gene Vectors as a Function of Plasma Concentration.* Langmuir, 2011. **27**(24): p. 15048-15053.

77. Wilson, R. and A. Turner, *Glucose oxidase: an ideal enzyme.* Biosensors and Bioelectronics, 1992. **7**(3): p. 165-185.

78. Aruoma, O.I., *Free radicals, oxidative stress, and antioxidants in human health and disease.* Journal of the American Oil Chemists' Society, 1998. **75**(2): p. 199-212.

79. Ben-Yoseph, O. and B. Ross, *Oxidation therapy: the use of a reactive oxygen species-generating enzyme system for tumour treatment.* British journal of cancer, 1994. **70**(6): p. 1131-1135.

80. Nathan, C.F. and Z.A. Cohn, *Antitumor effects of hydrogen peroxide in vivo.* Journal of Experimental Medicine, 1981. **154**(5): p. 1539-1553.

81. Zhao, W., J. Hu, and W. Gao, *Glucose Oxidase–Polymer Nanogels for Synergistic Cancer-Starving and Oxidation Therapy.* ACS applied materials & interfaces, 2017. **9**(28): p. 23528-23535.

82. Khalil, I.A., et al., *Uptake pathways and subsequent intracellular trafficking in nonviral gene delivery.* Pharmacol Rev, 2006. **58**(1): p. 32-45.

83. Woods, Y. and D. Lane, *Exploiting the p53 pathway for cancer diagnosis and therapy.* The Hematology Journal, 2013. **4**(1): p. 233-247.

84. Wang, M., et al., *Combinatorially Designed Lipid□like Nanoparticles for Intracellular Delivery of Cytotoxic Protein for Cancer Therapy.* Angewandte Chemie, 2014. **126**(11): p. 2937-2942.

85. Beitz, J.G., et al., *Antitumor Activity of Basic Fibroblast Growth Factor-Saporin Mitotoxin in Vitro and in Vivo.* Cancer Research, 1992. **52**(1): p. 227-230.

86. Wu, Y., et al., *A cytotoxic ribonuclease. Study of the mechanism of onconase cytotoxicity.* Journal of Biological Chemistry, 1993. **268**(14): p. 10686-10693.

87. Turkson, J., et al., *Phosphotyrosyl peptides block Stat3-mediated DNA binding activity, gene regulation, and cell transformation.* J Biol Chem, 2001. **276**(48): p. 45443-55.

88. Stebbins, E.G. and D. Mochly-Rosen, *Binding Specificity for RACK1 Resides in the V5 Region of βII Protein Kinase C.* Journal of Biological Chemistry, 2001. **276**(32): p. 29644-29650.

89. Kim, J., et al., *Centrosomal PKCβII and Pericentrin Are Critical for Human Prostate Cancer Growth and Angiogenesis.* Cancer Research, 2008. **68**(16): p. 6831-6839.

90. Ellerby, H.M., et al., *Anti-cancer activity of targeted pro-apoptotic peptides.* Nat Med, 1999. **5**(9): p. 1032-8.

91. Javadpour, M.M., et al., *De Novo Antimicrobial Peptides with Low Mammalian Cell Toxicity.* Journal of Medicinal Chemistry, 1996. **39**(16): p. 3107-3113.

92. Kell, D.B., P.D. Dobson, and S.G. Oliver, *Pharmaceutical drug transport: the issues and the implications that it is essentially carrier-mediated only.* Drug Discov Today, 2011. **16**(15-16): p. 704-14.

93. Di, L., et al., *Evidence-based approach to assess passive diffusion and carrier-mediated drug transport.* Drug Discov Today, 2012. **17**(15-16): p. 905-12.

94. Dobson, P.D. and D.B. Kell, *Carrier-mediated cellular uptake of pharmaceutical drugs: an exception or the rule?* Nat Rev Drug Discov, 2008. **7**(3): p. 205-20.

95. Sugano, K., et al., *Coexistence of passive and carrier-mediated processes in drug transport.* Nat Rev Drug Discov, 2010. **9**(8): p. 597-614.

96. Copolovici, D.M., et al., *Cell-penetrating peptides: design, synthesis, and applications.* ACS Nano, 2014. **8**(3): p. 1972-94.

97. Koren, E. and V.P. Torchilin, *Cell-penetrating peptides: breaking through to the other side.* Trends Mol Med, 2012. **18**(7): p. 385-93.

98. Alhakamy, N.A., et al., *Noncovalently associated cell-penetrating peptides for gene delivery applications.* Ther Deliv, 2013. **4**(6): p. 741-57.

99. Wang, F., et al., *Recent progress of cell-penetrating peptides as new carriers for intracellular cargo delivery.* J Control Release, 2014. **174**: p. 126-36.

100. Sternson, L.A., *Obstacles to polypeptide delivery.* Ann N Y Acad Sci, 1987. **507**: p. 19-21.

101. Frankel, A.D. and C.O. Pabo, *Cellular uptake of the tat protein from human immunodeficiency virus.* Cell, 1988. **55**(6): p. 1189-93.

102. Green, M. and P.M. Loewenstein, *Autonomous functional domains of chemically synthesized human immunodeficiency virus tat trans-activator protein.* Cell, 1988. **55**(6): p. 1179-88.

103. Vives, E., P. Brodin, and B. Lebleu, *A truncated HIV-1 Tat protein basic domain rapidly translocates through the plasma membrane and accumulates in the cell nucleus.* J Biol Chem, 1997. **272**(25): p. 16010-7.

104. Vivès, E., et al., *Structure–activity relationship study of the plasma membrane translocating potential of a short peptide from HIV-1 Tat protein.* Letters in Peptide Science, 1997. **4**(4-6): p. 429-436.

105. Park, J., et al., *Mutational analysis of a human immunodeficiency virus type 1 Tat protein transduction domain which is required for delivery of an exogenous protein into mammalian cells.* J Gen Virol, 2002. **83**(Pt 5): p. 1173-81.

106. Joliot, A., et al., *Antennapedia homeobox peptide regulates neural morphogenesis.* Proc Natl Acad Sci U S A, 1991. **88**(5): p. 1864-8.

107. Derossi, D., et al., *The third helix of the Antennapedia homeodomain translocates through biological membranes.* J Biol Chem, 1994. **269**(14): p. 10444-50.

108. Le Roux, I., et al., *Neurotrophic activity of the Antennapedia homeodomain depends on its specific DNA-binding properties.* Proceedings of the National Academy of Sciences, 1993. **90**(19): p. 9120-9124.

109. Frankel, A.D. and C.O. Pabo, *Cellular uptake of the tat protein from human immunodeficiency virus.* Cell, 1988. **55**(6): p. 1189-1193.

110. Green, M. and P.M. Loewenstein, *Autonomous functional domains of chemically synthesized human immunodeficiency virus Tat< I> Trans</I>-Activator Protein.* Cell, 1988. **55**(6): p. 1179-1188.

111. Vivès, E., P. Brodin, and B. Lebleu, *A Truncated HIV-1 Tat Protein Basic Domain Rapidly Translocates through the Plasma Membrane and Accumulates in the Cell Nucleus.* Journal of Biological Chemistry, 1997. **272**(25): p. 16010-16017.

112. Joliot, A., et al., *Antennapedia homeobox peptide regulates neural morphogenesis.* Proceedings of the National Academy of Sciences, 1991. **88**(5): p. 1864-1868.

113. Derossi, D., et al., *The third helix of the Antennapedia homeodomain translocates through biological membranes.* Journal of Biological Chemistry, 1994. **269**(14): p. 10444-10450.

114. Nigatu, A.S., et al., *Evaluation of cell-penetrating peptide/adenovirus particles for transduction of CAR-negative cells.* J Pharm Sci, 2013. **102**(6): p. 1981-93.

115. Nielsen, E.J.B., et al., *In vivo proof of concept of oral insulin delivery based on a co-administration strategy with the cell-penetrating peptide penetratin.* Journal of Controlled Release, 2014.

116. Alves, I.D., et al., *A proapoptotic peptide conjugated to penetratin selectively inhibits tumor cell growth.* Biochimica et Biophysica Acta (BBA)-Biomembranes, 2014. **1838**(8): p. 2087-2098.

117. Sharma, G., et al., *Cell penetrating peptide tethered bi-ligand liposomes for delivery to brain in vivo: Biodistribution and transfection.* Journal of Controlled Release, 2013. **167**(1): p. 1-10.

118. Wender, P.A., et al., *The design, synthesis, and evaluation of molecules that enable or enhance cellular uptake: peptoid molecular transporters.* Proceedings of the National Academy of Sciences, 2000. **97**(24): p. 13003-13008.

119. Zhang, C., et al., *siRNA-containing liposomes modified with polyarginine effectively silence the targeted gene.* Journal of Controlled Release, 2006. **112**(2): p. 229-239.

120. Tünnemann, G., et al., *Live-cell analysis of cell penetration ability and toxicity of oligo-arginines.* Journal of Peptide Science, 2008. **14**(4): p. 469-476.

121. Harreither, E., et al., *Characterization of a novel cell penetrating peptide derived from human Oct4.* Cell Regeneration, 2014. **3**(1): p. 2.

122. Massaoka, M.H., et al., *A novel cell-penetrating peptide derived from WT1 enhances p53 activity, induces cell senescence and displays antimelanoma activity in xeno- and syngeneic systems.* FEBS Open Bio, 2014. **4**(0): p. 153-161.

123. De Coupade, C., et al., *Novel human-derived cell-penetrating peptides for specific subcellular delivery of therapeutic biomolecules.* Biochem. J, 2005. **390**: p. 407-418.

124. Pooga, M., et al., *Cell penetration by transportan.* The FASEB Journal, 1998. **12**(1): p. 67-77.

125. Fisher, L., et al., *Cellular delivery of a double-stranded oligonucleotide NFκB decoy by hybridization to complementary PNA linked to a cell-penetrating peptide.* Gene therapy, 2004. **11**(16): p. 1264-1272.

126. Oehlke, J., et al., *Cellular uptake of an α-helical amphipathic model peptide with the potential to deliver polar compounds into the cell interior non-endocytically.* Biochimica et Biophysica Acta (BBA)-Biomembranes, 1998. **1414**(1): p. 127-139.

127. Elliott, G. and P. O'Hare, *Intercellular Trafficking and Protein Delivery by a Herpesvirus Structural Protein.* Cell, 1997. **88**(2): p. 223-233.

128. Zender, L., et al., *VP22-mediated intercellular transport of p53 in hepatoma cells in vitro and in vivo.* Cancer Gene Therapy, 2002. **9**(6): p. 489-496.

129. Dilber, M., et al., *Intercellular delivery of thymidine kinase prodrug activating enzyme by the herpes simplex virus protein, VP22.* Gene therapy, 1999. **6**(1): p. 12-21.

130. Morris, M.C., et al., *A peptide carrier for the delivery of biologically active proteins into mammalian cells.* Nature biotechnology, 2001. **19**(12): p. 1173-1176.

131. Kim, W., et al., *Neuroprotective effects of PEP-1-Cu, Zn-SOD against ischemic neuronal damage in the rabbit spinal cord.* Neurochemical research, 2012. **37**(2): p. 307-313.

132. Wei, Y., et al., *Design of novel cell penetrating peptides for the delivery of trehalose into mammalian cells.* Biochim Biophys Acta, 2014. **1838**(7): p. 1911-20.

133. Lin, Y.-Z., et al., *Inhibition of Nuclear Translocation of Transcription Factor NF-κB by a Synthetic Peptide Containing a Cell Membrane-permeable Motif and Nuclear Localization Sequence.* Journal of Biological Chemistry, 1995. **270**(24): p. 14255-14258.

134. Shin, I., et al., *Proapoptotic Activity of Cell-Permeable Anti-Akt Single-Chain Antibodies.* Cancer Research, 2005. **65**(7): p. 2815-2824.

135. Nakayama, F., et al., *Fibroblast Growth Factor-12 (FGF12) Translocation into Intestinal Epithelial Cells Is Dependent on a Novel Cell-penetrating Peptide Domain: INVOLVEMENT OF INTERNALIZATION IN THE IN VIVO ROLE OF EXOGENOUS FGF12.* Journal of Biological Chemistry, 2011. **286**(29): p. 25823-25834.

136. Nakayama, F., et al., *Cellular Internalization of Fibroblast Growth Factor-12 Exerts Radioprotective Effects on Intestinal Radiation Damage Independently of FGFR Signaling.* International Journal of Radiation Oncology*Biology*Physics, 2014. **88**(2): p. 377-384.

137. Liu, K., et al., *Identification of a functionally important sequence in the cytoplasmic tail of integrin beta 3 by using cell-permeable peptide analogs.* Proceedings of the National Academy of Sciences, 1996. **93**(21): p. 11819-11824.

138. Rhee, M. and P. Davis, *Mechanism of uptake of C105Y, a novel cell-penetrating peptide.* Journal of Biological Chemistry, 2006. **281**(2): p. 1233-1240.

139. Watkins, C.L., et al., *Cellular uptake, distribution and cytotoxicity of the hydrophobic cell penetrating peptide sequence PFVYLI linked to the proapoptotic domain peptide PAD.* Journal of Controlled Release, 2009. **140**(3): p. 237-244.

140. Cai, D., et al., *Hydrophobic penetrating peptide PFVYLI-modified stealth liposomes for doxorubicin delivery in breast cancer therapy.* Biomaterials, 2014. **35**(7): p. 2283-94.

141. Marks, J.R., et al., *Spontaneous membrane-translocating peptides by orthogonal high-throughput screening.* Journal of the American Chemical Society, 2011. **133**(23): p. 8995-9004.

142. He, J., et al., *Direct Cytosolic Delivery of Polar Cargo to Cells by Spontaneous Membrane-translocating Peptides.* Journal of Biological Chemistry, 2013. **288**(41): p. 29974-29986.

143. Sadler, K., et al., *Translocating Proline-Rich Peptides from the Antimicrobial Peptide Bactenecin 7†.* Biochemistry, 2002. **41**(48): p. 14150-14157.

144. Kobayashi, S., et al., *Interactions of the Novel Antimicrobial Peptide Buforin 2 with Lipid Bilayers: Proline as a Translocation Promoting Factor†.* Biochemistry, 2000. **39**(29): p. 8648-8654.

145. Jain, A., B.K. Yadav, and A. Chugh, *Marine antimicrobial peptide tachyplesin as an efficient nanocarrier for macromolecule delivery in plant and mammalian cells.* FEBS Journal, 2015: p. n/a-n/a.

146. Fennell, J.F., W.H. Shipman, and L.J. Cole, *Antibacterial action of melittin, a polypeptide from bee venom.* Experimental Biology and Medicine, 1968. **127**(3): p. 707-710.

147. Morris, M.C., et al., *A new peptide vector for efficient delivery of oligonucleotides into mammalian cells.* Nucleic Acids Research, 1997. **25**(14): p. 2730-2736.

148. Oehlke, J., et al., *Nonendocytic, amphipathicity dependent cellular uptake of helical model peptides.* Protein and Peptide Letters, 1996. **3**(6): p. 393-398.

149. Kamada, H., et al., *Creation of novel cell-penetrating peptides for intracellular drug delivery using systematic phage display technology originated from Tat transduction domain.* Biological and Pharmaceutical Bulletin, 2007. **30**(2): p. 218-223.

150. Sgolastra, F., et al., *Designing mimics of membrane active proteins.* Acc Chem Res, 2013. **46**(12): p. 2977-87.

151. Brock, R., *The uptake of arginine-rich cell-penetrating peptides: putting the puzzle together.* Bioconjug Chem, 2014. **25**(5): p. 863-8.

152. Lundberg, M. and M. Johansson, *Positively charged DNA-binding proteins cause apparent cell membrane translocation.* Biochem Biophys Res Commun, 2002. **291**(2): p. 367-71.

153. Richard, J.P., et al., *Cell-penetrating peptides. A reevaluation of the mechanism of cellular uptake.* J Biol Chem, 2003. **278**(1): p. 585-90.

154. Kaplan, I.M., J.S. Wadia, and S.F. Dowdy, *Cationic TAT peptide transduction domain enters cells by macropinocytosis.* Journal of Controlled Release, 2005. **102**(1): p. 247-253.

155. Richard, J.P., et al., *Cellular uptake of unconjugated TAT peptide involves clathrin-dependent endocytosis and heparan sulfate receptors.* J Biol Chem, 2005. **280**(15): p. 15300-6.

156. Ferrari, A., et al., *Caveolae-mediated internalization of extracellular HIV-1 tat fusion proteins visualized in real time.* Mol Ther, 2003. **8**(2): p. 284-94.

157. Fretz, M.M., et al., *Temperature-, concentration- and cholesterol-dependent translocation of L- and D-octa-arginine across the plasma and nuclear membrane of CD34+ leukaemia cells.* Biochem J, 2007. **403**(2): p. 335-42.

158. Kosuge, M., et al., *Cellular internalization and distribution of arginine-rich peptides as a function of extracellular peptide concentration, serum, and plasma membrane associated proteoglycans.* Bioconjug Chem, 2008. **19**(3): p. 656-64.

159. Derossi, D., et al., *Cell internalization of the third helix of the Antennapedia homeodomain is receptor-independent.* J Biol Chem, 1996. **271**(30): p. 18188-93.

160. Pouny, Y., et al., *Interaction of antimicrobial dermaseptin and its fluorescently labeled analogues with phospholipid membranes.* Biochemistry, 1992. **31**(49): p. 12416-23.

161. Herce, H.D. and A.E. Garcia, *Molecular dynamics simulations suggest a mechanism for translocation of the HIV-1 TAT peptide across lipid membranes.* Proc Natl Acad Sci U S A, 2007. **104**(52): p. 20805-10.

162. Palm-Apergi, C., et al., *The membrane repair response masks membrane disturbances caused by cell-penetrating peptide uptake.* FASEB J, 2009. **23**(1): p. 214-23.

163. Rothbard, J.B., T.C. Jessop, and P.A. Wender, *Adaptive translocation: the role of hydrogen bonding and membrane potential in the uptake of guanidinium-rich transporters into cells.* Adv Drug Deliv Rev, 2005. **57**(4): p. 495-504.

164. Hirose, H., et al., *Transient focal membrane deformation induced by arginine-rich peptides leads to their direct penetration into cells.* Mol Ther, 2012. **20**(5): p. 984-93.

165. Maiolo, J.R., M. Ferrer, and E.A. Ottinger, *Effects of cargo molecules on the cellular uptake of arginine-rich cell-penetrating peptides.* Biochim Biophys Acta, 2005. **1712**(2): p. 161-72.

166. Fittipaldi, A., et al., *Cell membrane lipid rafts mediate caveolar endocytosis of HIV-1 Tat fusion proteins.* J Biol Chem, 2003. **278**(36): p. 34141-9.

167. Tunnemann, G., et al., *Cargo-dependent mode of uptake and bioavailability of TAT-containing proteins and peptides in living cells.* FASEB J, 2006. **20**(11): p. 1775-84.

168. Holm, T., S.E. Andaloussi, and U. Langel, *Comparison of CPP uptake methods.* Methods Mol Biol, 2011. **683**: p. 207-17.

169. Pooga, M., et al., *Cell penetrating PNA constructs regulate galanin receptor levels and modify pain.* Nature biotechnology, 1998. **16**.

170. van Asbeck, A.H., et al., *Molecular Parameters of siRNA–Cell Penetrating Peptide Nanocomplexes for Efficient Cellular Delivery.* Acs Nano, 2013. **7**(5): p. 3797-3807.

171. Favaro, M., et al., *Development of a non-viral gene delivery vector based on the dynein light chain Rp3 and the TAT peptide.* Journal of biotechnology, 2014.

172. Lindberg, S., et al., *PepFect15, a novel endosomolytic cell-penetrating peptide for oligonucleotide delivery via scavenger receptors.* International journal of pharmaceutics, 2013. **441**(1): p. 242-247.

173. Hayashi, Y., et al., *Cell penetrating peptide-mediated systemic siRNA delivery to the liver.* International journal of pharmaceutics, 2011. **419**(1–2): p. 308-313.

174. Yamano, S., et al., *Long-term efficient gene delivery using polyethylenimine with modified Tat peptide.* Biomaterials, 2014. **35**(5): p. 1705-1715.

175. Yamano, S., et al., *Efficient in vivo gene delivery using modified Tat peptide with cationic lipids.* Biotechnology letters, 2014: p. 1-6.

176. Fang, B., et al., *A novel cell-penetrating peptide TAT-A1 delivers siRNA into tumor cells selectively.* Biochimie, 2013. **95**(2): p. 251-257.

177. Hu, Y., et al., *A mannosylated cell-penetrating peptide-graft-polyethylenimine as a gene delivery vector.* Biomaterials, 2014. **35**(13): p. 4236-46.

178. Jiang, Q.-Y., et al., *Gene delivery to tumor cells by cationic polymeric nanovectors coupled to folic acid and the cell-penetrating peptide octaarginine.* Biomaterials, 2011. **32**(29): p. 7253-7262.

179. Suk, J.S., et al., *Gene delivery to differentiated neurotypic cells with RGD and HIV Tat peptide functionalized polymeric nanoparticles.* Biomaterials, 2006. **27**(29): p. 5143-5150.

180. Cheng, C.J. and W.M. Saltzman, *Enhanced siRNA delivery into cells by exploiting the synergy between targeting ligands and cell-penetrating peptides.* Biomaterials, 2011. **32**(26): p. 6194-6203.

181. Chen, M., et al., *Topical delivery of siRNA into skin using SPACE-peptide carriers.* Journal of Controlled Release, 2014. **179**: p. 33-41.

182. Kanazawa, T., et al., *Prolongation of Life in Rats with Malignant Glioma by Intranasal siRNA/Drug Codelivery to the Brain with Cell-Penetrating Peptide-Modified Micelles.* Molecular Pharmaceutics, 2014. **11**(5): p. 1471-1478.

183. Eto, Y., et al., *Transduction of adenovirus vectors modified with cell-penetrating peptides.* Peptides, 2009. **30**(8): p. 1548-1552.

184. Liu, Y., et al., *Enhancing gene delivery of adeno-associated viruses by cell-permeable peptides.* Molecular Therapy—Methods & Clinical Development, 2014. **1**.

185. Chen, H.-Z., et al., *Membrane penetrating peptides greatly enhance baculovirus transduction efficiency into mammalian cells.* Biochemical and Biophysical Research Communications, 2011. **405**(2): p. 297-302.

186. Yu, D., et al., *Adenovirus with hexon Tat-protein transduction domain modification exhibits increased therapeutic effect in experimental neuroblastoma and neuroendocrine tumors.* Journal of Virology, 2011. **85**(24): p. 13114-13123.

187. Park, S., et al., *Branched oligomerization of cell-permeable peptides markedly enhances the transduction efficiency of adenovirus into mesenchymal stem cells.* Gene therapy, 2010. **17**(8): p. 1052-1061.

188. Bai, H., et al., *Antisense inhibition of gene expression and growth in gram-negative bacteria by cell-penetrating peptide conjugates of peptide nucleic acids targeted to< i> rpoD</i> gene.* Biomaterials, 2012. **33**(2): p. 659-667.

189. Rajasekaran, P., et al., *Peptide nucleic acids inhibit growth of Brucella suis in pure culture and in infected murine macrophages.* International Journal of Antimicrobial Agents, 2013. **41**(4): p. 358-362.

190. Rodriguez Plaza, J.G., et al., *Cell Penetrating Peptides and Cationic Antibacterial Peptides: two sides of the same coin.* Journal of Biological Chemistry, 2014.

191. Leader, B., Q.J. Baca, and D.E. Golan, *Protein therapeutics: a summary and pharmacological classification.* Nature Reviews Drug Discovery, 2008. **7**(1): p. 21-39.

192. Schwarze, S.R., et al., *In Vivo Protein Transduction: Delivery of a Biologically Active Protein into the Mouse.* Science, 1999. **285**(5433): p. 1569-1572.

193. Roeder, G.E., et al., *Herpes simplex virus VP22–human papillomavirus E2 fusion proteins produced in mammalian or bacterial cells enter mammalian cells and induce apoptotic cell death.* Biotechnology and applied biochemistry, 2004. **40**(2): p. 157-165.

194. Araki, D., et al., *Cell-penetrating D-isomer peptides of p53 C-terminus: long-term inhibitory effect on the growth of bladder cancer.* Urology, 2010. **75**(4): p. 813-819.

195. Fei, L., et al., *Tumor targeting of a cell penetrating peptide by fusing with a pH-sensitive histidine-glutamate co-oligopeptide.* Biomaterials, 2014. **35**(13): p. 4082-7.

196. Ramakrishna, S., et al., *Gene disruption by cell-penetrating peptide-mediated delivery of Cas9 protein and guide RNA.* Genome research, 2014. **24**(6): p. 1020-1027.

197. Liu, J., et al., *Cell-penetrating peptide-mediated delivery of TALEN proteins via bioconjugation for genome engineering.* Plos One, 2014. **9**(1): p. e85755.

198. Shin, M.J., et al., *Tat-glyoxalase protein inhibits against ischemic neuronal cell damage and ameliorates ischemic injury.* Free Radical Biology and Medicine, 2014. **67**: p. 195-210.

199. Kwon, H.Y., et al., *Transduction of Cu, Zn-superoxide dismutase mediated by an HIV-1 Tat protein basic domain into mammalian cells.* FEBS letters, 2000. **485**(2): p. 163-167.

200. Jin, L.H., et al., *Transduction of human catalase mediated by an HIV-1 TAT protein basic domain and arginine-rich peptides into mammalian cells.* Free Radical Biology and Medicine, 2001. **31**(11): p. 1509-1519.

201. Marchione, R., et al., *ZEBRA cell-penetrating peptide as an efficient delivery system in Candida albicans.* Biotechnol J, 2014.

202. Keller, A.A., et al., *Transduction of proteins into leishmania tarentolae by formation of non-covalent complexes with cell-penetrating peptides.* J Cell Biochem, 2014. **115**(2): p. 243-52.

203. Ma, J., et al., *Cell-penetrating peptides mediated protein cross-membrane delivery and its use in bacterial vector vaccine.* Fish Shellfish Immunol, 2014.

204. Nakase, I., et al., *Accumulation of arginine-rich cell-penetrating peptides in tumors and the potential for anticancer drug delivery in vivo.* Journal of Controlled Release, 2012. **159**(2): p. 181-188.

205. Lelle, M., et al., *Novel cleavable cell-penetrating peptide-drug conjugates: synthesis and characterization.* J Pept Sci, 2014. **20**(5): p. 323-33.

206. Nasrolahi Shirazi, A., et al., *Design and Biological Evaluation of Cell-Penetrating Peptide–Doxorubicin Conjugates as Prodrugs.* Molecular Pharmaceutics, 2013. **10**(2): p. 488-499.

207. Michiue, H., et al., *The acceleration of boron neutron capture therapy using multi-linked mercaptoundecahydrododecaborate (BSH) fused cell-penetrating peptide.* Biomaterials, 2014. **35**(10): p. 3396-405.

208. Meerovich, I., et al., *Photodamage of lipid bilayers by irradiation of a fluorescently labeled cell-penetrating peptide.* Biochim Biophys Acta, 2014. **1840**(1): p. 507-15.

209. Olson, E.S., et al., *In vivo characterization of activatable cell penetrating peptides for targeting protease activity in cancer.* Integrative Biology, 2009. **1**(5-6): p. 382-393.

210. Xia, H., et al., *Activatable Cell Penetrating Peptide-Conjugated Nanoparticles with Enhanced Permeability for Site-Specific Targeting Delivery of Anticancer Drug.* Bioconjugate Chemistry, 2013. **24**(3): p. 419-430.

211. Jin, E., et al., *Acid-active cell-penetrating peptides for in vivo tumor-targeted drug delivery.* Journal of the American Chemical Society, 2013. **135**(2): p. 933-940.

212. Delehanty, J.B., et al., *Self-Assembled Quantum Dot−Peptide Bioconjugates for Selective Intracellular Delivery.* Bioconjugate Chemistry, 2006. **17**(4): p. 920-927.

213. Liu, B.R., et al., *Intracellular delivery of quantum dots mediated by a histidine- and arginine-rich HR9 cell-penetrating peptide through the direct membrane translocation mechanism.* Biomaterials, 2011. **32**(13): p. 3520-3537.

214. Dmitriev, R.I., et al., *Intracellular oxygen-sensitive phosphorescent probes based on cell-penetrating peptides.* Analytical Biochemistry, 2010. **398**(1): p. 24-33.

215. Suh, J.S., et al., *Simultaneous imaging and restoration of cell function using cell permeable peptide probe.* Biomaterials, 2014. **35**(24): p. 6287-6298.

216. Jiang, T., et al., *Tumor imaging by means of proteolytic activation of cell-penetrating peptides.* Proceedings of the National Academy of Sciences of the United States of America, 2004. **101**(51): p. 17867-17872.

217. Olson, E.S., et al., *Activatable cell penetrating peptides linked to nanoparticles as dual probes for in vivo fluorescence and MR imaging of proteases.* Proceedings of the National Academy of Sciences, 2010. **107**(9): p. 4311-4316.

218. Nguyen, Q.T., et al., *Surgery with molecular fluorescence imaging using activatable cell-penetrating peptides decreases residual cancer and improves survival.* Proceedings of the National Academy of Sciences, 2010. **107**(9): p. 4317-4322.

219. Savariar, E.N., et al., *Real-time in vivo molecular detection of primary tumors and metastases with ratiometric activatable cell-penetrating peptides.* Cancer Research, 2013. **73**(2): p. 855-864.

220. Whitney, M., et al., *Ratiometric activatable cell-penetrating peptides provide rapid in vivo readout of thrombin activation.* Angew Chem Int Ed Engl, 2013. **52**(1): p. 325-30.

221. Weinstain, R., et al., *In Vivo Targeting of Hydrogen Peroxide by Activatable Cell-Penetrating Peptides.* Journal of the American Chemical Society, 2013. **136**(3): p. 874-877.

222. Gu, Z., et al., *Tailoring nanocarriers for intracellular protein delivery.* Chemical Society Reviews, 2011. **40**(7): p. 3638-3655.

223. Allen, C., D. Maysinger, and A. Eisenberg, *Nano-engineering block copolymer aggregates for drug delivery.* Colloids and Surfaces B: Biointerfaces, 1999. **16**(1): p. 3-27.

224. Stuart, M.A.C., et al., *Assembly of polyelectrolyte-containing block copolymers in aqueous media.* Current Opinion in Colloid & Interface Science, 2005. **10**(1-2): p. 30-36.

225. Kataoka, K., A. Harada, and Y. Nagasaki, *Block copolymer micelles for drug delivery: design, characterization and biological significance.* Advanced drug delivery reviews, 2001. **47**(1): p. 113-131.

226. Katayose, S. and K. Kataoka, *Water-soluble polyion complex associates of DNA and poly (ethylene glycol)-poly (L-lysine) block copolymer.* Bioconjugate Chemistry, 1997. **8**(5): p. 702-707.

227. Huang, N.-P., et al., *Poly (L-lysine)-g-poly (ethylene glycol) layers on metal oxide surfaces: surface-analytical characterization and resistance to serum and fibrinogen adsorption.* Langmuir, 2001. **17**(2): p. 489-498.

228. Veronese, F. and A. Mero, *The Impact of PEGylation on Biological Therapies.* BioDrugs, 2008. **22**(5): p. 315-329.

229. Otsuka, H., Y. Nagasaki, and K. Kataoka, *Self-assembly of poly(ethylene glycol)-based block copolymers for biomedical applications.* Current Opinion in Colloid & Interface Science, 2001. **6**(1): p. 3-10.

230. Kataoka, K., et al., *Spontaneous formation of polyion complex micelles with narrow distribution from antisense oligonucleotide and cationic block copolymer in physiological saline.* Macromolecules, 1996. **29**(26): p. 8556-8557.

231. Jaturanpinyo, M., et al., *Preparation of bionanoreactor based on core-shell structured polyion complex micelles entrapping trypsin in the core cross-linked with glutaraldehyde.* Bioconjugate Chemistry, 2004. **15**(2): p. 344-348.

232. Ragelle, H., et al., *Chitosan nanoparticles for siRNA delivery: Optimizing formulation to increase stability and efficiency.* Journal of Controlled Release, 2014. **176**: p. 54-63.

233. Singarapu, K., I. Pal, and J.D. Ramsey, *Polyethylene glycol–grafted polyethylenimine used to enhance adenovirus gene delivery.* Journal of Biomedical Materials Research Part A, 2013. **101**(7): p. 1857-1864.

234. Manickam, D.S., et al., *Well-defined cross-linked antioxidant nanozymes for treatment of ischemic brain injury.* Journal of Controlled Release, 2012. **162**(3): p. 636-645.

235. Yuan, X., et al., *Stabilization of lysozyme-incorporated polyion complex micelles by the ω-end derivatization of poly (ethylene glycol)-poly (α, β-aspartic acid) block copolymers with hydrophobic groups.* Langmuir, 2005. **21**(7): p. 2668-2674.

236. Batrakova, E.V., et al., *A macrophage-nanozyme delivery system for Parkinson's disease.* Bioconjugate Chemistry, 2007. **18**(5): p. 1498-1506.

237. Postupalenko, V., et al., *Intracellular delivery of functionally active proteins using self-assembling pyridylthiourea-polyethylenimine.* Journal of Controlled Release, 2014. **178**: p. 86-94.

238. Xu, Y. and Y. Du, *Effect of molecular structure of chitosan on protein delivery properties of chitosan nanoparticles.* International journal of pharmaceutics, 2003. **250**(1): p. 215-226.

239. Singh, H.D., et al., *Poly-l-lysine-coated albumin nanoparticles: Stability, mechanism for increasing in vitro enzymatic resilience, and siRNA release characteristics.* Acta Biomaterialia, 2010. **6**(11): p. 4277-4284.

240. Pippa, N., et al., *Insulin/Poly (ethylene glycol)-block-poly (L-lysine) Complexes: Physicochemical Properties and Protein Encapsulation.* The Journal of Physical Chemistry B, 2015.

241. Gaydess, A., et al., *Visualization of exogenous delivery of nanoformulated butyrylcholinesterase to the central nervous system.* Chemico-Biological Interactions, 2010. **187**(1-3): p. 295-298.

242. Lee, Y., et al., *Charge-Conversional Polyionic Complex Micelles—Efficient Nanocarriers for Protein Delivery into Cytoplasm.* Angewandte Chemie, 2009. **121**(29): p. 5413-5416.

243. Hunter, R.J., *Zeta potential in colloid science: principles and applications*. Vol. 2. 2013: Academic press.

244. Tove, S., *The esterolytic activity of serum albumin.* Biochimica et biophysica acta, 1962. **57**(1): p. 230-235.

245. Córdova, J., et al., *Esterase activity of bovine serum albumin up to 160 C: a new benchmark for biocatalysis.* Enzyme and Microbial Technology, 2008. **42**(3): p. 278-283.

246. Jones, L.J., et al., *Quenched BODIPY Dye-Labeled Casein Substrates for the Assay of Protease Activity by Direct Fluorescence Measurement.* Analytical Biochemistry, 1997. **251**(2): p. 144-152.

247. Migneault, I., et al., *Glutaraldehyde: behavior in aqueous solution, reaction with proteins, and application to enzyme crosslinking.* Biotechniques, 2004. **37**(5): p. 790-806.

248. Itaka, K., et al., *Polyion complex micelles from plasmid DNA and poly (ethylene glycol)–poly (l-lysine) block copolymer as serum-tolerable polyplex system: physicochemical properties of micelles relevant to gene transfection efficiency.* Biomaterials, 2003. **24**(24): p. 4495-4506.

249. Männistö, M., et al., *Structure–activity relationships of poly(l-lysines): effects of pegylation and molecular shape on physicochemical and biological properties in gene delivery.* Journal of Controlled Release, 2002. **83**(1): p. 169-182.

250. Sato, A., et al., *Polymer brush-stabilized polyplex for a siRNA carrier with long circulatory half-life.* Journal of Controlled Release, 2007. **122**(3): p. 209-216.

251. Wuelfing, W.P., et al., *Nanometer gold clusters protected by surface-bound monolayers of thiolated poly (ethylene glycol) polymer electrolyte.* Journal of the American Chemical Society, 1998. **120**(48): p. 12696-12697.

252. Wang, Y., W.L. Mattice, and D.H. Napper, *Simulation of the formation of micelles by diblock copolymers under weak segregation.* Langmuir, 1993. **9**(1): p. 66-70.

253. Kragh-Hansen, U., *Molecular and practical aspects of the enzymatic properties of human serum albumin and of albumin–ligand complexes.* Biochimica et Biophysica Acta (BBA) - General Subjects, 2013. **1830**(12): p. 5535-5544.

254. Yuan, X., et al., *Characterization of stable lysozyme-entrapped polyion complex (PIC) micelles with crosslinked core by glutaraldehyde.* Polymer, 2005. **46**(18): p. 7749-7758.

255. Jørgensen, L., S. Frokjaer, and H.M. Nielsen, *Issues in development of biodrug delivery systems.* Biodrug Delivery Systems: Fundamentals, Applications and Clinical Development, 2009: p. 13.

256. Pisal, D.S., M.P. Kosloski, and S.V. Balu-Iyer, *Delivery of therapeutic proteins.* Journal of Pharmaceutical Sciences, 2010. **99**(6): p. 2557-2575.

257. Klibanov, A.M., *Enzyme stabilization by immobilization.* Analytical Biochemistry, 1979. **93**(0): p. 1-25.

258. Appel, W., *Chymotrypsin: Molecular and catalytic properties.* Clinical Biochemistry, 1986. **19**(6): p. 317-322.

259. Katayose, S. and K. Kataoka, *Remarkable increase in nuclease resistance of plasmid DNA through supramolecular assembly with poly(ethylene glycol)—poly(L-lysine) block copolymer.* Journal of Pharmaceutical Sciences, 1998. **87**(2): p. 160-163.

260. Guidotti, G., L. Brambilla, and D. Rossi, *Cell-Penetrating Peptides: From Basic Research to Clinics.* Trends in Pharmacological Sciences, 2017. **38**(4): p. 406-424.

261. Milletti, F., *Cell-penetrating peptides: classes, origin, and current landscape.* Drug discovery today, 2012. **17**(15-16): p. 850-860.

262. Console, S., et al., *Antennapedia and HIV transactivator of transcription (TAT)"protein transduction domains" promote endocytosis of high molecular weight cargo upon binding to cell surface glycosaminoglycans.* Journal of Biological Chemistry, 2003. **278**(37): p. 35109-35114.

263. Ziegler, A. and J. Seelig, *Binding and Clustering of Glycosaminoglycans: A Common Property of Mono- and Multivalent Cell-Penetrating Compounds.* Biophysical Journal, 2008. **94**(6): p. 2142-2149.

264. C., F.H., et al., *Pharmacokinetics of Nanoscale Quantum Dots: In Vivo Distribution, Sequestration, and Clearance in the Rat.* Advanced Functional Materials, 2006. **16**(10): p. 1299-1305.

265. Gunawan, C., et al., *Nanoparticle–protein corona complexes govern the biological fates and functions of nanoparticles.* Journal of Materials Chemistry B, 2014. **2**(15): p. 2060-2083.

266. Nigatu, A.S., et al., *Evaluation of Cell-Penetrating Peptide/Adenovirus Particles for Transduction of CAR-Negative Cells.* Journal of Pharmaceutical Sciences, 2013. **102**(6): p. 1981-1993.

267. Kirsch, R.E., L.O.C. Frith, and S.J. Saunders, *Albumin catabolism in vitro by cultured peritoneal and pulmonary mononuclear phagocytes.* Biochimica et Biophysica Acta (BBA) - General Subjects, 1972. **279**(1): p. 87-91.

268. Buys, C., et al., *Rapid uptake by liver sinusoidal cells of serum albumin modified with retention of its compact conformation.* Biochimica et Biophysica Acta (BBA)-General Subjects, 1975. **392**(1): p. 95-100.

269. Green, M. and P.M. Loewenstein, *Autonomous functional domains of chemically synthesized human immunodeficiency virus tat trans-activator protein.* Cell, 1988. **55**(6): p. 1179-1188.

270. Huang, N.-P., et al., *Biotin-derivatized poly (L-lysine)-g-poly (ethylene glycol): A novel polymeric interface for bioaffinity sensing.* Langmuir, 2002. **18**(1): p. 220-230.

271. Ellman, G.L., et al., *A new and rapid colorimetric determination of acetylcholinesterase activity.* Biochemical pharmacology, 1961. **7**(2): p. 88IN191-9095.

272. Åkesson, A., et al., *The protein corona of dendrimers: PAMAM binds and activates complement proteins in human plasma in a generation dependent manner.* Rsc Advances, 2012. **2**(30): p. 11245-11248.

273. Zhuang, X., et al., *Fluorescence quenching: A tool for single-molecule protein-folding study.* Proceedings of the National Academy of Sciences, 2000. **97**(26): p. 14241-14244.

274. Keswani, R.K., M. Lazebnik, and D.W. Pack, *Intracellular trafficking of hybrid gene delivery vectors.* Journal of Controlled Release, 2015. **207**: p. 120-130.

275. Vercauteren, D., et al., *The use of inhibitors to study endocytic pathways of gene carriers: optimization and pitfalls.* Molecular Therapy, 2010. **18**(3): p. 561-569.

276. Hed, J., et al., *The use of fluorescence quenching in flow cytofluorometry to measure the attachment and ingestion phases in phagocytosis in peripheral blood without prior cell separation.* Journal of Immunological Methods, 1987. **101**(1): p. 119-125.

277. Wan, C.P., C.S. Park, and B.H. Lau, *A rapid and simple microfluorometric phagocytosis assay.* Journal of immunological methods, 1993. **162**(1): p. 1-7.

278. Varol, C., A. Mildner, and S. Jung, *Macrophages: Development and Tissue Specialization.* Annual Review of Immunology, 2015. **33**(1): p. 643-675.

279. Kawamura, A., et al., *Polyion complex micelles formed from glucose oxidase and comb□type polyelectrolyte with poly (ethylene glycol) grafts.* Journal of Polymer Science Part A: Polymer Chemistry, 2008. **46**(11): p. 3842-3852.

280. Xiang, S., et al., *Uptake mechanisms of non-viral gene delivery.* Journal of controlled release, 2012. **158**(3): p. 371-378.

281. Zani, I.A., et al., *Scavenger receptor structure and function in health and disease.* Cells, 2015. **4**(2): p. 178-201.

282. Van Haute, D., A.T. Liu, and J.M. Berlin, *Coating Metal Nanoparticle Surfaces With Small Organic Molecules Can Reduce Non-Specific Cell Uptake.* ACS nano, 2018.

283. Mitchell, D.J., et al., *Polyarginine enters cells more efficiently than other polycationic homopolymers.* Chemical Biology & Drug Design, 2000. **56**(5): p. 318-325.

284. Ramadass, M., B. Ghebrehiwet, and R.R. Kew, *Enhanced recognition of plasma proteins in a non-native state by complement C3b. A possible clearance mechanism for damaged proteins in blood.* Molecular immunology, 2015. **64**(1): p. 55-62.

285. Buttke, T.M. and P.A. Sandstrom, *Oxidative stress as a mediator of apoptosis.* Immunology today, 1994. **15**(1): p. 7-10.

286. Grune, T., T. Reinheckel, and K. Davies, *Degradation of oxidized proteins in mammalian cells.* The FASEB Journal, 1997. **11**(7): p. 526-534.

287. H. Sies, E.C., *Oxidative stress: damage to intact cells and organs.* Philosophical Transactions of the Royal Society of London. B, Biological Sciences, 1985. **311**(1152): p. 617-631.

288. Barzilai, A. and K.-I. Yamamoto, *DNA damage responses to oxidative stress.* DNA Repair, 2004. **3**(8): p. 1109-1115.

289. Yoshikawa, T., et al., *A novel cancer therapy based on oxygen radicals.* Cancer research, 1995. **55**(8): p. 1617-1620.

290. Singh, B.R., et al., *ROS-mediated apoptotic cell death in prostate cancer LNCaP cells induced by biosurfactant stabilized CdS quantum dots.* Biomaterials, 2012. **33**(23): p. 5753-5767.

291. Bankar, S.B., et al., *Glucose oxidase — An overview.* Biotechnology Advances, 2009. **27**(4): p. 489-501.

292. Fang, J., et al., *Tumor-targeted delivery of polyethylene glycol-conjugated D-amino acid oxidase for antitumor therapy via enzymatic generation of hydrogen peroxide.* Cancer research, 2002. **62**(11): p. 3138-3143.

293. Fan, W., et al., *Glucose-Responsive Sequential Generation of Hydrogen Peroxide and Nitric Oxide for Synergistic Cancer Starving-Like/Gas Therapy.* Angewandte Chemie International Edition, 2017. **56**(5): p. 1229-1233.

294. Kim, S.H., et al., *Folate receptor mediated intracellular protein delivery using PLL–PEG–FOL conjugate.* Journal of controlled release, 2005. **103**(3): p. 625-634.

295. Wolfert, M.A., et al., *Characterization of vectors for gene therapy formed by self-assembly of DNA with synthetic block co-polymers.* Human gene therapy, 1996. **7**(17): p. 2123-2133.

296. Oe, Y., et al., *Actively-targeted polyion complex micelles stabilized by cholesterol and disulfide cross-linking for systemic delivery of siRNA to solid tumors.* Biomaterials, 2014. **35**(27): p. 7887-7895.

297. Pippa, N., et al., *Insulin/poly (ethylene glycol)-block-poly (L-lysine) complexes: physicochemical properties and protein encapsulation.* The Journal of Physical Chemistry B, 2015. **119**(22): p. 6813-6819.

298. Choi, Y.H., et al., *Polyethylene glycol-grafted poly-L-lysine as polymeric gene carrier.* Journal of controlled release, 1998. **54**(1): p. 39-48.

299. O'Keefe, D.S., et al., *Prostate□specific suicide gene therapy using the prostate□specific membrane antigen promoter and enhancer.* The Prostate, 2000. **45**(2): p. 149-157.

300. Chang, S.S., et al., *Short term neoadjuvant androgen deprivation therapy does not affect prostate specific membrane antigen expression in prostate tissues.* Cancer, 2000. **88**(2): p. 407-415.

301. Su, S.L., et al., *Alternatively Spliced Variants of Prostate-specific Membrane Antigen RNA: Ratio of Expression as a Potential Measurement of Progression.* Cancer Research, 1995. **55**(7): p. 1441.

302. Liu, J., et al., *Biorecognition and Subcellular Trafficking of HPMA Copolymer−Anti-PSMA Antibody Conjugates by Prostate Cancer Cells.* Molecular pharmaceutics, 2009. **6**(3): p. 959-970.

303. Mahmoud, W., et al., *Advanced procedures for labeling of antibodies with quantum dots.* Analytical biochemistry, 2011. **416**(2): p. 180-185.

304. LeBel, C.P., H. Ischiropoulos, and S.C. Bondy, *Evaluation of the probe 2', 7'-dichlorofluorescin as an indicator of reactive oxygen species formation and oxidative stress.* Chemical research in toxicology, 1992. **5**(2): p. 227-231.

305. Eruslanov, E. and S. Kusmartsev, *Identification of ROS using oxidized DCFDA and flow-cytometry.* Advanced protocols in oxidative stress II, 2010: p. 57-72.

306. National Cancer Institute. *Cancer Stat Facts: Prostate Cancer*. 2017 [cited 2018 January 25, 2018]; Available from: https://seer.cancer.gov/statfacts/html/prost.html.

307. Warburg, O., F. Wind, and E. Negelein, *The metabolism of tumors in the body.* The Journal of general physiology, 1927. **8**(6): p. 519.

308. Ahmad, I.M., et al., *Mitochondrial and H2O2 Mediate Glucose Deprivation-induced Stress in Human Cancer Cells.* Journal of Biological Chemistry, 2005. **280**(6): p. 4254-4263.

309. Finkel, T. and N.J. Holbrook, *Oxidants, oxidative stress and the biology of ageing.* Nature, 2000. **408**(6809): p. 239-247.

310. Zhao, W., J. Hu, and W. Gao, *Glucose Oxidase–Polymer Nanogels for Synergistic Cancer-Starving and Oxidation Therapy.* ACS Applied Materials & Interfaces, 2017.

311. Jaturanpinyo, M., et al., *Preparation of Bionanoreactor Based on Core−Shell Structured Polyion Complex Micelles Entrapping Trypsin in the Core Cross-Linked with Glutaraldehyde.* Bioconjugate Chemistry, 2004. **15**(2): p. 344-348.

312. Elsässer-Beile, U., et al., *PET imaging of prostate cancer xenografts with a highly specific antibody against the prostate-specific membrane antigen.* Journal of Nuclear Medicine, 2009. **50**(4): p. 606-611.

313. Chiu, S.-J., N.T. Ueno, and R.J. Lee, *Tumor-targeted gene delivery via anti-HER2 antibody (trastuzumab, Herceptin®) conjugated polyethylenimine.* Journal of controlled release, 2004. **97**(2): p. 357-369.

314. Lühmann, T., et al., *Cellular Uptake and Intracellular Pathways of PLL-g-PEG-DNA Nanoparticles.* Bioconjugate Chemistry, 2008. **19**(9): p. 1907-1916.

APPENDICES

Supplementary Data

The grafting ratio of PEG onto PLL was determined using ^{1}H NMR spectroscopy. The number of PEG chains grafted onto the PLL was calculated by integrating the peaks in the PLL-g-PEG NMR spectrum that correspond to protons of the PLL (-CH- at 4.15 ppm) and PEG-amine linkage (-CH_2CO-NH at 2.55 ppm) portions of the copolymer. First, the average number of α carbon protons corresponding to the number of lysines per mol of PLL was calculated by using the median molecular weight of the high, medium and low PLL polymers (50,000 kDa, 22,500 kDa, and 9,500 kDa) (Equation 1). Next, the relative number of mols of PEG linkages to mols of lysine residues was calculated by taking the quotient of the PEG linkage peak and PLL monomer peak areas (Equations 2). Once the relative number of mols of PEG linkages to PLL monomers was determined, the grafting ratio was calculated by taking the product of the number of lysines per PLL chain with the relative number of mols of PEG linkage per the relative number of mols of lysines (Equation 3).The calculation used to determine the grafting ratio and a sample ^{1}HNMR spectrum may be found below:

S.1 Grafting Ratio Calculation and ^{1}HNMR

$$Number\ of\ lysines\ in\ PLL\ (N_{PLL}) = \frac{22500\ g}{mol\ PLL} \times \frac{1\ PLL\ mer}{146.17\ g} \times \frac{1\ H}{PLL\ mer\ (-CH-)} \quad 1.$$

$$Relative\ number\ of\ mols\ of\ PEG\ linkages\ per\ PLL\ lysines\ \left(\frac{mol\ PEG}{mol\ lysine}\right) = \frac{Area_{PEG}}{Area_{PLL}} \quad 2.$$

$$Grafting\ Ratio\ \frac{(mol\ PEG)}{(mol\ PLL)} = N_{PLL}\left(\frac{mol\ lysine}{mol\ PLL}\right) \times \left(\frac{mol\ PEG}{mol\ lysine}\right) \quad 3.$$

NMR Spectrum

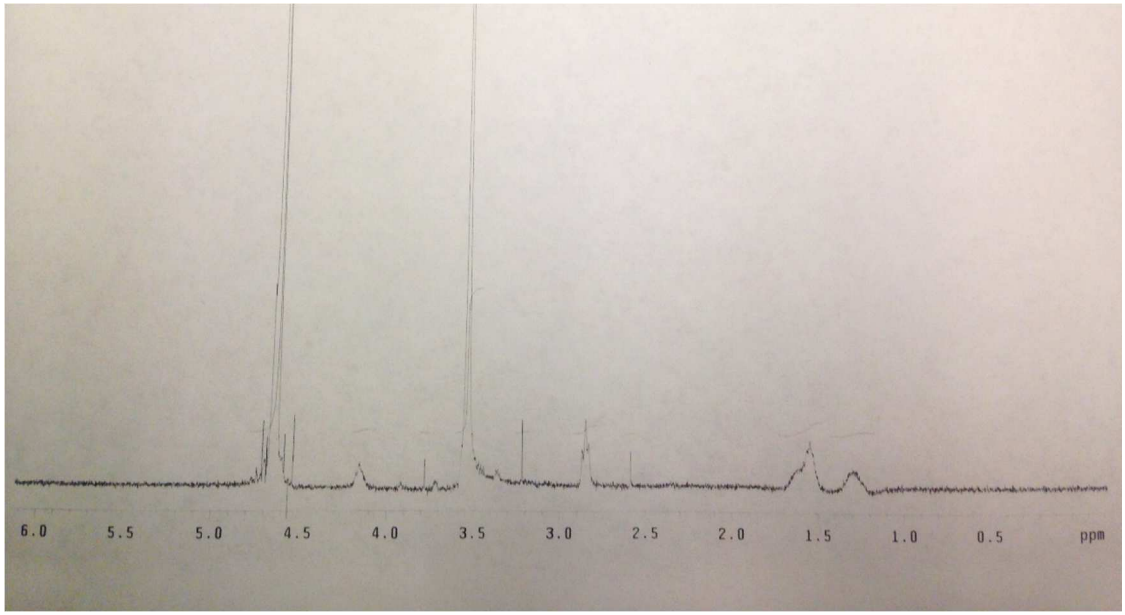

Figure S.1 ^{1}HNMR Spectrum for PLL-g-PEG. The spectrum is for MMW 10 copolymer. The peaks at 4.15 ppm (PLL -CH-) and 2.55 ppm (PEG-amine -CH_2CO-NH-) were used to calculate the grafting ratio.

VITA

Nicholas Flynn

Candidate for the Degree of

Doctor of Philosophy

Dissertation: SYNTHESIS AND FUNCTIONALIZATION OF POLY-L-LYSINE-GRAFTED-POLYETHYLENE GLYCOL COPOLYMER NANOPARTICLE COMPLEXES FOR PROTEIN DELIVERY

Major Field: Chemical Engineering

Biographical:

Education:

Completed the requirements for the Doctor of Philosophy in Chemical Engineering at Oklahoma State University, Stillwater, Oklahoma in July, 2018.

Completed the requirements for the Master of Science in Chemical Engineering at Oklahoma State University, Stillwater, Oklahoma in July, 2014.

Completed the requirements for the Bachelor of Science in Chemical Engineering at the University of Oklahoma, Norman, Oklahoma in May, 2011.

Experience:

Graduate Teaching and Research Assistant at the School of Chemical Engineering, Oklahoma State University, Stillwater, Oklahoma from January, 2012 through May, 2018.

Professional Memberships:

Membership in AIChE